공학박사학위논문

Geomechanical Study on Hydraulic Stimulation in Enhanced Geothermal System: Field Observation Analysis and Analytical Estimation

인공저류층 지열시스템에서의 수리자극을 위한
암반역학적 연구:
실증 자료 분석 및 이론적 예측

August 2016

Graduate School of Seoul National University

Department of Energy System Engineering

Linmao Xie

Geomechanical Study on Hydraulic Stimulation in Enhanced Geothermal System: Field Observation Analysis and Analytical Estimation

지도 교수 민 기 복

이 논문을 공학박사 학위논문으로 제출함

2016 년 06 월

서울대학교 대학원

에너지시스템공학부

Linmao Xie

Linmao Xie 의 공학박사 학위논문을 인준함

2016 년 07 월

위 원 장 :	전 석 원
부위원장 :	민 기 복
위 원 :	송 재 준
위 원 :	이 연 규
위 원 :	김 형 목

Abstract

Geomechanical Study on Hydraulic Stimulation in Enhanced Geothermal System: Field Observation Analysis and Analytical Estimation

Linmao Xie

Department of Energy Systems Engineering

The Graduate School

Seoul National University

Enhanced Geothermal System (EGS) technology which intends to extract deep geothermal resource from the hot crystalline basement has been a frontier for the geothermal industry for the past 30 years. Massive hydraulic stimulation is one key to improve the reservoir permeability to allow fluid circulation at rates of commercial interest during EGS development. The EGS stimulation targets to inject fluid into the long open hole section with an interval of tens to hundreds of meters in the crystalline formation. Numerous field stimulation tests have been performed and increasing efforts have been made to study the mechanisms of stimulation and interpret the test observation. However there is much knowledge gap for understanding the essential details of

the stimulation process, e.g., shearing initiation and propagation, and fracturing initiation and propagation, which is vital for interpreting the evolution of reservoir permeability and managing induced seismicity.

Key characteristic test and performance parameters of field hydraulic stimulation tests on seven EGS or HDR (Hot Dry Rock) projects were reviewed in geomechanical perspectives, followed by comparative correlation analysis on reservoir conditions, test parameters and test observations. The analysis indicates the differential stress condition plays a controlling role in hydroshearing and induced seismicity.

Generic geomechanical models were developed to estimate shearing initiation location, the required pressure and the overall shearing growth direction corresponding to hydroshearing mechanism. General studies on the effects of the stress condition on the shearing initiation and propagation captured some basic features related to the observed induced seismicity. Upward growth of shearing prevails for most stress conditions and a dense fluid favors downward shearing. The developed method is potentially applicable to provide primary assessment of shearing initiation and propagation during hydraulic stimulation in a fractured EGS reservoir.

For hydrofracturing mechanism, the proposed generic model can estimate the fracture initiation in open hole section and the overall fracturing propagation during stimulation. General studies on the effects

of in situ stress and open hole trajectory on hydraulic fracturing indicate that the fracture initiation at casing shoe section and the upward growth of vertical fracture prevails for common stress condition at deep EGS reservoir. An open hole with building up trajectory may shift fracture initiation location from cashing shoe to well toe by a lower breakdown pressure.

Keywords: Enhanced Geothermal System (EGS), hydraulic stimulation, induced seismicity, insitu stress, hydroshearing, hydrofracturing.

Student Number: 2011-31306

Publications during candidature

Publications related to the thesis

1. International Journal

Xie, L., Min, K. B., Song, Y., 2015. Observations of hydraulic stimulations in seven enhanced geothermal system projects. Renewable Energy, 79, 56-65.

Xie, L., Min, K. B., 2016. Initiation and propagation of fracture shearing during hydraulic stimulation in enhanced geothermal system. Geothermics, 59, 107-120.

Xie, L., Min, K. B., 2016. Hydraulic fracture initiation and propagation in EGS hydraulic stimulation (to be submitted).

2. National Journal

Min, K. B., Xie, L., Kim, H., Lee, J., 2014. EGS field case studies - UK Rosemanowes and Australian Cooper Basin projects. Journal of Korean Society for Rock Mechanics – tunnel and Underground Space, 24(1), 21-31.

3. International Conference

Xie, L., Min, K. B., 2013. Geo-mechanical issues associated with hydraulic stimulation in Enhanced Geothermal System. Asia-Pacific Forum on Renewable Energy, Jeju, Korea, paper No.: O-GE-003, P. 92.

Xie, L., Min, K. B., 2014. First Order Estimation of Hydraulic Fracture Initiation in Deviated Borehole for Enhanced Geothermal System. ISRM International Symposium - 8th Asian Rock Mechanics Symposium (ARMS8), Sapporo, Japan, P.2635-2643.

Xie, L., Min, K. B., Song, Y., Park, J., 2015. Role of Differential Stress in Induced Seismicity in Enhanced Geothermal System: a Review of Previous Hydraulic Stimulation Tests. World Geothermal Congress 2015 (WGC2015), Melbourne, Australia, paper No.: 31035.

Publications not included in the thesis

Xie, L., Min, K. B., Shen, B., 2016. Simulating interactions of hydraulic fractures and pre-existing fractures using Displacement Discontinuity Method. Journal of Natural Gas Science and Engineering, in press. doi:10.1016/j.jngse.2016.03.050.

Table of contents

List of tables

Chapter 2

Chapter 3

Chapter 4

List of figures

Chapter 1

Chapter 2

Chapter 3

Chapter 4

Nomenclature

E	Elastic modulus of formation material
g	Acceleration of gravity
h	Depth below surface
h_c, h_t	Depth of casing shoe and well toe, respectively
h_{cr}	Breakout location in open hole section
k	Ratio of maximum principle stress to minimum one
k_1, k_2, k_3	Ratios of S_1, S_2, and S_3 to vertical principle stress, respectively
k_c	Coefficient associated with frictional angle used for P_{cm} computation
k_{cf}	Critical pressure for shearing equal to σ_3 in normalized form
k_{cm}	Minimum critical pressure used to slide the most optimally oriented joint in normalized form
k_{co}	Cut-off critical pressure for defining the range of orientations with high tendency for shearing in normalized form

k_{H} , k_{h}	Ratios of maximum and minimum horizontal stresses to vertical one, respectively
k_{pp} , k_{pc}	Injection pressure and critical pressure for shearing in normalized form
l	Direction cosine between joint normal and maximum principle stress
m	Direction cosine between joint normal and intermediate principle stress
n	Direction cosine between joint normal and minimum principle stress
P_{b}	Breakout pressure at bottom hole
P_{bwh}	Breakout pressure at wellhead
P_{c}	Critical pressure required for shearing
P_{c}'	Gradient of critical pressure for shearing
P_{cf}	Critical pressure for shearing equal to σ_3
P_{cm}	Minimum critical pressure used to slide the most optimally oriented joint
P_{f}	Fracture initiation pressure for given depth at bottom hole
P_{f}'	Fracture pressure gradient
P_{fwh}	Fracture initiation pressure for given depth at wellhead

P_{o}	In situ pore pressure
P_{p}	Injection pressure
P_{p}'	Injection pressure gradient
P_{st}	Hydrostatic fluid column pressure
P_{wh}	Wellhead pressure
S_1, S_2, S_3	Maximum, intermediate and minimum principal stress, respectively
S_1^{e}, S_2^{e}, S_3^{e}	Effective maximum, intermediate and minimum principle stresses, respectively
$S_x, S_y, S_z, S_{xy}, S_{yz}, S_{zx}$	Components of in situ stress tensor in Cartesian coordinate
S_{v}, S_{H}, S_{h}	Vertical, maximum horizontal and minimum horizontal principle stresses, respectively
S_{h}'	Minimum in situ horizontal stress gradient
α	Thermal expansion coefficient
β	Wellbore azimuth angle from S_{h} measured counterclockwise
ε	Angle between wellbore axis and hydraulic fracture trace line
η	Angle of S_{h} direction from the East measured counterclockwise
θ	Wellbore circumferential angle

θ_{cr}	Angular position of fracture initiation for given depth
λ_{c}	Coefficient of critical pressure gradient for shearing
λ_{co}	Coefficient used to estimate the cut-off critical pressure P_{co}
λ_{f}	Coefficient of fracture pressure gradient
λ_{σ}, λ_{τ}	Coefficients of normal and shear stress gradients, respectively
μ	Joint frictional coefficient
ν	Poisson's ratio of formation material
ρ_{r}	Overburden rock density
ρ_{w}	Density of injection fluid
σ	Resolved normal stress on the joint plane
σ'	Gradient of normal stress
σ_1, σ_2, σ_3	Maximum, intermediate and minimum principle stresses on wellbore wall, respectively
$\sigma_r, \sigma_\theta, \sigma_z, \sigma_{r\theta}, \sigma_{rz}, \sigma_{z\theta}$	Components of stress tensor on wellbore wall in cylinder coordinate
σ_{T}	Thermal stress on wellbore wall
τ	Resolved shear stress on the joint plane
τ'	Gradient of shear stress

τ_f	Shear strength of single rock joint
ϕ	Joint frictional angle
ψ	Wellbore inclination angle from vertical

Chapter 1. Introduction

1.1 Enhanced Geothermal System

The heat beneath the earth is a huge source of renewable and clean energy. The geothermal energy is considered to be inexhaustible due to the fact that the heat continuously flowing from the Earth's interior is estimated to be equivalent to 42 million MW of power, and is expected to remain so for billions of years to come (Kagel et al., 2005). Geothermal energy can be used directly in the form of heat such as the ground source heat pumps (GSHP) or converted to electricity. Ever since the first geothermal electricity production in Larderello (Italy), the human beings have the experience of harnessing the earth heat for electricity generation for more than one century. It is increasingly accepted that geothermal electricity generation has become an attractive option to serve as a CO2-emission-free, base-road renewable energy source (DiPippo, 2012). The total installed capacity from worldwide geothermal power plant increased to 12.7 GW until 2015 and an increase rate of 17% has been achieved in the five year term 2010-2015 (Bertani, 2016).

Only a small fraction of geothermal energy is currently converted to electricity and geothermal power accounts for only 0.3% of the global electricity supply due to the limited geologically viable locations where

the natural heat, water and rock permeability are sufficient for economical heat resource extraction (Van der Hoeven, 2013). It is known that most hydrothermal resources are within the volcanic regions near tectonic plate boundaries that form the Ring of Fire (Sanyal, 2010) and those used for geothermal power generation are just pinpoints on a map of global scale (Jung, 2013). The huge amounts of geothermal resources within the drillable depth are stored in the formations that are deficient in water or permeability. For example in the US, only 2% of the total thermal energy stored between 3 km to 10 km reservoir is sufficient to provide the US primary energy for 2,800 years (MIT, 2006).

To reduce the dependency of heat extraction on reservoir natural permeability, the scientists and engineers are seeking alternative solutions to create technically and economically viable reservoirs. This alternative is referred to as Enhanced Geothermal System (EGS). The report by MIT (2006) defined EGS as the extraction of economical amount of heat from low permeability and/or porosity geothermal resources that are initially not in commercial interests and require engineering enhancement or stimulation. Actually, there is no universal definition of EGS and it should date back to the early 1970s when Los Alamos National Laboratory initiated the Hot Dry Rock (HDR) project at Fenton Hill. In general, the EGS concept involves drilling boreholes to depths where the temperature condition is sufficient for commercial interest and then artificially enhancing or creating the permeability of the reservoir to allow the heat to be extracted efficiently by circulating

fluid/steam through injection and production wells. Broad definition of EGS may include the engineering to bring uneconomic hydrothermal systems into production by improving their underground conditions by stimulation (Majer et al., 2007). The successful implementation of EGS system can significantly enlarge the retrievable amount of geothermal resources. These cost-effective ways to mine heat from deep crystalline basement make geothermal energy a world wide energy contributor regardless of geological limitations.

Figure 1.1 shows a typical doublet EGS system comprised of ground and underground facilities. The potential site for EGS development can be identified through surface, geologic and geophysical characterization of associated geomechanical properties and temperature condition. Deep wells are drilled into crystalline basement rocks until a sufficient temperature condition is achieved (usually 3-5 km). In addition to deep drilling, another key operation for creating EGS reservoir is hydraulic stimulation which involves injecting massive volume of fluid into the target formation to reduce the flow resistivity. The basic goal is to create fluid pathways to allow fluid pass through the hot rock at rates of commercial interest at a low pressure level (Genter et al., 2010). During hydraulic stimulation, a reliable seismic monitoring system is required to monitor the induced seismicity, which reflects the evolution of the stimulated reservoir in real time. Once the surface facilities are installed, the circulation loop of fluid, injected from injection well, flowing through the enhanced reservoir and pumped to the surface by production

wells, brings the crust heat to driver turbines. A multi-well system may be adopted to optimize heat extraction efficiency.

First attempts to access this deep geothermal resource date back to the early 1970s when the Fenton Hill project was put forward in the USA. This sparks numerous research and commercial projects in various countries over the past four decades such as Rosemanowe in UK, Soultz in France, Ogachi in Janpan, Basel in Switzerland, Cooper Basin in Australia and Pohang in Korea.

The Pohang EGS project in Korea was launched in 2010, which is the first attempt to realize geothermal power generation in Korea (Song et al., 2015). The project targets to reach a MW scale power generation by the heat in granite basement using a doublet system. First deep well, PX-1, was completed at 4127 m depth in 2013 and the second one, PX-2 was drilled to 4348 m in 2015. Subsequently, first hydraulic stimulation was carried out in February, 2016 at PX-2 deep well.

General review of the EGS development form its origins to the current state of the art and the projects world wide is available in Breede et al. (2013) and Olasolo et al. (2016). They highlight the EGS is sill on a learning curve and much more efforts are required to make it technologically and commercially viable.

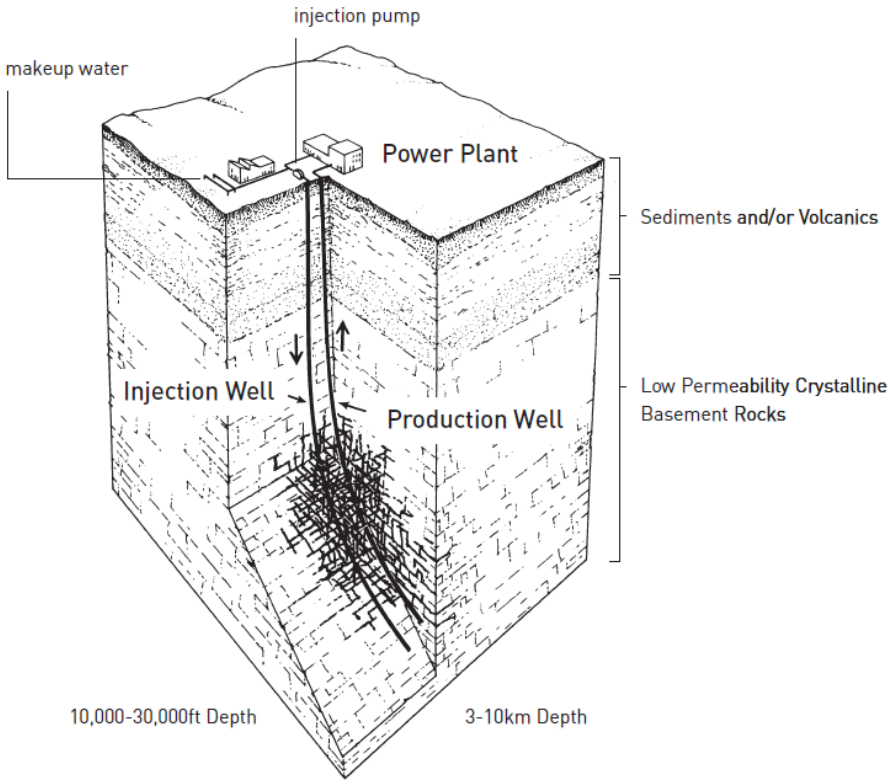

Figure 1.1 A diagram of a typical doublet enhanced geothermal system (MIT, 2006).

1.2 EGS hydraulic stimulation

How to achieve the required flow rate through the reservoir by a sufficient low parasitic pump power is one key to make a breakthrough of EGS play into the energy market (Regenauer-Lieb et al., 2015). This requires enhancing the hydraulic performance of the reservoir, whose natural permeability is very low due to low porosity of rock matrix and poor connectivity of natural fracture system. For this issue, the key

technique is operating hydraulic stimulation to increase the permeability of heat reservoir and make artificial hydraulic linkage between two or more boreholes to allow fluid circulation through the hot rock at rates of commercial interest (Genter et al, 2010). Hydraulic stimulation has become an essential operation for EGS or HDR projects. The stimulation is basically complicated geo-mechanical process. Improving the understanding of reservoir geo-mechanics has become critical towards the hydraulic stimulation research and site operation optimization. It is desired to permit the target circulation through hot rock mass without inducing excessive induced seismicity.

As demonstrated in Figure 1.2, basically, two conceptual models of hydraulic stimulation were designed and tested over the previous EGS development experience: 1) hydrofracturing, creating new fractures or reopening the pre-existing fractures which has been widely used in hydrocarbon production and 2) hydroshearing, that is the slip of pre-existing fractures associated with shear dilation.

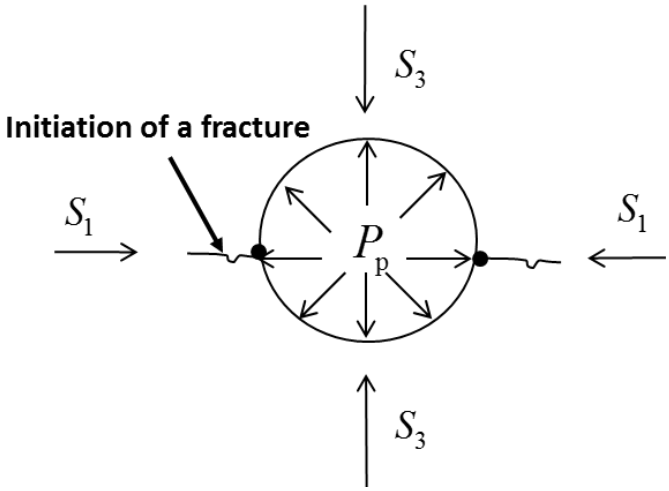

(a) Hydrofracturing

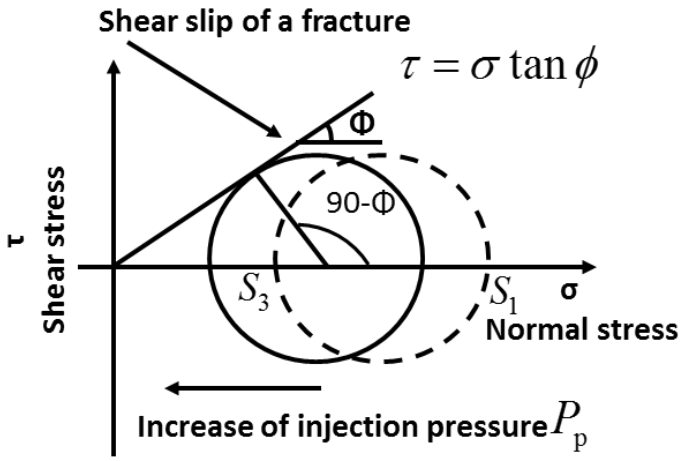

(b)Hydroshearing

Figure 1.2 Basic mechanisms of hydraulic stimulation: (a) hydrofracturing (creating a new fracture) and (b) hydroshearing (shear slip of an existing fracture).

When the original concept of HDR was proposed by the research team at Los Alamos National Laboratory in the early 1970s, the conventional hydraulic fracturing idea for oil and gas engineering was applied to HDR directly (Duchane and Brown, 2002). The classical hydraulic fracturing model suggests the opening mode fracture propagates perpendicular to the least compressive principal stress. And thus the Fenton Hill Project was designed to drill two wells parallel to the azimuth of the lease compressive principal stress and they were expected to be connected by a set of hydraulic fractures created by hydraulic fracturing in the isolated sections. Obviously, this concept does not consider the effects of pre-existing natural fractures and then the EGS concept was promoted to accounting the roles of these natural discontinuities.

Realizing the existence and significant effects of the pre-existing fractures, the mechanism of stimulation in EGS reservoir was adjusted to the shear slip on pre-existing fractures (Evans, 2005; Murphy and Fehler, 1986; Pine and Batchelor, 1984; Wyborn, 2010). Field monitoring of heavy induced seismicity when the injection pressure was lower than the minimum principal stress supports that the shearing of fractures and faults is the primary mechanism of permeability enhancement. The existence of natural fractures in the deep formation has been confirmed by various sources. Drilling parameters, borehole image survey, caliper logging, temperature and flow logging provide the solid proof of pre-existing fracture occurrence. The widely accepted

cubic relationship between fracture trasmissivity and aperture suggests that the shear induced fracture dilation significantly contributes to the improvement of the transmissivity. The compilation of dilation angles measured by direct shear tests indicted a range of 0° to 20° depending on rock type and the applied normal loading (Lee, 2014).

In reality, considering the complexity of underground discontinuities and stimulation operation, increasing attention has been paid to the mixed mechanism of fracturing and shearing, which emphasized that both newly forming and pre-existing fractures are important for permeability enhancement. (McClure and Horne, 2014). The mixed mechanism provides a plausible explanation to the observed continuous flow over the extended depth interval for GPK4 stimulation in Soultz EGS project where the maximum pressure applied approached the minimum principal stress (Tischner et al., 2007).

The orientation and distribution of natural fractures and the state of field stress play controlling roles in the determination of reservoir responses subjected to hydraulic stimulation. Principally, both the stress measurement methods and discontinuity structure logging techniques developed in oil and gas field can be applied at EGS project sites (Valley, 2007). However, more uncertainties must be faced considering these two situations associated with EGS development: 1) the reliability of measurement devices can be reduced when subjected to a high temperature and pressure condition existing at deep EGS reservoir and

2) the available data is limited due to the high cost of measurement and a small number of deep wells.

The conversion of HDR fracturing concept to EGS shearing concept results in changes in terms of deep well and hydraulic stimulation design (Jung, 2013). One consequence is that no high-temperature open hole packers are required for technical simplicity and very long open hole sections containing numerous natural fractures are stimulated by injecting massive volume of water. This long open hole design is beneficial to present continuous communication throughout the production interval and reduce the cost by simplifying the well completion (Polsky et al., 2008).

Overall, the behaviors of EGS hydraulic stimulation are far more complex than those shown in Figure 1.2 because of the above presented facts related to 1) the difficulty and uncertainty of determining in-situ stress condition and characterizing pre-existing fracture system and reservoir properties, 2) the limited understanding of stimulation mechanisms and 3) the adoption of long open hole injection. They are often not well understood even after the site stimulation operations have been performed, letting alone the prediction of stimulation performance before operation. Extensive improvement of knowledge on hydraulic stimulation, both stimulation performance and mechanism, is critically important for meeting the requirements raised by the challenging issues with respect to EGS project development.

1.3 Scope of the dissertation

Besides to the general description of EGS and hydraulic stimulation in this chapter, three main chapters (2, 3 and 4) are included. They are organized in a form similar as the structure of journal publication followed by Chapter 5 for conclusion and discussion.

Chapter 2 provides an overview of the hydraulic stimulation tests carried out on seven EGS or HDR projects in a geomechanical perspective (Xie et al., 2015). Some key characterization and performance parameters of field hydraulic stimulation tests were proposed, and they were collected through extensive survey of stimulation results. Further efforts are made for the correlation analysis among performance parameters, test parameters and reservoir fundamental conditions.

Chapter 3 deals with the issue of shearing initiation and propagation during EGS hydraulic stimulation corresponding to the hydroshearing concept (Xie and Min, 2016). The generic models are developed to estimate the location of the shearing onset, the required critical pressure and the overall shearing growth direction. The proposed models are applied to general studies on the effects of the stress condition on shearing initiation and propagation and to the selected field stimulation tests in major EGS projects.

Chapter 4 studies the fracturing initiation and propagation during EGS stimulation corresponding to the hydrofracturing concept (Xie and Min, to be submitted). The generic models for estimating the fracture initiation in open hole section and the overall fracturing propagation are presented. There are general studies on the effects of the stress condition and open hole trajectory on hydraulic fracturing, followed by the field case study of fracturing initiation for Jolokia-1 hydraulic stimulation at Cooper Basin site in Australia.

Chapter 5 presents major conclusions and discussions integrating the recommendations for further study.

Chapter 2. Observations of hydraulic stimulations in EGS projects[1]

2.1 Observations during hydraulic stimulation tests

For hydraulic stimulation operation in EGS projects, both the hydraulic and induced seismicity (IS) data are monitored and recorded throughout the treatment, and the monitoring process even continues for a long time after stimulation. These monitoring works play an important role in stimulation process management and the associated reservoir behavior interpretation (e.g., the evolution of stimulated volume).

Real time recordings of injection rate and fluid pressure are fundamental for evaluating the hydraulic performance of the system as well as the deep reservoir hydraulic properties. Both wellhead pressure (WHP) and bottom hole pressure (BHP) are of interest for engineers and researchers, but the complete reliable high quality BHP measurement is seldom available due to high cost and poor performance of measurement devices subject to high temperature and pressure conditions. Thus many stimulation tests could provide only WHP data, and the BHP can usually be estimated as the summation of measured WHP and the corresponding hydrostatic fluid column pressure as Eq. (2.1).

[1] Major content of this chapter is published in Xie et al., (2015).

$$BHP = WHP + \rho_{\mathrm{w}} gh \tag{2.1}$$

where ρ_{w} is the density of injection fluid and h is the depth for pressure computation.

Monitoring of induced seismicity has become one of the best tools for understanding reservoir development and estimating the stimulation effects (Ghassemi, 2012). Locating induced seismic events provides direct proof of stimulated volume or the permeability-enhanced region, which is one of the pre-set stimulation target parameters. Additionally, extensive investigations of these events can be very useful in understanding their focal mechanisms, field stress state and its variation, nature of existing fractures, and the fluid flow pathways. In order to detect these seismic events induced by fluid injection, the seismic monitoring network, including surface and down-hole stations, must be constructed and validated prior to the stimulation operations. Nowadays, the advanced seismic acquisition and processing system can record and map the events in real time.

Figure 2.1 is a clear demonstration to show the complete set observations during a field stimulation test at Basel project, Switzerland in 2006 (Häring et al., 2008), where there were 6 days of continuous injection and several more days of post stimulation. The observation recorded the histories of injection rate, wellhead pressure, triggered seismic event rate in hour and earthquake event magnitudes determined by Swiss Seismological Survey (SED). The seismic event locations were

also mapped to account for the stimulated region and a plate-like structure of seismic cloud is obvious from top view (Figure 2.2).

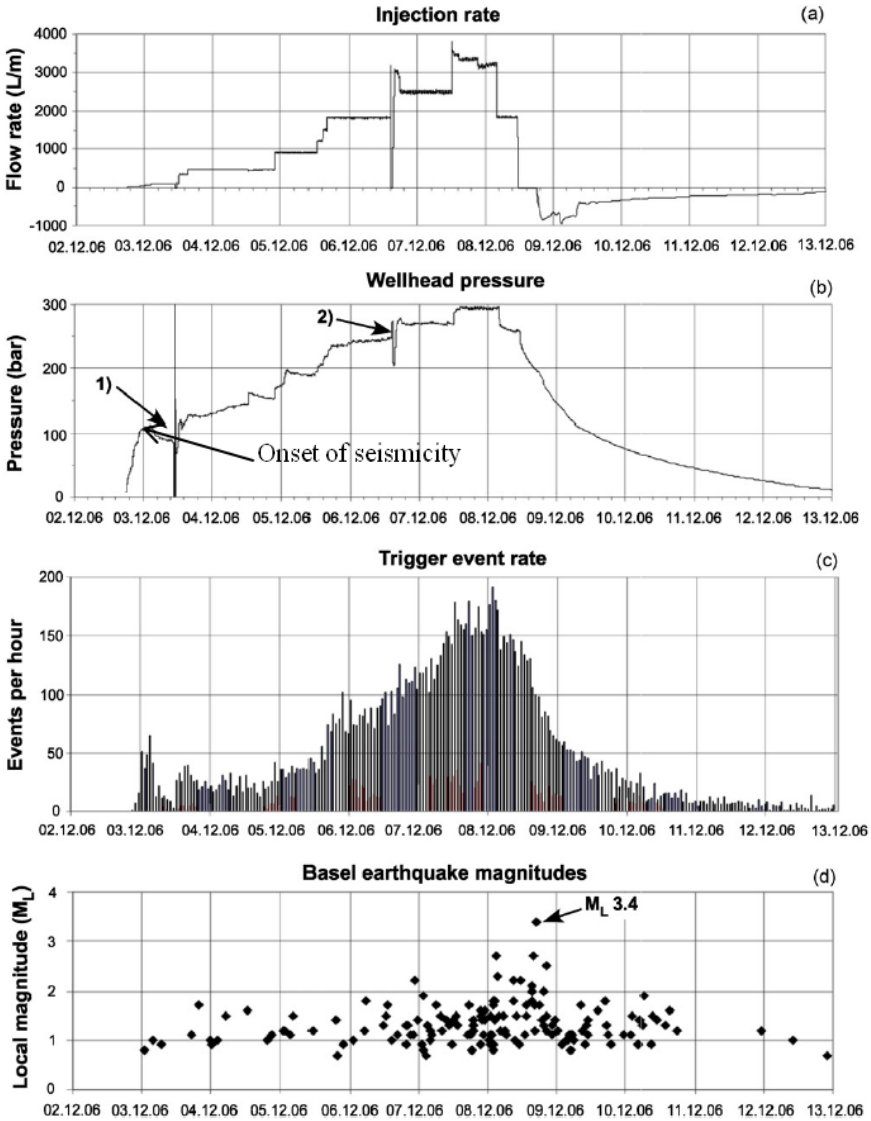

Figure 2.1 Stimulation observations of test on well Basel 1, Switzerland . History of (a) injection rate, (b) wellhead pressure where two pressure abnormalities are detected and pressure at onset of seismicity is defined, (c) seismic event rate and (d) event magnitude (Häring et al., 2008)

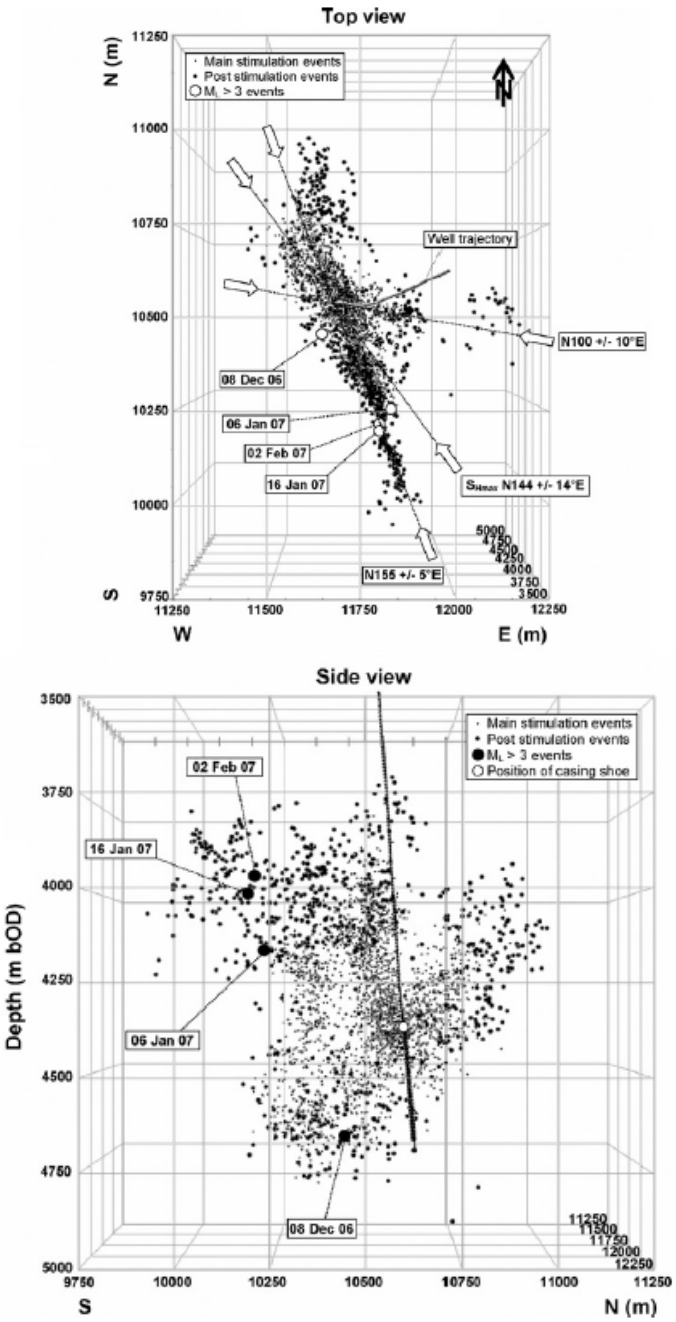

Figure 2.2 Stimulation observations of test on well Basel 1, Switzerland : mapped event locations during and post injection, the occurring times of large magnitude events (M_L > 2) and field stress orientation (Häring et al., 2008).

An extensive survey of the observations and results of stimulation tests of major EGS projects was carried out to study the general correlation among test observations, test parameters and reservoir conditions. It should be highlighted that these projects are sparsely distributed on earth and the reservoir conditions can be quite variable. In this chapter, seven EGS or HDR projects were determined as test data sources. Basically, they are selected based on three criteria: 1) the reservoir host rock is crystalline; 2) a massive volume of fluid was injected into the well open section with interval of tens to hundreds meters from casing shoe to well toe; and 3) relatively sufficient access to the field test data is available.

Moreover, the key test and performance parameters, thought to be able to characterize the stimulation test conditions and to evaluate stimulation effects in terms of hydraulic and seismic responses, were defined as follows and collected as Table 2.1.

Table 2.1 Hydraulic stimulation test and performance parameters of major EGS (HDR) projects

	Date Sti. year	Sti. Int. km	V_{in} m^3	Max. Q_{in} L/sec	Max. WHP MPa	A_{sei} km^2	T_{in} hour	Sei. No.	$D_{sei.}$ km	Sei.WHP MPa	M_L	Ref.
Soutlz GPK1	1993	2.85-3.4	25300	36	9	1			3.0			[1]
Soutlz GPK2	1995	3.21-3.87	28000	56	12	0.8	168					[1-2]
Soutlz GPK2	2000	4.4-5.09	23400	50	13.5	3	144	13986	4.8	4	2.6	[3]
Soutlz GPK3	2003	4.56-5	34000	50	15.5		264	21600	4.8	2.6	2.9	[4-5]
Soutlz GPK4	2004	4.49-4.98	9134	30	17		84	5700	4.9	8	2	[5-9]
Soutlz GPK4	2005	4.49-4.98	13000	45	18.3		96	3000	4.9	13	2.6	[5-9]
Ogachi OGC1	1991	0.99-1.0[a]	10140	11	19	0.5	264	1553		17	2	[10-11]
Hijiori HDR1	1992	2.15-2.2	2115	67	26	0.25	15	106	2.2	19	0.3	[10, 12]
Basel1	2006	4.63-5	11570	55	29.6	0.9	144	11200	4.7	11	3.4	[13]
Roseman. RH12	1982	1.7-2.06	18500	90	14.2	0.6	120		2.5	4.5		[1, 14-15]
Roseman. RH15	1986	??-2.6	5700	200	15	0.04						[16]
Cooper B. Hab.1	2003	4.14-4.42	16350	24	65	2.5	168	5029	4.3	47	3.7	[10]
Cooper B. Hab.1	2005	4.14-4.43	22500	32	62	4	312	16454	4.3	56	3	[10, 17]

Cooper B. Hab.2	2005	3.92-4.36	7000	7	63	0.4		1283	4.3			[16-18]
Cooper B. Hab.3	2008	4.05-4.2	2200	55	62	0.2		452	4.2			[16-18]
Cooper B. Hab.4	2012	4.05-4.2	34200	48	49	2	336	24000	4.1		3	[19]
Cooper B. Jol.1	2010	4.32-4.91		70	69		312	200				[20]
Fenton H. EE-2[b]	1983	3.45-3.47	21000	108	38	0.72	63	1800	3.5		1.0[c]	[21-23]

Sti. Int.: well open section interval, Dia.: well open section diameter, V_{in}: injected volume, Max. Q_{in}: maximum injection rate, Max. WHP: maximum well head pressure, A_{sei}: area of 'seismic cloud', T_{in}: injection duration, Sei. No.: seismic event number, D_{sei}: mean depth of seismic cloud, Sei. WHP: well head pressure at onset of seismicity, M_L.: maximum event magnitude.

a: The injection was carried out on a relatively short open hole section where a number of natural fractures exist with an average spacing of 8 cm (Kaieda et al., 2010). (b: It is the massive hydraulic fracturing test (MHF): Expt. 2032 in 1983. c: It is the magnitude of the largest induced seismic event ever observed throughout the Fenton Hill project duration (Fehler, 1989).

[1]: (Jung, 2013); [2]: (Baumgartner et al., 1996); [3]: (Weidler et al., 2002); [4]: (Baria et al., 2005); [5]: (Tischner et al., 2007); [6]: (Baria et al., 2006); [7]: (Charléty et al., 2007); [8]: (Schindler et al., 2010); [9]: (Valley and Evans, 2007); [10]: (Kaieda et al., 2010); [11]: (Shin et al., 2000); [12]: (Oikawa and Yamaguchi, 2000); [13]: (Häring et al., 2008); [14]: (Pine and Batchelor, 1984): [15]: (Batchelor et al., 1983); [16]: (Parker, 1999); [17]: (Baisch et al., 2009); [18]: (D Chen and Wyborn, 2009); [19]: (Baisch and McMahon, 2014); [20]: (Jeffrey et al., 2012); [21]: (Dreesen and Nicholson, 1985); [22]: (Brown et al., 2012); [23]: (Fehler, 1989).

Stimulation interval. It is the uncased open section where the potential fluid flow paths intersect the well and the fluid pressure diffuses. A longer open section intuitively indicates more chances to have natural fractures available to accept injected fluid.

Injected fluid volume. Generally, a massive volume of fluid (up to tens of thousands of cubic meters) is injected accounting for the long stimulation interval and a large stimulated reservoir volume which is expected for economic issue.

Maximum injection rate and maximum injection pressure. Stimulation tests can be performed with a stepwise increase of flow rate and the corresponding pressure responses are complicated. The maximum injection pressure and the maximum injection rate are two characterization parameters that can indicate the hydraulic performance of reservoir. In addition, they are often thought to be closely related to the induced seismicity (IS) especially the large magnitude events (LME) and are regularly listed as main controlling parameters with respect to the seismic risk management.

Seismic cloud area. Strictly speaking, the seismic cloud volume should be the measure of the size of a stimulated region considering that the triggered events must be distributed in the space. The seismic cloud area is, however, used in accordance with the earlier studies to account for the often observed planar feature of seismic clouds and the strong influence of the location error on their thickness (Jung, 2013).

Fluid pressure at onset of seismicity. The onset of seismicity can be treated as a strong indicator of the beginning of shear slip and thus the fluid pressure at onset of seismicity would be meaningful to understand the stress state and fracture nature. It should be noted that the observation of onset of seismicity heavily depends on many factors such as seismic monitoring network configuration, seismic sensor resolution and the pre-defined threshold of recording events. Because of very limited accessible data, it is almost impossible to define a universal criterion of onset of seismicity. Here either the stated fluid pressure directly from the specific reference was adopted or the one from pressure history data was picked up when the seismic event was firstly recorded as demonstrated in Figure 2.1b. In this way, actions were taken to simply stick to the determination of onset of seismicity the same as the references.

Mean depth of induced seismic cloud. The massive volume injection into a long open section usually induces a big seismic cloud and, intuitively, the mean depth of seismic cloud can be more representative to feature the overall seismic event distribution in depth. For efficiency, the stress state at mean depth of seismic cloud is adopted when characterizing and discussing the roles of field stress condition in induced seismicity.

Maximum seismic event magnitude. The injection induced seismicity is a controversial issue and the potential of inducing LME is a challenge for project development. The investigation of LME not only

helps to study the mechanisms of IS but also contributes to the seismic risk management which could benefit the project and the site vicinity community. The site stimulation tests find that LME can occur during injection or after shut-in.

These test parameters and results summarized in Table 2.1 form the data base for the following correlation analysis and they also provide a direct reference for future stimulation designs. Due to the difficulty and cost of field data measurement or the limited access to the full set of data, some of the key parameters listed above for some stimulation tests may not be available in Table 2.1. However, conscientious efforts to draw meaningful lessons and implications are still desired. The correlation analysis, among performance parameters, test parameters and reservoir fundamental conditions, and the general discussion were addressed to provide more insight into hydraulic stimulations during EGS development.

2.2 Analysis of stimulation test observation and discussion

It should be highlighted that 1) the number of hydraulic stimulation tests in EGS or HDR projects is relatively limited, 2) within these limited samples, the reliable data was sparse and 3) the test conditions were variable except that they were involved with massive volume injection into a long bottom hole open section in crystalline host rock. In this regard, it is very difficult to draw firm conclusions. Intensive

investigations were carried out to study general correlation analysis between test parameters and observations.

2.2.1 Reservoir stress state

The state of stress in reservoir is a fundamental geomechanical parameter that plays a critical role in the reservoir response to hydraulic stimulation and one of the determinant components in permeability evolution as well as the migration of IS. In the basic conceptual models of stimulation, in situ stress is an important factor in evaluating injection pressure required for activating stimulation, e.g., Figure 1.2 which suggests the determinant role of field stress with respect to the breakdown pressure.

Figure 2.3 shows the stress state of reservoir at mean depth of seismic cloud for these projects, expressed in terms of stress regime plot to show project stress regimes and the stress magnitude plot. There is no intention to discuss the in situ stress estimation methods used and the associated differences of evaluated stress information from different methods, thus the stress information in the plots represent a general estimation for each project. The whole stress regime is represented as the upper left half of plot in Figure 2.3a where normal faulting, strike slip faulting and reverse faulting stress conditions are distinguished by three dashed auxiliary lines. These auxiliary lines correspond to special cases where two of three principal stress components equalize.

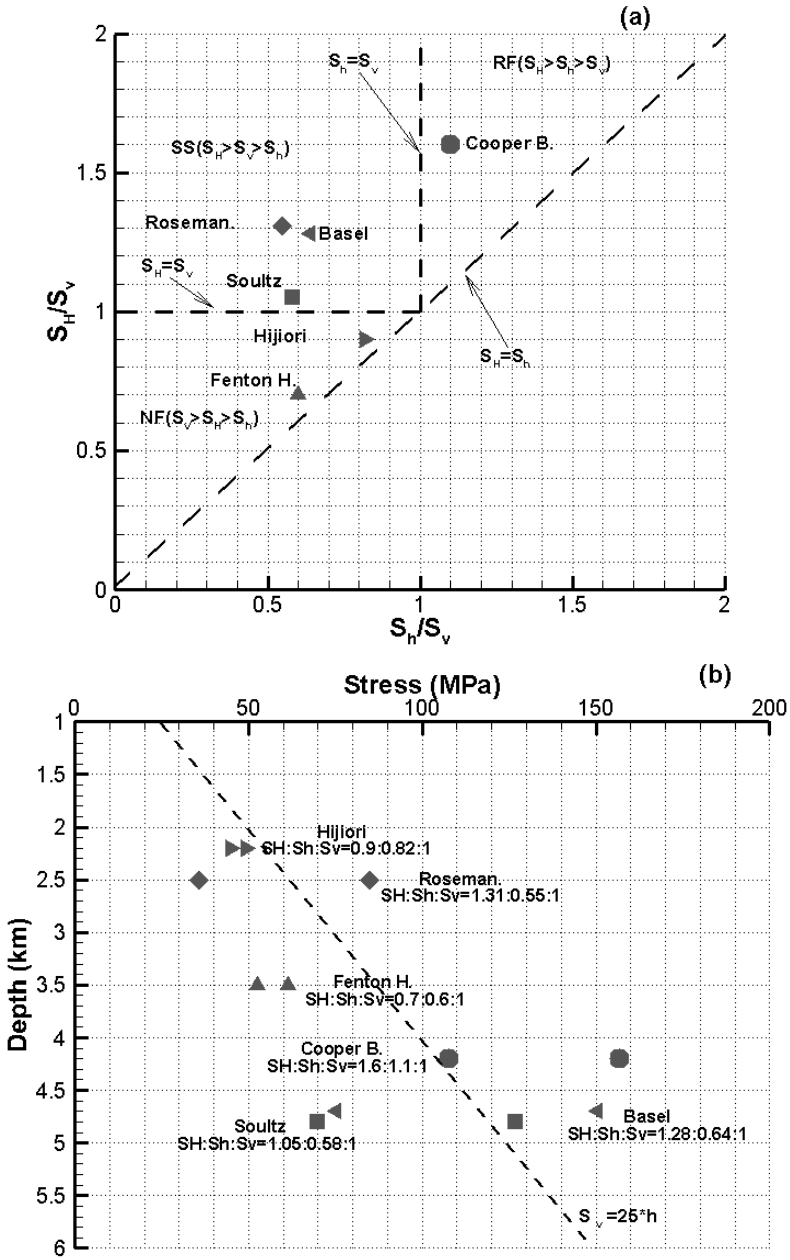

Figure 2.3 Stress state of reservoir at mean depth of seismic cloud. (a) Stress regime plot where S_H and S_h are normalized to S_v; (b) stress magnitude plot where S_H and S_h are solid symbols and S_v, represented by dashed line, is treated as the overburden load with formation mass density of 2,500kg/m^3.

In general, these projects cover all stress regimes from normal faulting to reverse faulting stress state. The projects in West European countries (Soultz, Basel and Rosemanowes) are consistently in a relatively extreme strike slip stress condition and the Cooper Basin project is in an intermediate reverse faulting stress regime. No arguments related to the optimal stress regime for the success of stimulation were found; however, it is definite that in situ stress conditions influence the development of stimulated rock regions or migration of IS. Indeed, it was reported that the seismic clouds appear as vertical or sub-vertical in strike slip stress regimes (Resemanowes, Soultz and Basel), moderately dipping in normal faulting stress regime (Fenton Hill and Hijiori) and horizontal or sub-horizontal for reverse faulting stress conditions (Cooper Basin) (Jung, 2013). In this regard, the reverse faulting stress regime, where the horizontally or sub-horizontally oriented stimulated region is very possible, is good for the arrangement of a multiple-well system in order to scale up the power generation.

Not only does the stress regime influence the stimulated region but also the stress magnitude ratios of three principal components, or the stress difference impacts the stimulation performance. The Mohr diagram is a useful tool in visualizing the effect of differential stress on the pressure required for fractures to be critically stressed for slip. Ito and Hayashi (2003) adopted the Mohr diagram to estimate the possible orientations of flow pathways by analyzing the critically stressed fractures. Figure 2.4 shows the Mohr stress circles at depth of induced

seismicity center for each project before stimulation, where the effective normal stress is treated as the total stress minus the hydrostatic water column pressure. For Cooper Basin project, a significant pressure with the magnitude of 72.7 MPa at 4100 m depth was detected in the reservoir, which represents an overpressure of around 34 MPa (Holl and Barton, 2015). Thus this overpressure should be deducted from total stress when calculating the effective normal stress.

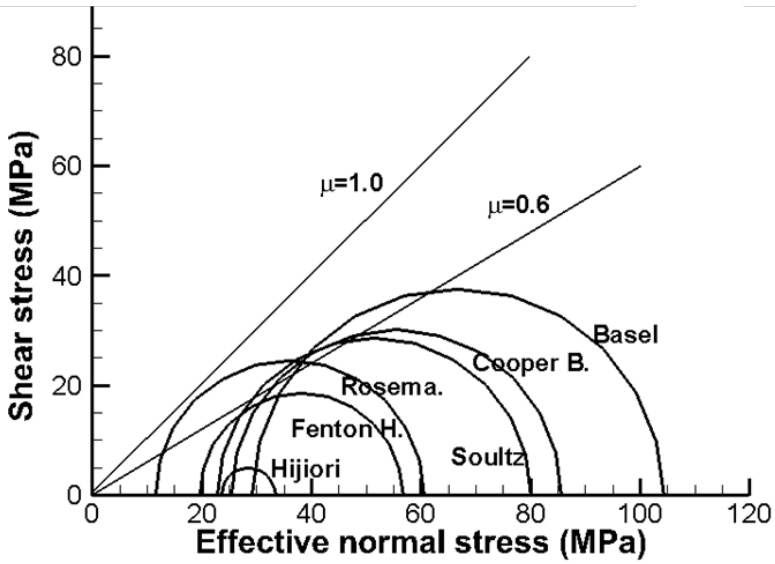

Figure 2.4 Mohr stress circles showing the stress state at mean depth of seismic cloud. Solid straight lines are the Coulomb failure envelopes when coefficient of friction is 1.0 and 0.6 without accounting for cohesion strength.

The solid straight lines are the Coulomb failure envelopes when the coefficient of friction is 1.0 and 0.6 respectively without accounting for the cohesion. The region between them covers all possibilities with frictional coefficient value ranging from 0.6 and 1.0. This range of

coefficient is considered as the common friction of rocks based on the experimental results compiled by Byerlee (1978). It is obvious that the cases with large differential stress require less additional fluid pressure to activate the shear slip of natural fractures or it is closer to critically stressed for significant differential stress conditions. Taking Hijiori project as the example, even though it is the least stressed, it requires the most effort to trigger shear slip or to move its Mohr stress circle to meet the failure envelope.

2.2.2 Hydraulic performance

The main purpose of hydraulic stimulation is to improve the reservoir hydraulic connectivity to a certain degree to satisfy the commercial production and to avoid a hydraulic short circuit by stimulating a large rock volume. The injectivity index which can be defined as the injection flow rate per unit wellhead pressure is a parameter to characterize the hydraulic impedance of reservoir. The hydraulic resistance (or wellbore impedance) is a key issue considering that the parasitic pumping power to circulate the fluid is an important factor in the overall efficiency of the system.

The hydraulic injectivity information of the previous tests was collected as Figure 2.5. The injectivity was calculated as the ratio of maximum injection flow rate and the associated wellhead pressure if a zero pressure at surface of production well is assumed or it can be

interpreted that the pressure at wellhead of production is totally released. So the pressure difference between injection and production well is basically WHP measured at injection well. Here the injectivity ever achieved in Cooper Basin is treated as the ratio of maximum injection rate over the measured WHP at injection well. It is admitted that this treatment for Cooper Basin case may lead to an underestimation of the injectivity due to the natural overpressure condition in the reservoir

The maximum injection flow rate was selected to characterize reservoir performance based on the recognition that 1) the maximum value is easier to spot in the flow rate monitoring histories and mostly reported in the literatures and project reports; 2) the dominant stimulation mechanism was interpreted as shearing of natural fractures. One can assume that the fracture permeability enhancement induced by shear slip is irreversible. This is a self-proppant behavior unlike that of tensile opening induced improvement of permeability which relies on the application of proppant. In this regard, the stimulated fractures retain their hydraulic conductivity even after stimulation, and thus the injectivity index ever made by stimulation plays a predictive role after circulation and production stage. Indeed, the study of injectivity and productivity of stimulation and post stimulation on all three deep wells (GPK2, GPK3 and GPK4) in Soultz project supported that the productivity after stimulation was essentially the same as that ever achieved during stimulation (Tischner et al., 2007).

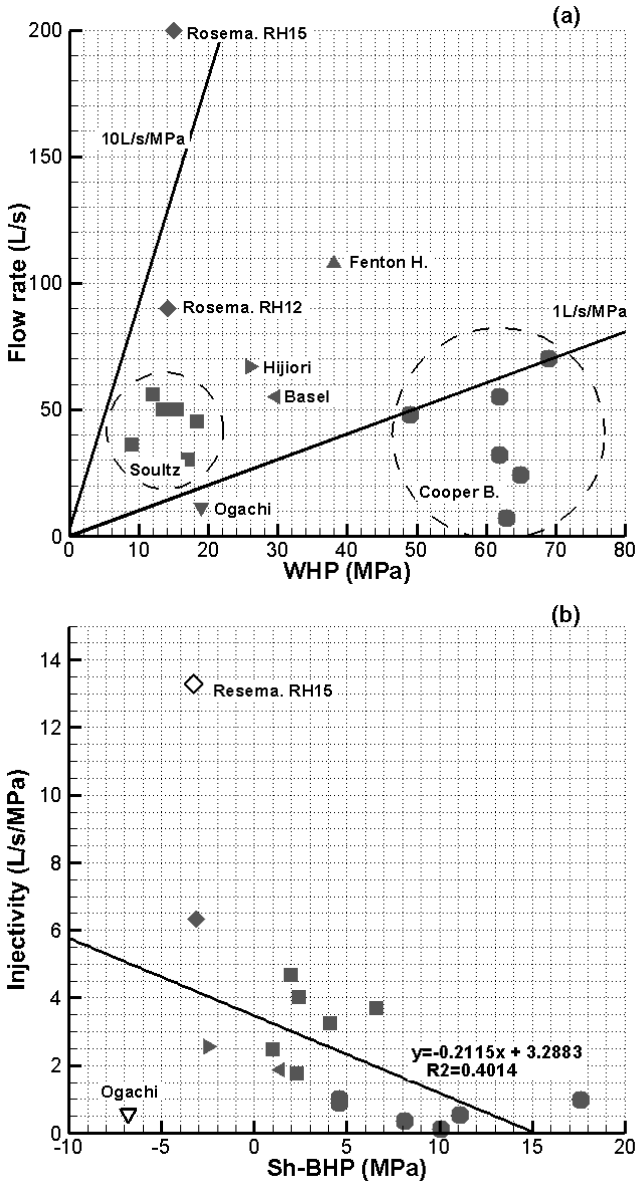

Figure 2.5 Hydraulic performance of previous stimulation tests. (a) Maximum injection rate and the associated wellhead pressure, encircled are tests within the same project, solid lines represent the injectivity of 10 L/s/MPa and 1 L/s/MPa, respectively; (b) Correlation of injectivity and the difference between minimum horizontal principal stress and bottom hole pressure at mean depth of seismic cloud, the fitting line and coefficients of determination are for solid data points.

It is observed that the injection performance is relatively convergent within the same project (data points encircled in Figure 2.5a of Soultz and Cooper Basin project). The estimated target injectivity/productivity required for economic competitiveness was set 10 l/sec/MPa (Baria et al., 2006), the solid line in Figure 2.5a, however, it is shown that most test results are much lower than the preferred level except the Resemanowes case.

In Figure 2.5b, more effort was made to the correlation analysis of injectivity (slope of data points in Figure 2.5b) and the difference between S_h and BHP (the sum of WHP and hydrostatic fluid column pressure) at depth of seismic center (S_h – BHP). This difference can be understood as an indicator of effective normal stress states of natural fractures even though their orientations are widely ranged. It is known that the decrease of fracture normal effective stress tends to lead to fracture slip followed by the increase of permeability, and thus the expected phenomenon is the increase of overall injectivity. There is a clear trend that the injectivity index increases with the decrease of (S_h – BHP) as depicted by Figure 2.5b and even approximately linear correlation can be determined based on the previous test results. When (S_h – BHP) becomes negative, there are two possible outcomes: opening of natural fractures and creating new fractures or propagating the existing ones in a tensile mode. Both help to improve the injectivity. For the Ogachi case, an extremely low injectivity was observed even for a negative difference of stress and injection pressure because the well has

an injection interval of 10 meters where the number of flow paths may be very limited (Baria et al., 1999). Combining the recognition that the injectivity index achieved by stimulation injection can be retained during the circulation of production, it is realized that a higher injection rate, which leads to a higher injection pressure, can improve hydraulic performance during stimulation and consequently afterwards.

2.2.3 Seismic Responses during Stimulations

Induced seismicity is a controversial issue associated with EGS development (Ghassemi, 2012; Majer et al., 2007). On one hand, people have realized the seismicity-based reservoir characterization method is the irreplaceable tool for evaluating the stimulation effects (stimulated volume and fracture network growth); on the other hand, the increasing concern regarding the potential of IS risk has been a big challenge for the EGS development. All of this calls for more efforts to study the mechanisms of IS and to identity the factors that control the event magnitude, and then come up with a more comprehensive but efficient seismic management scheme.

Previous studies have found that the injection volume controlled characteristics of stimulated region based on the field experience (Fehler, 1989; Jung, 2013; Phillips et al., 2002), and that the long term stimulation experience in Fenton Hill Phase II revealed that the stimulated region corresponds linearly to the increase of the volume of injected water

(Brown, 1995). Here attempts are made to study this feature more specifically on those tests subjected to the granite formation and to discuss its implications on possible alternative strategies for reducing seismic risks.

Figure 2.6a shows the general trend of the increase of seismic events with the injected volume and this feature becomes more obvious and consistent when investigating the tests on different wells in the same project (dashed line segments connecting tests on different wells in Soultz and Cooper Basin project, respectively). Within the same project, the test conditions such as reservoir stress state, and seismic monitoring systems are more likely to be similar except that the injection volumes applied were variable and this fact highlights the volume-controlled stimulation behavior. It is observed that the second stimulation of GPK4 in 2005 produced just half the seismic events induced by the first stimulation in 2004, even though the second stimulation consumed much more water. This is mainly due to the fact that no seismic events were observed during the first two-day injection of 2005 stimulation until the injection pressure of the 2005 stimulation reached the level achieved in 2004 stimulation (Charléty et al., 2007). In other words it is kind of a Kaiser effect which remembers the maximum stress exerted on the system.

In terms of the size of stimulated region, Figure 2.6b shows that the data demonstrates a clear correlation between the seismic cloud area and

injected volume. All data except the test of Rosema. RH15 well can be fitted by a power expression with the exponent of 0.77 even the reservoir conditions and test operations were variable. In this plot, the seismic cloud area was used rather than the stimulated rock volume, which accounts for the common planar nature of seismic clouds and the significant impact of location error on their thickness. Similar exponential correlation was reported by Jung (2013), however, the data of most Fenton Hill tests where the injection was applied on very small well interval using zonal isolation packers was excluded here since it was dedicated to investigate massive volume injection along long well open section. This feature of injection volume controlled stimulation is not only observed in the EGS stimulation tests, bus also found in the shale gas hydraulic treatments for enhancing production (Mayerhofer et al., 2010).

Recognizing that the seismic response under injection is controlled by injected volume, the final stimulated region or seismic cloud size is hoped to be identical while the total injection volume stays the same. Instead of injecting the fluid to the long open hole section, one alternative strategy is to stimulate the selected intervals one after another using a smaller amount of fluid volume for each stimulation, thus reduce the seismicity strength. A similar suggestion was reported as multifrac stimulation concept to reduce the seismic risk (Tischner et al., 2007). The discrete element modeling of hydraulic stimulation treatment by Zang suggested that the cyclic treatment, where the injection was interrupted

frequently, is a safer alternative to conventional step-wise increase injection scheme as it reduces the IS (Zang et al., 2013). It can be expected that the seismicity strength (both occurring rate of seismic events and magnitude) may decrease if either extending the stimulation in time (cyclic injection with interruptions) or separating the stimulation in space (multifrac injection).

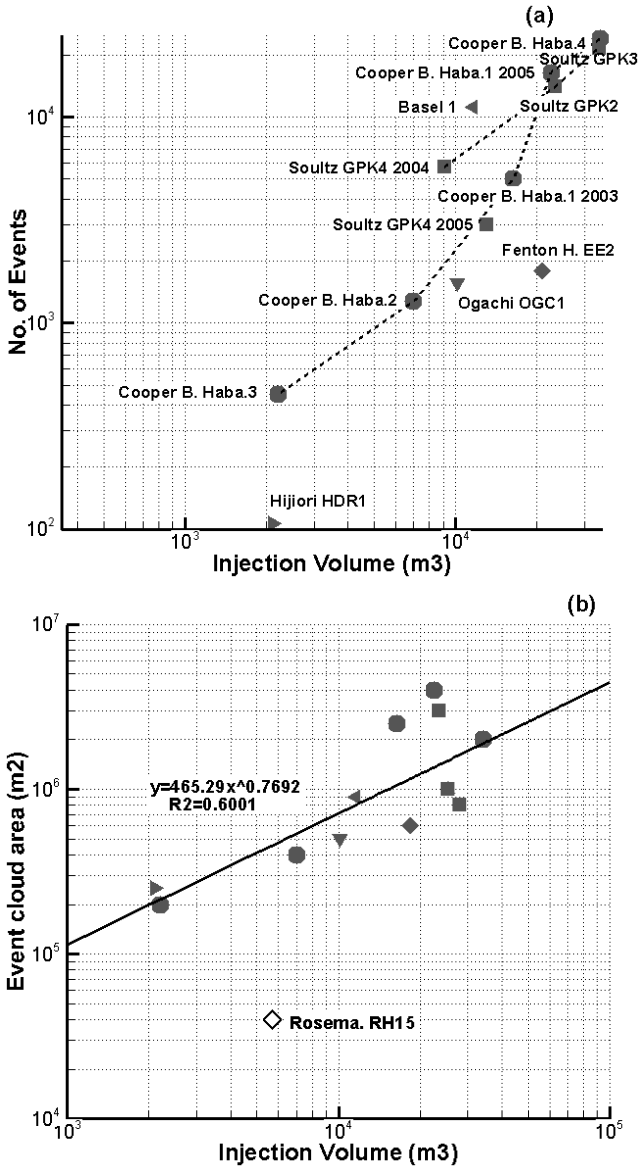

Figure 2.6 Results of seismic monitoring of previous stimulation tests, the injection volume controlled stimulation. (a) Number of seismic events vs. injection volume, dashed line segments connecting the tests on wells in the same project, stimulations operated twice for Soultz GPK2 and Cooper B. Haba.1, (b) seismic event cloud area vs. injection volume, fitting line and coefficients of determination are for solid data points.

Figure 2.7 plots the recorded maximum event magnitude during the hydraulic stimulation tests and its correlation with (a) the difference between maximum field principal stress and minimum one which is normalized against the vertical principal stress, and (b) the pressure difference of maximum WHP and WHP at onset of seismicity. A seismic event of magnitude larger than 2.0 can be felt at surface and these seismic events are referred as 'large magnitude events (LME)' (Evans et al., 2012). As analyzed in section 3.1, the significant differential stress condition is preferable for fractures to be critically stressed to slip; a similar trend is spotted in terms of the existence of LME. It is found that LMEs occurred in the projects which were subject to large differential stress conditions under strike slip or reverse faulting stress regime (Soultz, Basel and Cooper Basin). But no LME was detected for the projects with relatively even stress condition (Fenton Hill and Hijiori). Obviously, the differential stress condition is a necessary factor to raise the LME and a strong correlation between them is found (Figure 2.7a).

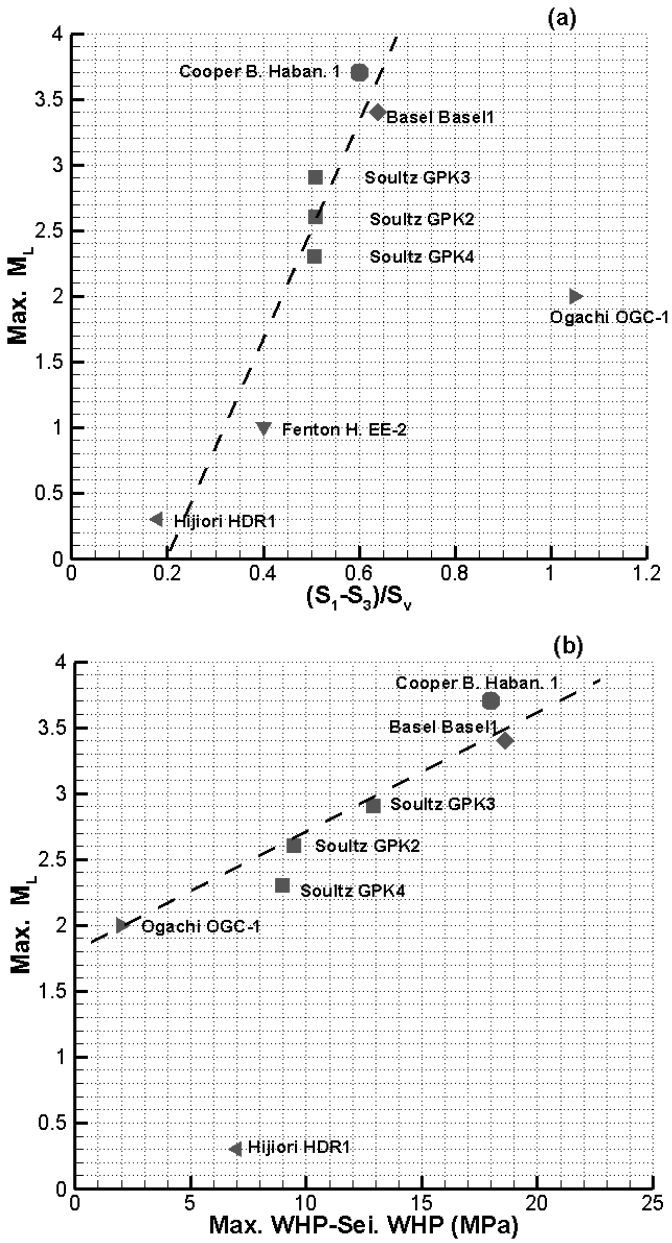

Figure 2.7 Maximum event magnitude observed and its correlation with (a) the normalized difference between maximum field principal stress and minimum one, (b) the pressure difference of maximum WHP and WHP at onset of seismicity

Many other factors can contribute to the triggering of LME. Some researchers discussed the effects of the existence of fault zones in the well vicinity on the induced big events and found a close relationship between them (Evans et al., 2012; McClure and Horne, 2012). The correlation between the maximum injection pressure and LME was also investigated and no evidence was found to support their correlation (Evans et al., 2012; Mukuhira et al., 2013). However, as found in Figure 2.7b, the amount of achieved maximum pressure over that at onset of seismicity (Max. WHP – Sei. WHP) is a very important additional condition to induce LME and a strong correlation between them is observed. This finding is very meaningful in practice. The field stress condition is natural and almost impossible to change; however, people may control the maximum pressure to decrease seismic magnitude. Bear in mind that a high injection pressure improves the injectivity index as discussed in section 3.2. Thus how to achieve expected injectivity improvement while reducing LME is certainly a challenging issue. More work is needed to study the mechanisms of inducing LME and to identify the factors controlling the event magnitude since the evaluation of the potential of LME induced by fluid injection is one of the main issues in EGS project.

2.3 Summary

In this chapter, efforts were made to review the hydraulic stimulation tests carried out on seven EGS or HDR projects where the massive

volume of fluid was injected into the well open section with interval of tens to hundreds meters in the granite formation. The key characteristic test and performance parameters were documented based on extensive investigation of stimulation test observations. Furthermore, the general correlation analysis among reservoir conditions, test parameters and test observations was attempted and more insightful discussion was presented.

The existing projects cover all stress regimes from normal faulting to reverse faulting stress regime. The stress regime influences the growth of stimulation region and the reverse faulting stress condition, where a horizontally or sub-horizontally oriented stimulated zone is very likely, is good for the layout of a multiple well system. The injection pressure for activating shear slip and the associated seismic onset is mainly field stress controlled and a significantly differential stress condition allows more possibility for the fractures to be critically stressed for slip.

The injectivity index for most tested wells is lower than the pre-set target value, 10 l/sec/MPa for economic feasibility. The dependency of injectivity on injection pressure is observed and it implies that a high injection pressure can make an improved hydraulic injectivity during stimulation and consequently after circulation.

The clear correlation between seismic cloud or stimulated region and injected volume is confirmed. Both the stimulated region and the induced seismic event are mainly injection volume controlled and the

potential strategy to reduce the seismic risks is either to extend stimulation in time or to separate stimulation in space. The differential stress condition is one of the necessary factors to raise LME and the difference of maximum injection pressure achieved over that at onset of seismicity is an important additional factor to induce LME.

Chapter 3. Initiation and propagation of fracture shearing during EGS hydraulic stimulation[2]

3.1 Introduction

The accumulated field observations revealed that deep rocks are naturally fractured and many seismic events were detected when the injection pressure was much lower than the magnitude of minimum principal stress. It was realized that the hydroshearing of fractures and faults is the primary mechanism of permeability enhancement (Jung, 2013). However, there is poor knowledge with respect to the essential details of this shearing process, which are vital for understanding the reservoir permeability evolution and managing the induced seismicity (IS). It is realized that there are several distinctive features of EGS stimulation compared with common hydraulic treatments in the hydrocarbon field: 1) an EGS well is usually completed with a long open section with interval of tens to hundreds of meters; 2) the application of an isolation packer is very limited; 3) a large fluid volume is injected into a naturally fractured reservoir with the expectation to form a stimulated region with discrete fracture networks; and 4) a deviated well design with a varying well trajectory can be adopted for favorable heat extraction. In this regard, the pressure accumulates along the whole open hole section

[2] Major content of this chapter is published in Xie and Min (2016).

during fluid injection. It is essential to estimate the location of shearing onset, the required pressure, and the shear slip growth direction because these will determine the volume of the geothermal heat exchanger and the design of the hydraulic stimulation for the desired connectivity between wells.

Numerous previous studies are related to the methodology and applications for characterizing the fracture and fault slip caused by hydraulic injections. Ito and Hayashi (2003) presented a procedure to estimate the orientations of critically stressed fractures. The slip tendency concept, which is defined as the ratio of the resolved shear stress to resolved normal stress acting on a fracture plane (Morris et al., 1996), was applied to investigate the potential for fracture slip and dilation in a deep geothermal reservoir at the Groß Schönebeck site in the Northeast German Basin (Moeck et al., 2009). Meller et al. (2012) proposed an approach for estimating the shearing probability of the fractures based on statistical analyses of the fracture distribution, orientation and clusters, and applied this to the case of the Soultz EGS project. Pine and Batchelor (1984) presented a theoretical basis to explain the downward growth of induced seismicity during hydraulic injections at the Rosemanowes EGS site, in which two dimensional explicit equations were provided by considering the shear slip on vertical joints that are aligned most critically with respect to the anisotropic strike slip faulting stress condition. This specific study on the downward migration of induced seismicity in the Rosemanowes project stimulates

the development of a generic model which can be applicable for various stress conditions and joint orientations.

In this chapter, the generic models are developed, based on the hydroshearing concept, to estimate the location of the shearing onset, the required injection pressure, and the overall shearing growth direction during EGS hydraulic stimulation. The proposed models are applied to general studies on the effects of the stress condition on shearing initiation and propagation. The models are also applied to the selected field stimulation tests in major EGS projects in order to validate its usefulness.

3.2 Shearing initiation and propagation in EGS hydraulic stimulation

Two types of shear strength criterion for rock joints have been widely used, simple linear shear strength envelope for Mohr-Coulomb model and empirical nonlinear envelope for Barton-Bandis model. In general, the linear Coulomb type has been customarily fit to the results of shear tests on rock joints under high normal stress conditions (Barton, 1973). Here for the simplicity and the great normal stress on joints due to tectonic stress at depth, the Coulomb type is adopted to define the shear strength of a single rock joint.

$$\tau_f = \mu\sigma \tag{3.1}$$

where τ_f is the shear strength, σ is the resolved normal stress on the joint and μ is the frictional coefficient, which is the tangent of the friction angle ϕ.

It should be highlighted that the cohesion of fracture at significant depth is neglected (Zoback et al., 2003) because the fracture cohesive strength contributes little compared to the compressive field stresses at a depth of several kilometers in an EGS reservoir.

From the geomechanical point of view, the elevated fluid pressure due to hydraulic injection weakens the shear strength of rock joints. The hydroshearing of a specific fracture occurs when the applied injection pressure is sufficient to reduce its shear strength to the resolved shear stress τ on the joint plane. Here the Mohr diagram and the movement of stress circles, as shown in Figure 3.1, are used to demonstrate such a physical process. A leftward shift of the stress circles corresponds to a reduction of the effective stress by fluid injection. The stress state on a specifically oriented joint is represented by a point (e.g., point A in Figure 3.1) located within the area that is bounded by the biggest stress circle with the other two circles removed. The critical pressure required for shearing such a specifically oriented joint should be able to move point A past the failure envelope (as shown in Figure 3.1b) and the exact magnitude of the critical pressure is

$$P_c = \sigma - \frac{\tau}{\mu} \tag{3.2}$$

In order to determine the critical pressure for shearing, the resolved normal and shear stresses on the joint plane have to be calculated. The normal and shear stresses acting on a given joint plane are

$$\sigma = l^2 S_1 + m^2 S_2 + n^2 S_3 \tag{3.3}$$

$$\tau = [(\mathrm{S}_1 - S_2)^2 l^2 m^2 + (\mathrm{S}_2 - S_3)^2 m^2 n^2 + (\mathrm{S}_3 - S_1)^2 l^2 n^2]^{1/2} \tag{3.4}$$

where l , m and n are the direction cosines of the joint plane normal with respect to the principal stress axes, S_1 , S_2 and S_3, respectively. Putting Eqs. (3.3) and (3.4) back into Eq. (3.2), the critical injection pressure to activate the shear slip on a specifically oriented joint can be determined for a given state of stress and a given frictional coefficient. As for the shaded region in Figure 3.1b, it represents all the joints that would have been slid at the current injection pressure level of P_c. It is obvious that the critical injection pressure for shearing varies with the joint orientation.

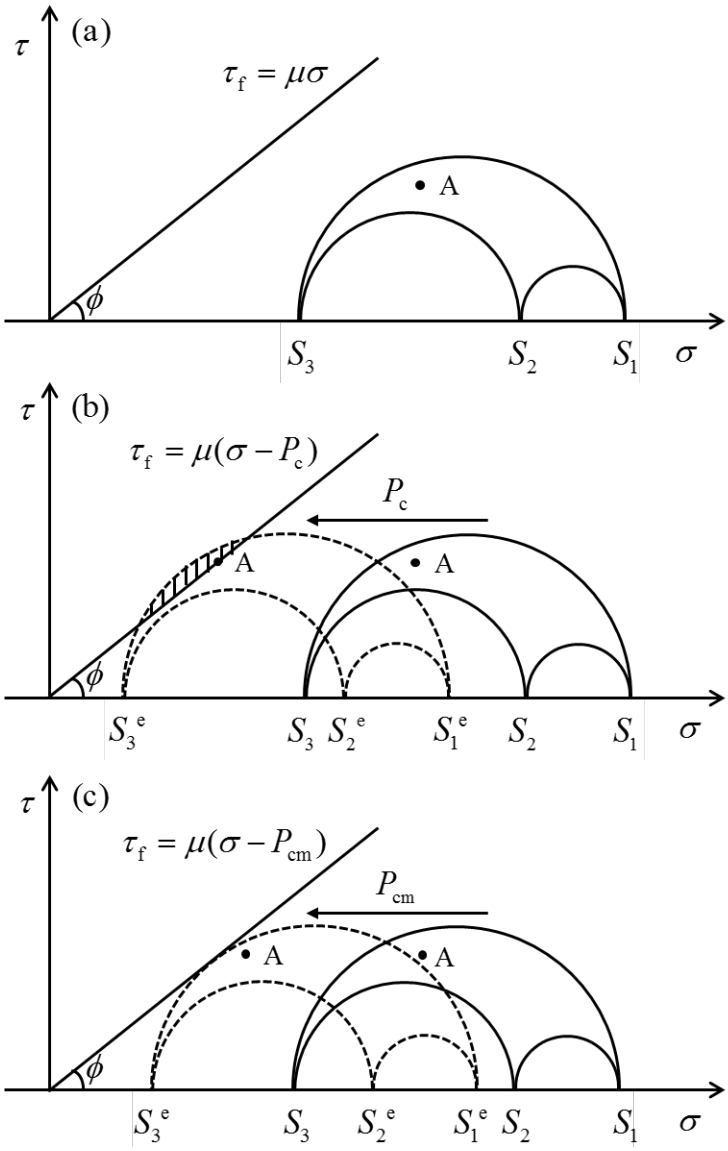

Figure 3.1 Concept of hydroshearing and definition of critical pressure for shearing. The effect of the injection pressure is to horizontally move the stress circles left by an amount equal to the magnitude of the injection pressure. (a) Initial state without fluid pressure, (b) critical pressure, P_c, required to slide a specifically oriented joint and (c) critical pressure, P_{cm}, required to slide the most optimally oriented joint which is the minimum pressure to cause shearing.

The most optimally oriented joint for shearing requires a minimum additional pressure to make a slip occur, and this pressure is used to move the biggest stress circle composed of S_1 and S_3 to be tangent to the failure envelope (as shown in Figure 3.1c). This most vulnerable joint for slip is oriented with its normal vector perpendicular to S_2 and at an angle of $\frac{\pi}{4}+\frac{\phi}{2}$ to S_1. The magnitude of the minimum critical pressure (P_{cm}) is explicitly expressed as

$$P_{cm} = \frac{k_c - k}{k_c - 1} S_3 \tag{3.5}$$

$$k = \frac{S_1}{S_3},\ k_c = \frac{1+\sin\phi}{1-\sin\phi} \tag{3.6}$$

Once shearing is initiated, it is natural and essential to study the direction of shearing growth as well as the location where shearing starts in the open well interval. The location of shearing and the direction of its growth determine potential location and direction of permeability enhancement. Considering that the propagation of fracture shearing is reflected by the monitored migration of induced seismicity, the terminology shearing propagation and shearing migration are used alternatively.

The diagrams in Figure 3.2 are adopted to demonstrate the process of predicting the shearing initiation location of the open well and the shearing migration direction. For a specifically oriented fracture set

existing across the whole open hole section, one can compute the magnitudes of critical pressure using Eq. (3.2) for different depths, and the depth profile of the critical pressure is shown as the solid line in the plots of Figure 3.2.

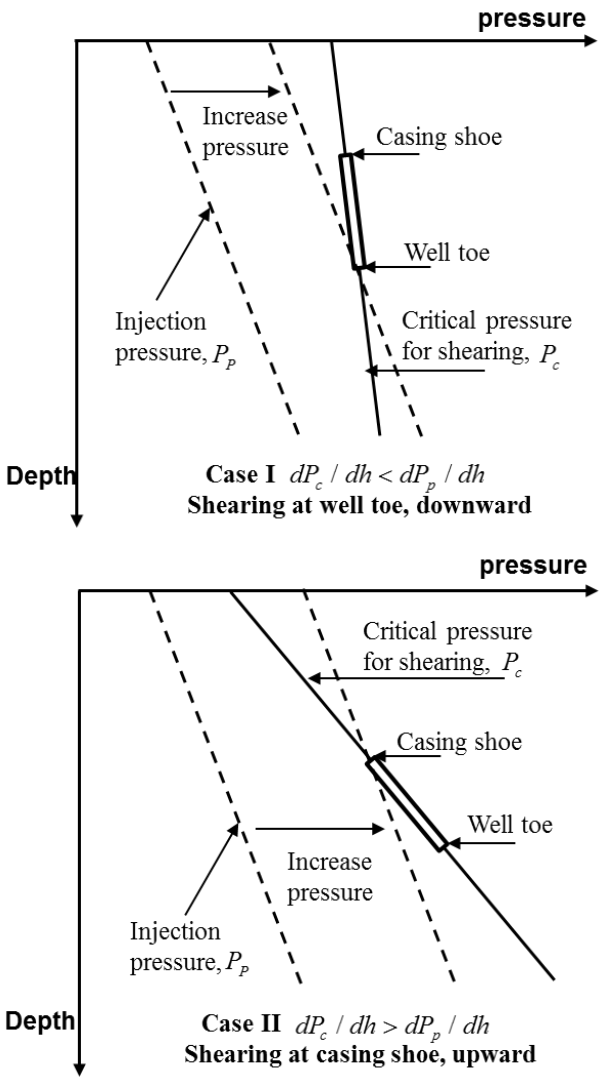

Figure 3.2 Demonstrating diagrams to determine shearing initiation location of open hole section and shearing migration direction.

It should be noticed that the critical pressure may not have to be linearly increased with depth, or, in other words, the depth gradient of the critical pressure may not have to be constant. Actually, a constant depth gradient of critical pressure for a fracture set is valid for the given stress configurations, which will be discussed later.

With continuous injection, the injection pressure profile (dashed lines in the plots of Figure 3.2) moves toward the right until it first meets the profile of critical pressure for the interval of the open well, which means the shear slip is activated. If the injection pressure profile first meets the critical pressure profile at the well toe location (case I in Figure 3.2), which is mathematically expressed as the gradient of the injection pressure being larger than the gradient of the critical pressure, the shearing shall initiate at the well toe location. It is also found that the injection pressure applied on the wellbore wall below the well toe location already exceeds the required pressure for shearing, which means the shear slip tends to grow downward. In the contrast, as shown by case II in Figure 3.2, if the injection pressure profile first meets the critical pressure profile at the casing shoe location, the shearing shall activate at casing shoe location with an upward migration. For case II, the gradient of the injection pressure is less than the gradient of the critical pressure.

In what follows, the gradients of the critical pressure and injection pressure are derived.

The injection pressure shall linearly increases with depth if the hydrostatic column pressure is set as

$$P_{\mathrm{st}} = \rho_{\mathrm{w}} gh \tag{3.7}$$

where ρ_{w} is the density of the applied injection fluid. The frictional pressure loss along the wellbore interval from the surface to the target depth is ignored, also the loss along the fracture planes. Because of this ignorance, the evaluated critical pressure is underestimated, also the gradient of critical pressure. As measuring friction loss in wellbore and fracture plane is not straightforward, one can make the critical shearing pressure more conservative by adopting a higher frictional coefficient. The injection pressure acting on the wellbore wall is the sum of the applied wellhead pressure P_{wh} and the hydrostatic pressure P_{st}.

$$P_{\mathrm{p}} = P_{\mathrm{wh}} + \rho_{\mathrm{w}} gh \tag{3.8}$$

The gradient of the injection pressure is expressed as

$$P_{\mathrm{p}}' = \rho_{\mathrm{w}} g \tag{3.9}$$

In the Earth's crust, especially deep underground, it is widely assumed that one principal stress is vertical, S_{v}, and the other two are horizontal, S_{H} and S_{h} (Amadei and Stephansson, 1997; Jaeger et al., 2007; Zoback et al., 2003). Three stress regimes are defined depending on the relative magnitude of these three principal stresses (Anderson, 1951). They are normal faulting (NF) when $S_{\mathrm{V}} > S_{\mathrm{H}} > S_{\mathrm{h}}$, strike slip

faulting (SS) when $S_{\mathrm{H}} > S_{\mathrm{V}} > S_{\mathrm{h}}$ and reverse faulting (RF) when $S_{\mathrm{H}} > S_{\mathrm{h}} > S_{\mathrm{V}}$.

The magnitude of the vertical stress is commonly treated as the overburden weight and mathematically, it is calculated by integrating the rock densities from the surface to the depth of interest.

$$S_{\mathrm{v}} = \rho_{\mathrm{r}} g h \tag{3.10}$$

where ρ_{r} is the overburden rock density.

In kilometer-scale EGS reservoir of interest, the stress magnitudes are generally thought to increase linearly with depth (e.g., stress state of Soultz site proposed by Valley and Evans (2007), and stress state of KTB scientific drill site determined by Brudy et al. (1997)). The two horizontal stresses are expressed as

$$S_{\mathrm{H}} = k_{\mathrm{H}} \rho_{\mathrm{r}} g h \tag{3.11}$$

$$S_{\mathrm{h}} = k_{\mathrm{h}} \rho_{\mathrm{r}} g h \tag{3.12}$$

where k_{H} and k_{h} are the ratios of the maximum and minimum horizontal to vertical stresses, respectively. It is assumed here that the stress ratios are constant for the kilometer-scale reservoir, even though the variation may exists in reality. Such an assumption guarantees that the critical pressure for shearing a specifically oriented fracture is proportional to the depth, or the gradient of the critical pressure is constant, which is adopted in Figure 3.2. This proportionality of the critical pressure to the

depth can also be demonstrated in the Mohr diagrams (Figure 3.1) if the normalized stresses are used. The locations and sizes of stress circles are fixed when k_{H} and k_{h} are constant, also the location of the point representing the stress state on a specifically oriented fracture. Therefore the horizontal distance of the Coulomb failure line relative to the point is identical regardless of the depth, which means the magnitude of critical pressure required for shearing a specifically oriented fracture is proportional to the depth. Similar stress assumption is also adopted by Ito and Hayashi (2003). In the following, the constant gradient of the critical pressure in the reservoir will be mathematically demonstrated.

Let the principal stresses be expressed in terms of the vertical stress.

$$S_1 = k_1 S_{\mathrm{v}} \tag{3.13}$$

$$S_2 = k_2 S_{\mathrm{v}} \tag{3.14}$$

$$S_3 = k_3 S_{\mathrm{v}} \tag{3.15}$$

One of the three stress ratios must be equal to one, which depends on the given stress regime. k_1, k_2 and k_3 are one for normal, strike slip and reverse faulting stress regimes, respectively.

Then the derivative of the critical pressure for shearing with respect to the depth is expressed as,

$$P_{\mathrm{c}}' = \sigma' - \frac{1}{\mu}\tau' \tag{3.16}$$

The gradients of the normal and shear stresses are obtained from Eq. (3.3) and (3.4), respectively.

$$\sigma' = (l^2 k_1 + m^2 k_2 + n^2 k_3)\rho_r g = \lambda_\sigma g \tag{3.17}$$

$$\tau' = [(k_1 - k_2)^2 l^2 m^2 + (k_2 - k_3)^2 m^2 n^2 + (k_3 - k_1)^2 l^2 n^2]^{1/2} \rho_r g = \lambda_\tau g \tag{3.18}$$

λ_σ and λ_τ are defined as the coefficients of the normal stress gradient and shear stress gradient, respectively. Putting Eqs. (3.17) and (3.18) back into Eq. (3.16), the expression for the gradient of the critical pressure is obtained,

$$P_{\mathrm{c}}' = \lambda_\sigma g - \frac{\lambda_\tau g}{\mu} = \lambda_{\mathrm{c}} g \tag{3.19}$$

where λ_{c} is the coefficient of the critical pressure gradient. It is noted that, for a specifically oriented joint set, Eqs. (3.16)–(3.19) indicate that the gradient of critical pressure is constant for the provided stress condition and frictional coefficient.

According to the proposed methodology shown in Figure 3.2, the determination of the shearing initiation location of the open section and shearing growth direction is expressed as follows.

Shearing at casing shoe with upward growth $\lambda_{\mathrm{c}} > \rho_{\mathrm{w}}$ (3.20)

Shearing at well toe with downward growth $\lambda_{\mathrm{c}} < \rho_{\mathrm{w}}$ (3.21)

In theory, upward growth naturally occurs from casing shoe location while downward growth occurs from well toe location. The derivation

process indicates that the upward or downward shearing depends on the fracture orientation, stress condition, fracture frictional coefficient, and injection fluid density. The effects of μ and ρ_{w} are straightforward, smaller μ and larger ρ_{w} tending to cause downward growth, while the impacts of the fracture orientation and stress condition are coupled.

3.3 Results and discussions

3.3.1 General configurations of studies

In order to enhance the generality of the study and make the associated results applicable to various depth conditions for an open well, the stresses and pressures are expressed in normalized forms by dividing them by S_{v}. The normalized stress magnitudes are, k_{H} as the maximum horizontal stress, k_{h} as the minimum horizontal stress, and one as the vertical stress. It is assumed that k_{H} and k_{h} are constant for the kilometer-scale EGS reservoir at depth. Different stress regimes are distinguished as NF when $1 > k_{\mathrm{H}} > k_{\mathrm{h}}$, SS when $k_{\mathrm{H}} > 1 > k_{\mathrm{h}}$ and RF when $k_{\mathrm{H}} > k_{\mathrm{h}} > 1$. Similarly the normalized injection pressure and critical pressure with respect to vertical stress are obtained,

$$k_{\mathrm{pp}} = \frac{P_{\mathrm{p}}}{S_{\mathrm{v}}} \tag{3.22}$$

$$k_{\mathrm{pc}} = \frac{P_{\mathrm{c}}}{S_{\mathrm{v}}} \tag{3.23}$$

In this section for generic studies, minor attention is paid to the sensitivity of μ and ρ_{w} because their effects on shearing initiation and migration are straightforward. μ is set as 0.8, which is the intermediate of the common rock friction range, 0.6-1.0 (Byerlee, 1978). Pure water injection (ρ_{w} =1000 kg/m^3) is considered unless otherwise specifically stated.

The impacts of the fracture orientation and stress condition on the shearing initiation and migration are coupled and complicated. As for general studies, random fracture orientations with a uniform distribution are assumed, which means to cover all possible fracture orientations. Moreover, it is considered that these randomly oriented fractures exist across the whole open hole section, which means that the fractures are ubiquitous in terms of the depth. It should be highlighted that they may not always stand in reality, and the results shown in this section still can provide general implications. In this regard, first-order estimations are available, and more accurate results shall be obtained by accounting for site specific conditions. For example, the shearing initiation location is highly dependent on the location where the optimal fracture exists in the open hole section.

The general studies in this section consider a range of stress ratios from 0.5 to 2.0 as EGS wells are commonly completed at a depth of

several kilometers. As for the stress direction, the N-S orientation is adopted for S_H . A study of the relationships between the measured in situ stresses and the depth by Brown and Hoek (1978) suggested a range of 0.5 to 2.0 for the horizontal to vertical stress ratio at depths below 1000 m. Collected field stress states at the reservoir depth for seven EGS sites and their stress ratios presented in the previous chapter are within the above mentioned range. Regarding these, it is reasonable to study this stress range for the effects of field stress on initiation and propagation of fracture shear slip.

A polygonal plot of the stress was adopted in Figure 3.3 to show the stress conditions studied in a straightforward way. The whole stress range covered here is represented as a triangle in the lower left, and two more auxiliary dashed lines are added to distinguish the NF, SS and RF stress regimes. In addition, such polygonal plots are used with respect to the presentation of the contours of the obtained results to highlight the effects of the stress conditions on the shearing in the EGS open section.

In order to visualize how far from failure the rock mass is in the proposed stress range, two stress polygons are added in Figure 3.3, which represent the possible stress ratios for keeping fault stability. They are prepared following the method used in Zoback et al. (2003) for zero and hydrostatic pore pressure conditions with the friction coefficient of 0.8. The studied stress condition in this section is reasonably within the limitations of fault stability except a small region of SS condition

violating the stress limit for hydrostatic case. For this extreme SS condition where the ratio between maximum and minimum stress is high, the shear slip of rock discontinuities is expected to easily happen during the injection.

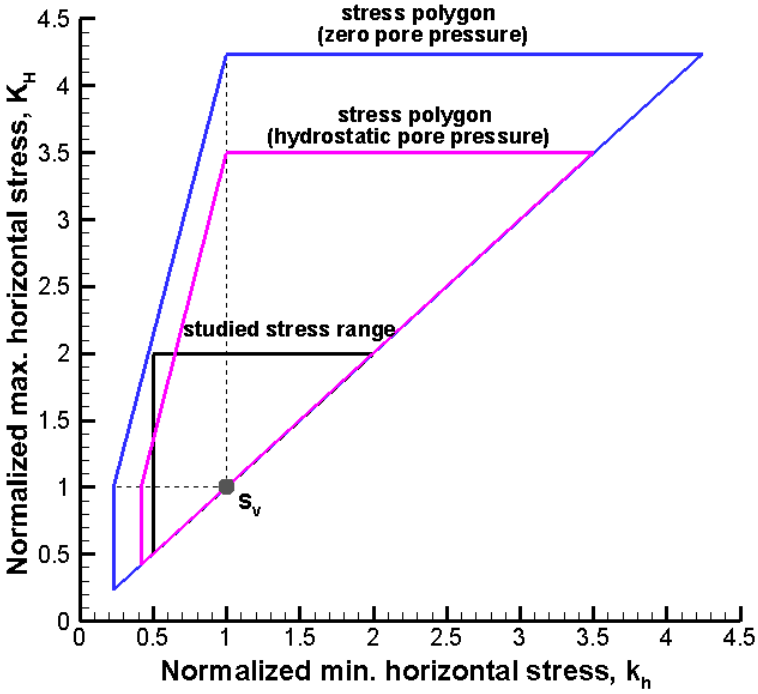

Figure 3.3 Stress range considered in general study (black triangle), stress polygons constrained by fault stability for zero pore pressure (blue polygon) and hydrostatic pore pressure (pink polygon). The stress limits are computed using a friction coefficient of 0.8.

Based on these pre-defined configurations, the proposed methodology was applied to generally study the shearing during EGS stimulation in terms of the minimum critical pressure for shearing, critical pressure for shearing, shearing probability, shearing initiation location and downward shearing probability.

3.3.2 Minimum critical pressure to activate shearing

Because the monitored induced seismicity is usually related to the shear slip on fracture planes, people may treat the onset of seismicity as an indicator of shearing activation in the reservoir. Actually the seismic events caused by tensile fracture opening are difficult to detect mainly due to two facts in terms of data monitoring: 1) the frequency of downhole amplifier is not sufficiently high and 2) the events are small and weak (Gaucher et al, 2015). In this way, the minimum critical pressure to activate shearing becomes a useful parameter applicable in practice, because it represents the injection pressure at the onset of seismicity. In return, the observed fluid pressure at the onset of seismicity can be helpful for understanding the reservoir stress state and fracture system. Similar scenario was reported in Jeanne et al. (2014) where they treated the strong increase of seismic event rate as the indicator of beginning of fault zone reactivation.

The normalized minimum critical pressure, k_{cm}, required to activate shearing in the reservoir with a randomly oriented fracture system can simply be evaluated using Eq. (3.5) when the most optimally oriented fracture is sheared. Even though the most optimally oriented fracture may not always exist at a real site, such an estimated k_{cm} provides a general but simple indicator of how difficult it is to activate shear slip and the associated onset of seismicity.

Figure 3.4 shows the computed results of k_{cm} for various stress conditions. It is obvious that the case at the RF stress regime requires a high injection pressure to cause shear slip on the fracture, which means a large energy consumption is expected to pump in fluid with a high pressure. In addition, the selected pump and pipes must be capable of handling such a high pressure. The results suggest that the regions with significant NF or SS stress conditions seem to be favorable for shear slip by relatively small injection pressure. In general, RF stress regime requires higher injection pressure since overall stress magnitude is greater compared to the NF or SS stress regimes because the vertical stress is the minimum. Similarly, NF stress regime in general requires less injection pressure. These findings are supported by the results of some real site stimulation tests (refer to Figure 3.9 in Chapter 3.4). For example, stimulations at the Habanero site of the Cooper Basin project in Australia, which has an RF stress regime, were completed with high injection pressure (Baisch et al., 2009; Chen, 2010), whereas a small injection pressure was observed for the tests at the Rosemanowes project in the UK, where an extreme SS condition exists (Pine and Batchelor, 1984).

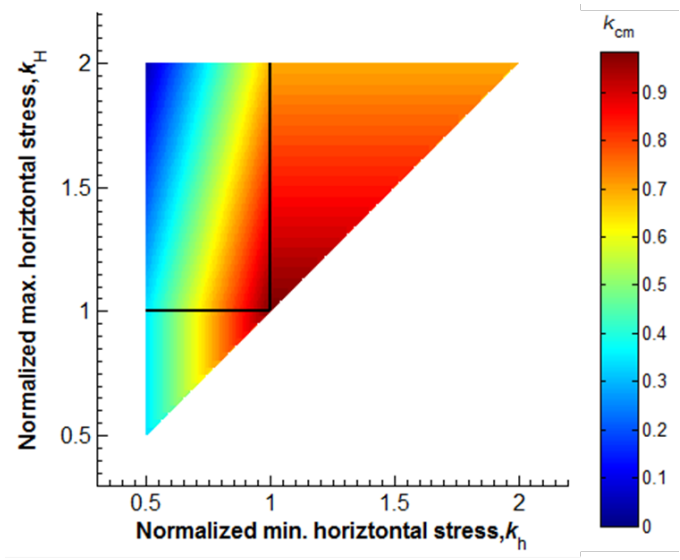

Figure 3.4 Normalized minimum critical pressure (k_{cm}) for shearing activation computed from Eq. (3.5) for various stress configurations. It was prepared using 0.02 increments for k_H and k_h .

3.3.3 Critical pressure for shearing and probability of shearing

Using Eqs. (3.2)-(3.4), the critical pressure for shearing a specifically oriented fracture can be computed, and a lower hemisphere stereo plot is employed to include information of the critical pressures of all the possible fracture orientations for the given stress condition (left column of Figure 3.5). In the stereo plot, the color overlaid at the position of a fracture pole represents the computed k_{pc} for shearing that specifically oriented fracture. Such a stereo plot permits a rapid and visual assessment of the range of critically stressed orientations for a provided injection pressure. Two auxiliary contour lines are included. They are raised for the attempts to conceptually compute the orientations possible

for shearing and the orientations with high tendency for shearing in practice. One represents the magnitude of the critical pressure equal to the magnitude of s_3,

$$k_{cf} = k_3 \tag{3.24}$$

k_{cf} is considered to be the critical pressure required to activate the fracture opening. Here the fracture opening means the openness of natural fractures in the tensile mode, in other words, the detachment of natural fracture planes. The fracture opening is potential to happen when the injection pressure exceeds the magnitude of s_3. Considering the fact that the opening of the fracture significantly improves its permeability, it is very difficult to further increase the injection pressure, because the injected fluid can diffuse away easily. In this regard, the fractures that require a critical pressure greater than k_{cf} can hardly be sheared, and the fractures with orientations within this contour line are expected to be sheared before the fracture opening occurs. Therefor k_{cf} can be the cut-off critical pressure to define the range of orientations possible for shearing in practice.

The other inner contour line represents the cut-off critical pressure for defining the range of orientations with high tendency for shearing in practice. A cut-off critical pressure is suggested as

$$k_{\mathrm{co}} = k_{\mathrm{cm}} + \lambda_{\mathrm{co}}(k_{\mathrm{cf}} - k_{\mathrm{cm}}) \tag{3.25}$$

where the coefficient λ_{co} is bigger than 0 and less than 1, correspondingly $k_{cm} < k_{co} < k_{cf}$, which means k_{co} shall be sufficient to slide the most optimally orientated fracture and does not allow fracture opening to occur. This concept of high tendency for shearing in practice corresponds to the phenomenon that the injection pressure increase rate decreases with improved reservoir permeability and the associated enhancement of fluid diffusivity. This has been observed from the recorded pressure-injection histories of many EGS field stimulation tests such as those operated at the Soultz EGS site (Dorbath et al., 2009) and Basel EGS site (Häring et al., 2008). Physically, such a phenomenon can also be understandable. With a continuous injection and increase of the injection pressure, more significant fracture slips are expected to occur, improving the overall reservoir permeability, and the injected fluid diffuses more easily from the open well interval. Therefore, pressure accumulation becomes more difficult, or the pressure increase rate decreases. In a practical point of view, the fractures with high tendency for shearing are those requiring a critical pressure that is relatively easy to be achieved during the injection operation.

It is difficult to determine λ_{co} precisely because there are many impacting factors, including the borehole geometry, reservoir rock properties, injection fluid properties, and fracture connectivity to name a few. Some field investigations suggested that the fractures close to being critically stressed for shearing are likely to be naturally more conductive

(Barton et al., 1995; Ito and Zoback, 2000), and this feature tends to make the pressure accumulation difficult. In addition, the previous field stimulation tests observed that induced seismic events consistently occurred along those planes that are favorably aligned for shear slip with respect to the current field stress (Jung, 2013; Xie et al., 2015). The slips on those fractures which require a relatively low critical pressure for shearing may compose significant permeability enhancement. Regarding these, a relatively small value of λ_{co} is suggested to be more applicable in general. All the results presented in Figure 3.5 and Figure 3.6 were obtained by adopting a value of $\frac{1}{3}$ for coefficient λ_{co}. It should be highlighted that such a specific value is used for better demonstration of the study results.

In order to show the spatial distribution of orientations for shearing with increasing pore pressure for different stress regimes, especially the features of orientations for possible shearing and with high tendency for shearing in practice, three demonstrating examples are provided (Figure 3.5). The stress magnitudes adopted for these examples are (a) the NF stress regime, S_{Hmax}:S_{hmin}:S_v = 0.75:0.5:1, (b) SS stress regime, S_{Hmax}:S_{hmin}:S_v = 1.4:0.6:1, and (c) RF regime, S_{Hmax}:S_{hmin}:S_v = 1.5:1.25:1. They are featured as 1) high ratio of maximum to minimum principal stress is adopted because it is favorable for shearing, 2) they can be comparable with the reservoir stress states of some well-known EGS sites, e.g., 0.6 of S_{hmin} in SS case is similar to that of Soultz and Basel

sites, and 3) the average of maximum and minimum principal stress is used for the intermediate principal stress.

The equal area stereo plot[3] in Figure 3.5 includes the k_{pc} values for all possible fracture orientations and the color overlaid at the position of a fracture pole represents the required k_{pc} for shearing that specifically oriented fracture. The blue zone represents the orientations which need a lower pressure for shearing to happen. Obviously, the fractures with poles laying in the blue zone are prevailing for shear slip when applying fluid injection. The outer contour line of k_{pc}, whose value equals the magnitude of minimum principal stress, defines the range of orientations possible for shearing before fracture opening. The k_{pc} for these orientations satisfies

$$k_{\mathrm{pc}} < k_3 \tag{3.26}$$

While the inner contour line, whose value is computed from Eq. (3.25), constrains the range of orientations with high tendency for shearing from a practical point of view. The k_{pc} for these orientations satisfies

[3] The equal area stereo plot was adopted to preserve the area in the projection to reflect the probability of shearing. The corresponding plots in journal publication are equal angle projection (Xie and Min, 2016).

$$k_{pc} < k_{co} \tag{3.27}$$

From Figure 3.5, it is obvious that the stress regime impacts the spatial features of orientations for possible shearing and with high tendency for shearing in practice. It is observed that the optimally oriented fractures for shearing are moderately dipped, highly dipped (sub-vertical) and slightly dipped (sub-horizontal) for the NF, SS and RF stress conditions, respectively. More interestingly, this claim is generally consistent with the monitored seismic clouds in some field tests of hydraulic stimulation. It was summarized by (Jung, 2013) that the seismic clouds appeared to be moderately dipped at the Fenton Hill and Hijiori projects (NF stress regime); sub-vertical or highly dipped at the Resemanowes, Soultz and Basel projects (SS stress regime); and sub-horizontal at the Cooper Basin project (RF stress regime).

(a)NF, S_H:S_h:S_v = 0.75:0.5:1

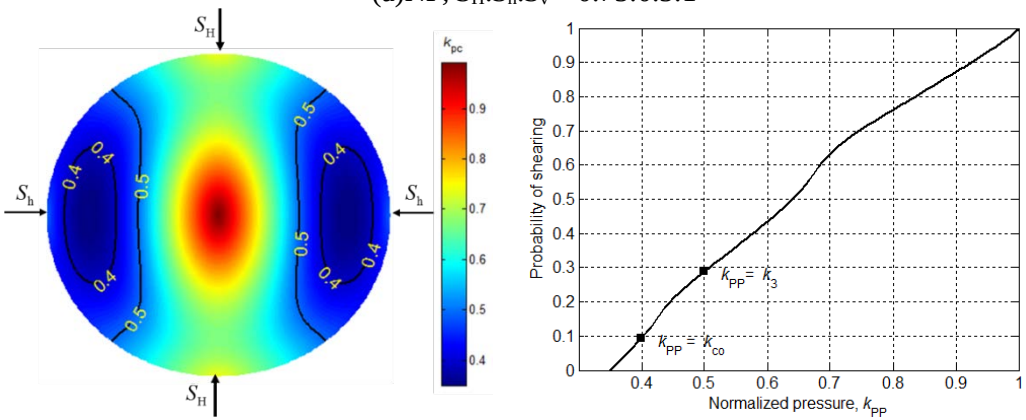

(b) SS, S_H:S_h:S_v = 1.4:0.6:1

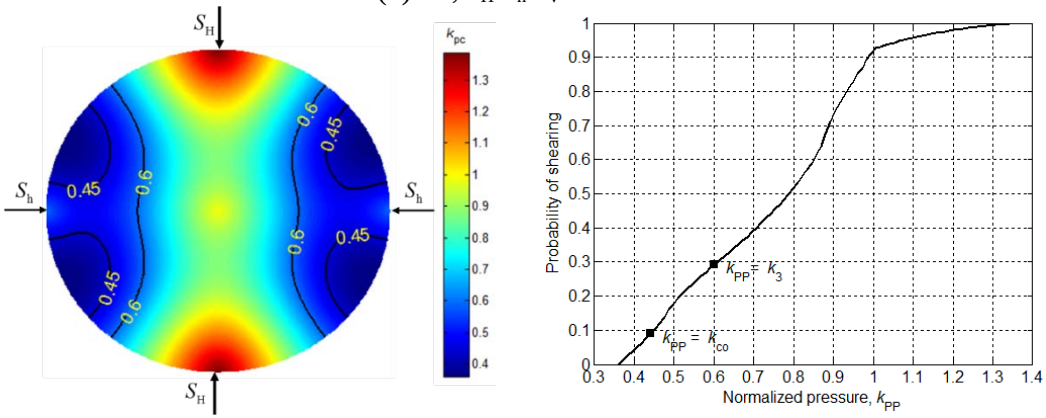

(c) RF, S_H:S_h:S_v = 1.5:1.25:1

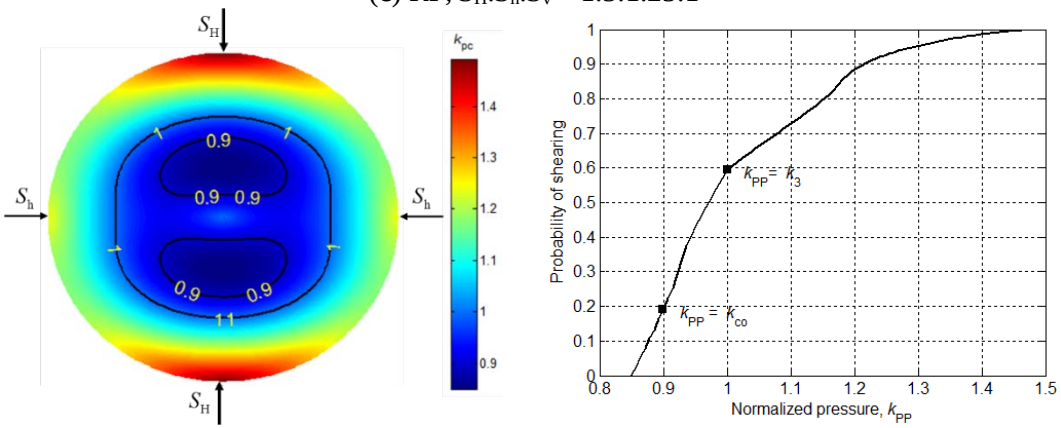

Figure 3.5 Left column: equal area stereo plot of contour of critical pressure in lower hemisphere. The color overlaid at the position of a fracture pole represents the required k_{pc} for shearing that specifically oriented fracture. It was prepared using one degree increments of both the fracture dip and dip direction. The outer contour line defines the range of orientations possible for shearing before fracture opening, and the inner contour line defines the range of orientations with high tendency for shearing in practice. Right column: evolution of probability of shearing with respect to increasing injection pressure. The two square marks represent the probabilities of shearing when the applied injection pressure equals k_{co} and k_3, respectively. The examples shown are (a) the NF stress regime, S_{Hmax}:S_{hmin}:S_v = 0.75:0.5:1, (b) SS stress regime, S_{Hmax}:S_{hmin}:S_v = 1.4:0.6:1, and (c) RF regime, S_{Hmax}:S_{hmin}:S_v = 1.5:1.25:1.

The plots in the right column of Figure 3.5 record the evolution of the shearing probability with respect to the increasing injection pressure, and two square marks represent the probabilities of shearing with the applied injection pressure equals k_{co} and S_3 , respectively. The probability of shearing is simply defined as the portion of critically stressed orientations for the applied pressure because randomly distributed fracture orientations are considered. In this regard, such a shearing probability plot may further provide a quantitative assessment of the portion of critically stressed orientations for the given pressure condition. A higher shearing probability indicates more diverse orientation slips, which contribute to form a three-dimensionally stimulated volume rather than a two-dimensionally featured stimulated plane with a small thickness. For the cases presented in Figure 3.5, it is interesting that the portion of orientations with high tendency for shearing is higher for the RF condition compared with those of the NF and SS cases, even though a much higher critical pressure is required. It is notable that the shearing probability develops quicker for the case of the RF stress condition, which implicates that the portion of critically stressed orientations expands easily with the increasing pressure.

The contour plot of Figure 3.6a shows the computed k_{co} from Eq. (3.25) for various stress configurations by adopting a coefficient λ_{co} of $\frac{1}{3}$, and they are used to define the portions of orientations with high

tendency for shearing in Figure 3.6b. In general, the range of orientations with high tendency for shearing is small for most stress conditions except the cases nearby the transition between SS and RF. The probability with high tendency for shearing is relatively high for the RF stress condition, while for most cases of NF and SS stress regimes, a very narrow range of orientations is with high tendency for shearing in practice. This means that the fractures that can be sheared in practice may not be very diversely oriented and this situation is not favorable for achieving a three-dimensionally stimulated reservoir for EGS development. In fact, the majority of field stimulation tests for EGS projects have demonstrated that the observed seismic clouds are mainly two dimensionally shaped with relatively small thicknesses (Jung, 2013). The obtained general study result, a narrow portion of orientations holding high tendency for shearing in practice, can provide some insights with respect to such a feature of observed seismic clouds.

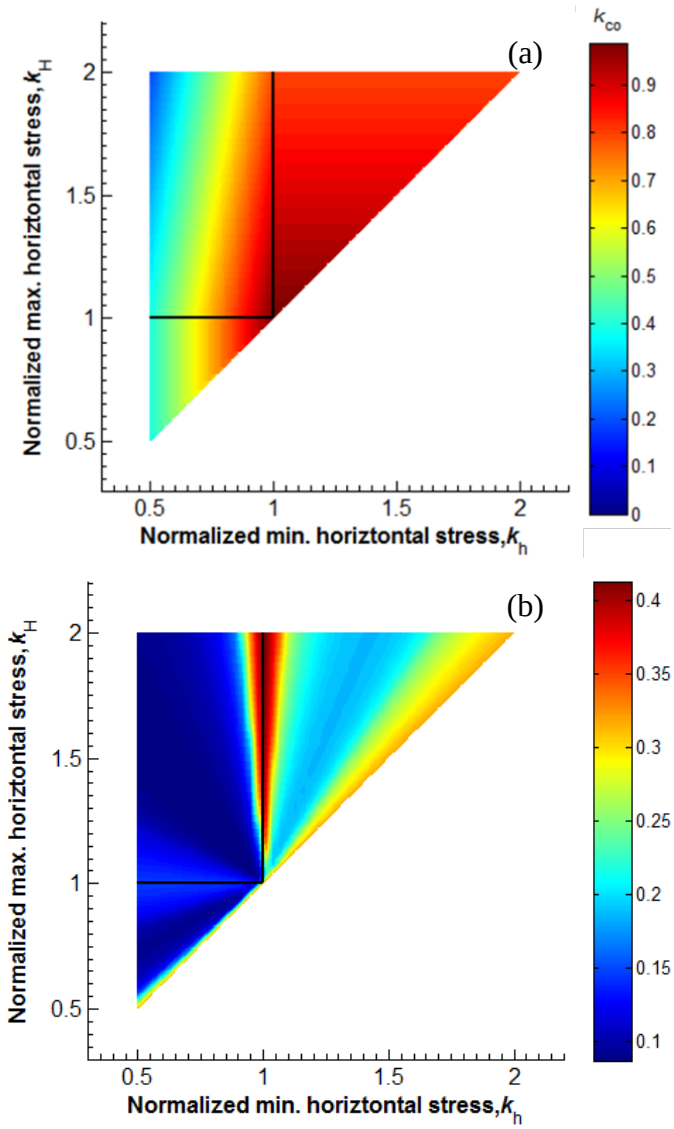

Figure 3.6 (a) Computed k_{co} used for defining orientations with high tendency for shearing in practice by adopting a coefficient λ_{co} of $\frac{1}{3}$. (b) Probability with high tendency for shearing for various stress conditions. They were prepared using 0.02 increments for k_H and k_h.

3.3.4 Shearing initiation location and growth direction

According to the methodology proposed in section 3.2, the shearing initiation location and growth direction depend on the comparison between the gradient of the critical pressure and the gradient of the injection pressure. For a specifically oriented fracture set, the shearing tends to initiate at casing shoe location with upward migration if the gradient of the critical pressure is larger than the gradient of the injection pressure. Otherwise, the shearing tends to start at the well toe location with a downward migration. The gradient of the critical pressure for shearing is computed using Eqs. (3.17 – 3.19), and its counterpart, the gradient of the injection pressure, is computed using Eq. (3.9). In this section, the gradient of the injection pressure is 9.8 MPa/km because pure water injection is adopted.

Figure 3.7 shows stereo plots of the contours of the computed critical pressure gradients for the given stress conditions. A distinguisher contour line of 9.8 MPa/km is also included if it exists. The fracture sets with orientations located within this distinguisher contour line tend to initiate shearing at well toe with downward growth because the gradient of the critical pressure is smaller than the gradient of the injection pressure. Such a stereo plot allows a rapid and visual assessment of the shearing initiation location and migration direction. It is observed that no distinguisher contour appears for the example of the RF stress configuration, which means there is no possibility of downward growth

of shearing. Actually, the vertical component of the shear growth is less significant for RF stress conditions because the optimal orientations for shearing are sub-horizontal. For the other two examples of NF and SS stress conditions, there is a certain range of fracture orientations that favor downward growth of shearing.

Further, it is found that these fracture orientations allowing downward shearing development are almost within those of optimal shearing, as shown in the stereo plot of the critical pressure contour in Figure 3.5. Such a phenomenon is due to the considerations with respect to the in situ stresses as described in section 3.2. For the kilometer-scale EGS reservoir at depth, it is assumed that the magnitudes of the three in situ principal stresses vary linearly with the depth, and the stress magnitude ratios are constant. This makes the critical pressure for shearing a specifically oriented fracture directly related to the gradient of the critical pressure as

$$P_c = P'_c \cdot h \tag{3.28}$$

(a) NF, S_H:S_h:S_v = 0.75:0.5:1 (b) SS, S_H:S_h:S_v = 1.4:0.6:1 (c) RF, S_H:S_h:S_v = 1.5:1.25:1

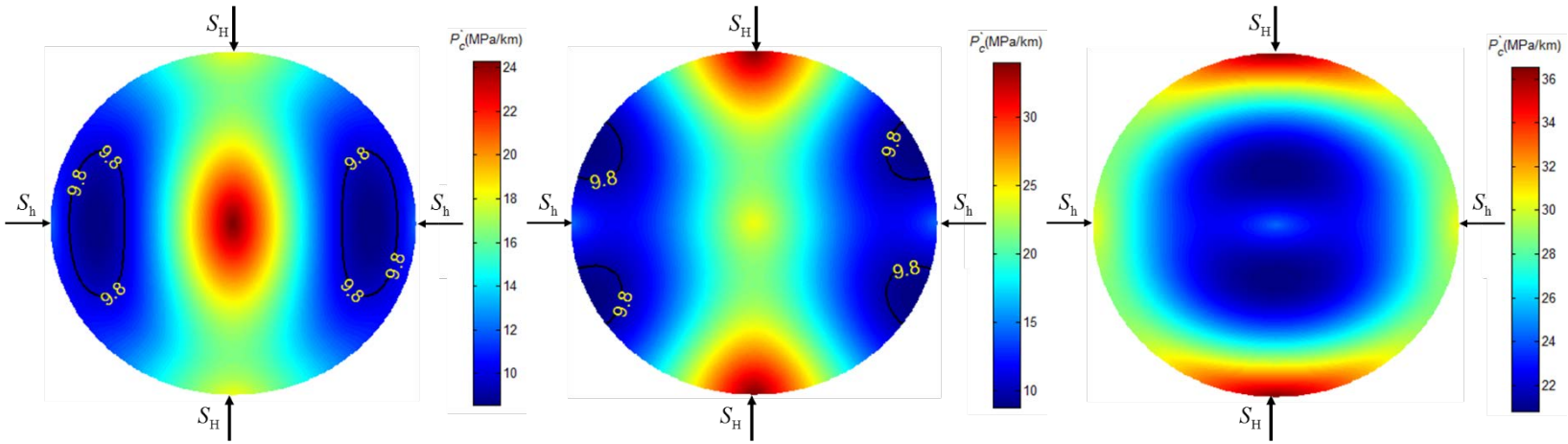

Figure 3.7 Equal area stereo plot of contour of critical pressure gradient in lower hemisphere. It was prepared using one degree increments of both the fracture dip and dip direction. A distinguisher contour line of 9.8 MPa/km is included if it exists. The tested examples are (a) the NF stress regime, S_{Hmax}:S_{hmin}:S_v = 0.75:0.5:1, (b) SS stress regime, S_{Hmax}:S_{hmin}:S_v = 1.4:0.6:1 and (c) RF regime, S_{Hmax}:S_{hmin}:S_v = 1.5:1.25:1.

In this regard, the critical pressure is positive proportional to its gradient. Fractures with smaller gradients of critical pressure correspond to those of smaller critical pressures, which means such fractures are optimally oriented for shearing. In this regard, only optimal orientations for shearing may permit downward growth of shearing, and this is a necessary but not sufficient condition. This implies that downward shearing initiated at the well toe location shall occur first if it is possible during the stimulation operation. However, it is emphasized that the shearing initiation location is actually determined by the location where optimal fractures exist in reality.

Figure 3.8 presents the probability of downward growth of shearing for various stress settings. The probability is defined as the portion of orientations for which downward growth of shearing tends to occur. Figure 3.8a is the case of water injection with a density of 1000 kg/m^3, while Figure 3.8b is the case of a denser fluid injection with a density of 1100 kg/ m^3. It is obvious that only a small range of stress conditions (extreme NF and SS stress condition) allows downward growth of shearing to occur. For the EGS development, this is not really a favorable finding because upward growth of shearing prevails for most stress conditions. Compared to those allowing downward growth, the cases with upward growth of shearing require deeper EGS wells in order to reach similar hot resources.

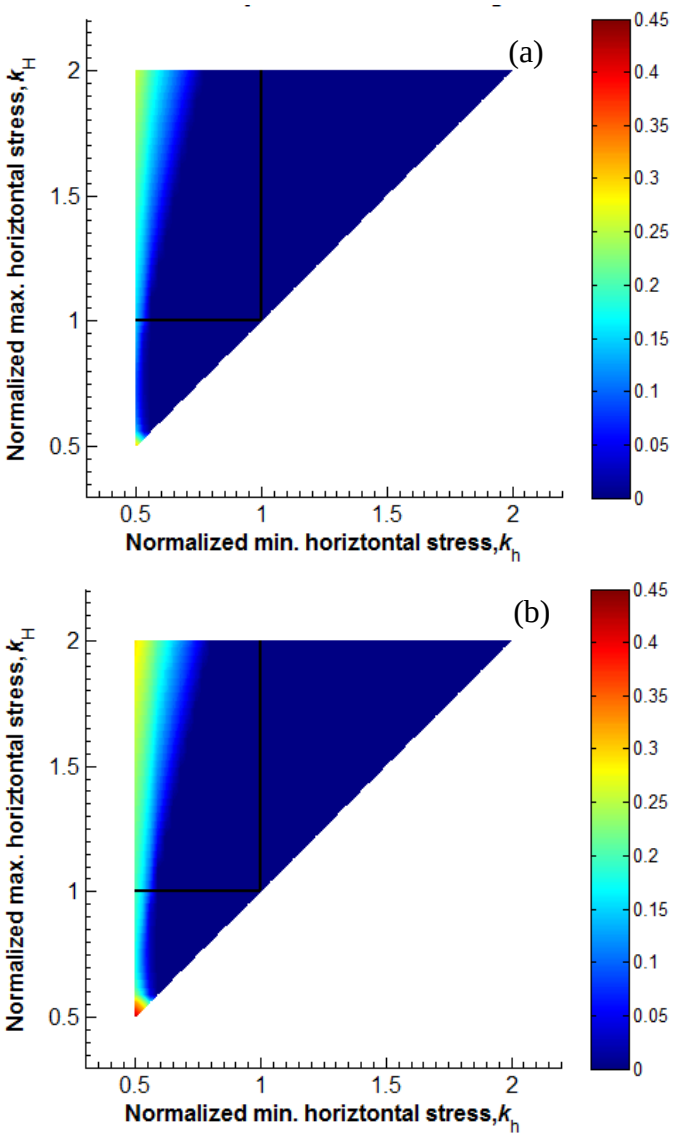

Figure 3.8 Probability of downward growth of shearing for various stress conditions when (a) applying pure water injection with density of 1000 kg/ m^3 and (b) applying dense brine injection with density of 1100 kg/ m^3.

It is very meaningful to discuss the potential measures to initiate downward growth of shearing which contributes to reaching hotter heat resources by stimulating a deeper rock mass for EGS project

development. It is demonstrated in section 3.2 that the shearing initiation location and growth direction depend on the fracture orientation, stress condition, fracture frictional coefficient, and applied fluid density. The fracture orientation and stress condition are basically naturally formed and cannot be controlled. As for the fracture frictional properties, chemical stimulation may contribute to reduce the frictional resistance to some degree. In reality, it is more practical to use a denser brine rather than pure water for approaching downward growth of shearing. In particular, at an early stage of stimulation, employing a heavy brine is a good practice to initiate shearing at a deeper location of an open well with downward migration. Because shear slip improves fracture permeability, the fluid injected at a following stage is more possible to flow from a deeper section of the open well even if no more dense fluid is used after the early stage. Such a strategy was applied to the stimulation of GPK 2 at the Soultz project in order to make shearing occur at a deeper part of the open well, which was achieved by injecting 400 m^3 of heavy brine with a density of 1200 kg/m^3 at the first stage (Weidler et al., 2002). As shown in Figure 3.8b, our general study also showed the expansion of the stress range allowing downward growth of shearing and the increase of probability.

3.4 Field case studies

In this section, efforts are made to estimate the pressure required to activate shear slip and the shearing migration direction for the major

EGS stimulations at Soultz, France; Basel, Switzerland; Rosemanowes, UK; and Cooper Basin, Australia. Specifically, the pressure for shearing activation was computed from Eq. (3.5) based on the Mohr Coulomb law for sliding while the newly proposed method was applied for shearing migration direction estimation by following the procedures presented in section 3.3.4. Then, the estimations were compared with the actual observations of field tests. Here, these four sites were selected for study based on two considerations: 1) a massive volume was injected into fractured crystalline rock through a long open hole section with an interval of hundreds of meters and 2) the data associated with the present analysis were well recorded.

The characterizing test and performance parameters are listed in Table 3.1 for these field tests. Some explanations of these parameters and the origins of the parameter values were also given below the table. Among them, the pressure at onset of seismicity and insitu stress magnitude are crucial parameters for the evaluation and discussion. If the onset of seismicity can be treated as an indicator of the beginning of shear slip, the observed pressure at onset of seismicity would be meaningful in practice because it represents the minimum pressure required for activating shear slip in the site. The pressure at onset of seismicity recorded in Table 3.1 was simply taken from the pressure-seismicity-injection history curves in the specific reference by naked eyes. Using this simple method, it is impossible to determine the pressures at onset of seismicity for Soultz GPK3 and GPK4 cases

because the pressure increased too fast at the early stage of stimulation, almost vertical pressure-time history curves (Dorbath et al., 2009). For the depth used to compute the stress magnitudes listed in Table 3.1, it is the center of open hole section for Soultz and Basel cases, well toe depth for Rosemanowes case because the seismic cloud is mainly developed downward from well toe section, and the depth where the main fracture zone is detected for Cooper Basin case. Details on how to define and determine these parameters can be found elsewhere, e.g., in Xie et al. (2015).

Table 3.1 Summary of hydraulic stimulation tests for field case studies

	Date Sti.	Sti. Int.	V_{in}	Max. Q_{in}	Max. WHP	Sei. WHP	Sei. cloud	Sei. Gro.	Str. Dep.	S_v	S_H	S_h
	year	km	m^3	L/sec	MPa	MPa			km	MPa	MPa	MPa
Soutlz GPK1	1993	2.85-3.4	25300	36	9[a]	4.5[a]	Sub-ver.[a]	Down[a]	3.0	75[d]	76[d]	38[d]
Soutlz GPK2	2000	4.4-5.09	23400	50[b]	14.5[b]	4[b]	Sub-ver.[c]	Down[c]	4.75	121[d]	135[d]	65[d]
Soultz GPK3	2003	4.55-5.0	34000	50	16[b]		Sub-ver.[c]	Down[c]	4.75	121[d]	135[d]	65[d]
Soultz GPK4	2004	4.5-5.0	9134	30	17[b]		Sub-ver[c]	Down[c]		121[d]	135[d]	65[d]
Basel Basel 1	2006	4.63-5	11570	55[e]	29[e]	11[e]	Sub-ver.[f]	Up[f]	4.8	120[g]	154[g]	77[g]
Rosema. RH12	1982	1.7-2.06	18500	90[h]	14[h]	4[j]	Sub-ver.[k]	Down[k]	2.0	52[i]	71[i]	30[i]
Cooper B. Hab. 1	2003	4.14-4.42	16350	24[l]	65[l]	47[l]	Sub-hor.[m]		4.3	100[n]	160[n]	110[n]

Sti. Int.: open hole section interval, V_{in}: injected volume, Max. Q_{in}: maximum injection rate, Max. WHP: maximum well head pressure, Sei. WHP: well head pressure at onset of seismicity, Sei. cloud: dip of stimulated seismic cloud, Sei. Gro.: overall growth direction of seismic cloud; Str. Dep.: the depth used to compute the stress magnitudes listed in the table. For Soultz and Basel, center depth of open hole section, for Rosemanowes, well toe depth as the seismic cloud is mainly developed downward from well toe section, and for Cooper Basin, depth where main fracture zone exits.

a: Figure 14 & 16 in Evans et al. (2005); b: Estimated from Figure 3 in Dorbath et al. (2009); c: Figure 4, 7 & 9 from Dorbath et al. (2009); d: Eq. 2 from Cornet et al. (2007); e: Figure 5 from Häring et al. (2008); f: Figure 3 from Ladner and Häring (2009) and Figure 8 in Terakawa et al. (2012); g: Eq. 7 in Mukuhira et al. (2013); h: Figure 4 in Batchelor et al. (1983); i: Figure 6 in Pine and Batchelor (1984); j: Figure 3 in Pine and Batchelor (1984); k: Eq. 1-3 in Pine and Batchelor (1984); l: Figure 2 in Baisch et al. (2009) and Figure 3 in Kaieda et al. (2010); m: Figure 4 in Baisch et al. (2009); n: Eq. 1-3 in Chen (2010).

In Figure 3.9, the vertical line represents the computed range of minimum pressure required for activating shearing by Eq. (3.5) with μ from 0.6 to 1.0, and the black horizontal bar mark stands for the actual site observation of well head pressure (WHP) at the onset of seismicity. As discussed in section 3.3.2, the estimated minimum critical pressure would correspond to the pressure at the onset of seismicity if the seismicity onset is treated as an indicator of shearing activation during the stimulation operation.

It is found, in general, that the observed pressures at the onset of seismicity are within the range of analytical estimations. Moreover, it seems that the site observations agree well with the estimations using a μ of 1.0. This agreement may not directly indicate that the frictional coefficient is 1.0 in the reservoir. In reality, the critical pressure computed by adopting a smaller μ other than 1.0 for less optimally oriented fractures can be identical to that from Eq. (3.5) using μ of 1.0 for the most optimally oriented fracture. In this regard, employing the μ of 1.0 in Eq. (3.5) to evaluate the pressure for initiating shear slip can be a good practice, which somehow counteracts the effects induced by the fact that the most optimally oriented fracture may not exist at the site. Additionally, applying a large magnitude of μ also counteracts the impacts caused by neglecting of fracture cohesive strength to some degree. It may be concluded that the injection pressure for activating fracture shear slip and the associated seismic onset are mainly field stress

controlled. Besides this stress-controlled pressure for activating fracture slip, the research by Ito and Hayashi (2003) suggests a feature of stress-controlled flow pathways in HDR geothermal reservoir. It seems this is a quick but still reliable way to assess the required minimum pressure for shearing activation by Eq. (3.5) with μ of 1.0. But it must be kept in mind that there are many uncertainties included in this way of evaluation, such as those related with stress condition and fracture frictional properties. Also the uncertainty may be caused by the difficulty and ambiguity of defining and detecting the onset of seismicity in site. It is also noticed that the estimated minimum pressure at the surface could be small or even negative, which means the fractures and discontinuities at depth are close to the critical state for sliding, and a small additional pressure can cause shear failure to occur along the optimally oriented fractures.

Besides, the pressure necessary for tensile opening, which is treated to be equal to the minimum principal stress, is also shown in Figure 3.9. Obviously, the pressure level at onset of seismicity is not sufficient for tensile opening and this confirms the shearing mechanism for induced seismicity at the beginning of stimulation.

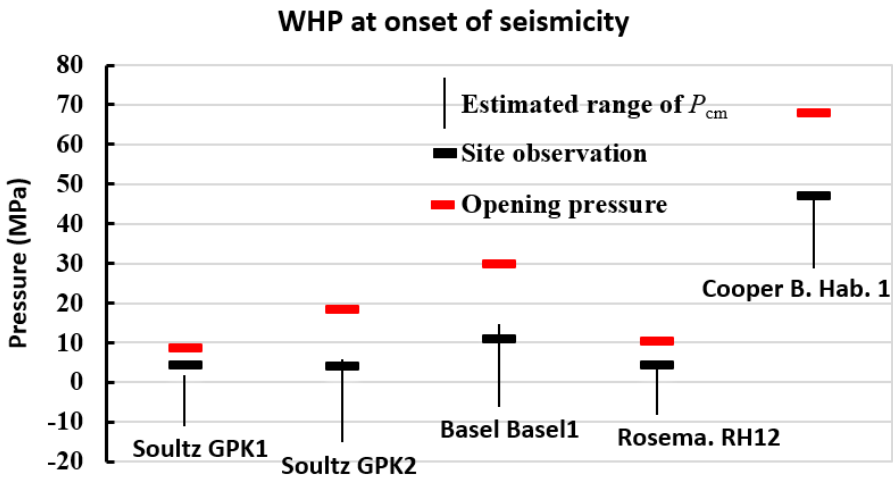

Figure 3.9 Estimated range of minimum pressure P_{cm} for shear slip activation (vertical line), estimated minimum pressure required for tensile opening (horizontal red bar) and observed WHP at onset of seismicity of field tests (horizontal black Bar). A vertical line represents an estimation of P_{cm} corresponding to a range of μ between 0.6 and 1.0.

Both downward and upward featured growth of induced seismicity cloud was observed from existing EGS site stimulations (Table 1). Rosemanowes RH12 stimulation is a typical example for downward migration of shearing with significant downward growth of seismicity. Pine and Batchelor (1984) presented a 2D geomechanical model to successfully explain the observed downward migration of seismicity, mainly because the major fracture sets are steeply dipped, almost vertical. During the massive stimulation of Basel EGS site, induced seismicity showed the feature of upward growth even though it is not so significant. Referred to the previous evaluation for the probability of downward growth of shearing (Figure 3.8a), the Basel reservoir stress condition

($k_{\mathrm{H}} = 1.28$ and $k_{\mathrm{h}} = 0.64$) corresponds to an extremely low probability, less than 0.05, which means only a small range of orientations is possible for downward shearing. In other words, the Basel reservoir stress condition is favorable for upward shearing. Note that the probability presented here is based on an uniform distribution of fracture orientations and in reality certain fracture orientations may dominate. Theoretically speaking, more exact analysis, similar to the following Soultz case, can be performed if the detailed fracture zone information with confidence is available. As for the Cooper Basin project, the observed seismic cloud is sub-horizontal with a minor component of vertical growth.

Another example of downward migration of the seismicity is Soultz EGS project where 4 wells were completed and several stimulations were performed. The downward growth of induced seismicity was consistently observed for the stimulations carried out on different wells in Soultz site. Because of a better access to reservoir properties and test data for the Soult site, a detailed analysis of shearing initiation and propagation can be provided using the prescribed methodology in section 3.2 and 3.3.

Dezayes et al. (2010) determined the characteristics of fracture zones in Soultz site. These fracture zones are permeable for which either important mud loss was detected during drilling operations or high water loss was related during stimulations. Therefore the fracture zones indicate potential main paths for fluid flow. The orientations of fracture

zones in the reservoir depth were collected (Table 3.2) where main stimulations were involved.

Table 3.2 Orientations of fracture zones in the reservoir depth of Soultz site (after Dezayes et al. 2010)

Well	Name	Depth (m)	Dip direction (°)	Dip (°)
GPK1	GPK1-FZ2815	2815	230	70
	GPK1-FZ3220	3223	50	75
	GPK1-FZ3490	3492	257	63
GPK2	GPK2-FZ4760	4760	250	65
GPK3	GPK2-FZ4890	4890	250	65
	GPK2-FZ5060	5060	250	65
	GPK3-FZ4770	4775	234	64
GPK4	GPK4-FZ4620	4620	285	78
	GPK4-FZ4710	4712	212	50
	GPK4-FZ4970	4973	276	81
	GPK4-FZ5050	5012	257	85
	GPK4-FZ5100	5100	255	69

Figure 3.10 shows equal area stereo plots of estimated critical pressure k_{pc} for shearing (left column) and critical pressure gradient (right column) in lower hemisphere for Soultz site. They were obtained following the same procedures as those in section 3.3.3 and 3.3.4, also

the attached contour lines keep the same definitions and physical interpretations (referred to texts used to explain Figure 3.5a and Figure 3.7). Moreover, the poles of detected fracture zones in the reservoir depth of Soultz site are included (white dots). The results were sub-divided into two cases due to the different stress conditions: $k_{\mathrm{H}} = 1.02$ and $k_{\mathrm{h}} = 0.5$ for relatively shallow reservoir (GPK1) and $k_{\mathrm{H}} = 1.12$ and $k_{\mathrm{h}} = 0.53$ for deep reservoir (GPK2-4). The orientation of maximum horizontal stress is N170°E (Valley and Evans, 2007). The water stimulation is considered and an intermediate frictional coefficient, 0.8, is adopted. The results in Figure 3.10 highlight that:

1) All the poles of fracture zones except one (212/50) are placed within the region defined by the outer contour line in the critical pressure k_{pc} plot, which means they can be sheared before the existence of fracture opening. In this regard, the analysis predicts a shearing dominated mechanism for stimulation.
2) Most of the poles of fracture zones are also located within the region constrained by the inner contour line in the critical pressure k_{pc} plot, which indicates they are with high tendency for shearing and can play significant roles with respect to stimulated region development and the seismicity.
3) All the poles for GPK1 and most of the poles for deep reservoir are well laid in the region defined by the distinguisher contour line of 9.8 MPa/km in the critical pressure gradient plot. According to the

proposed criterion for estimating shearing growth direction, Eq. (3.21), the analysis predicts the downward growth of shearing (induced seismicity) is predominant during the stimulation.

These findings are in general consistent with captured site observations even if there are much room for improvement in terms of the calibration with the exact depth information of permeable fracture zones and the pressure loss along the fracture and wellbore. However, this agreement of model predictions and site observations indicates that the proposed method can be potentially applicable to provide a primary evaluation in terms of the overall shearing development and the associated seismicity growth.

critical pressure k_{pc} for shearing

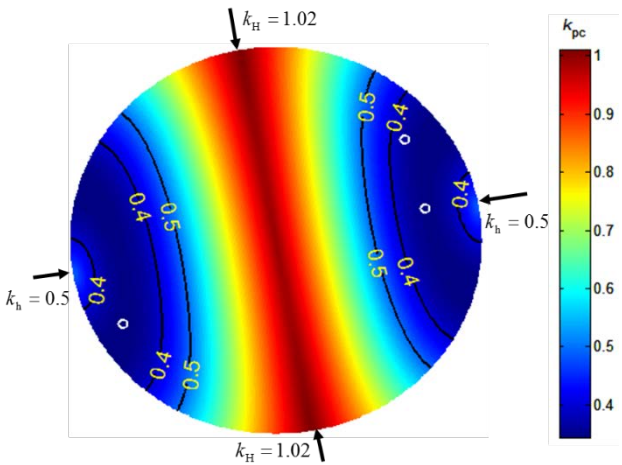

critical pressure gradient

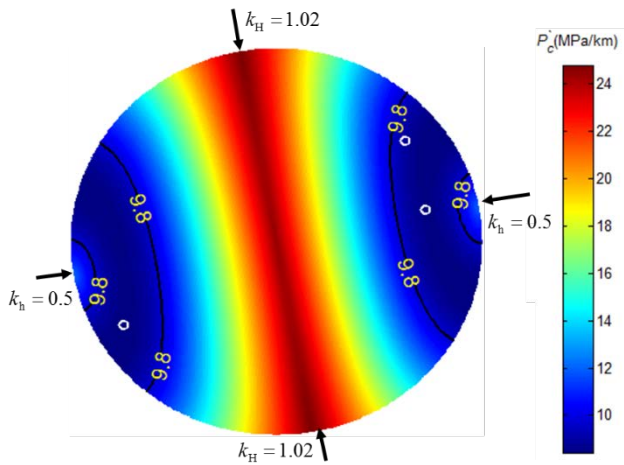

GPK1 (k_H=1.02, k_h=0.5)

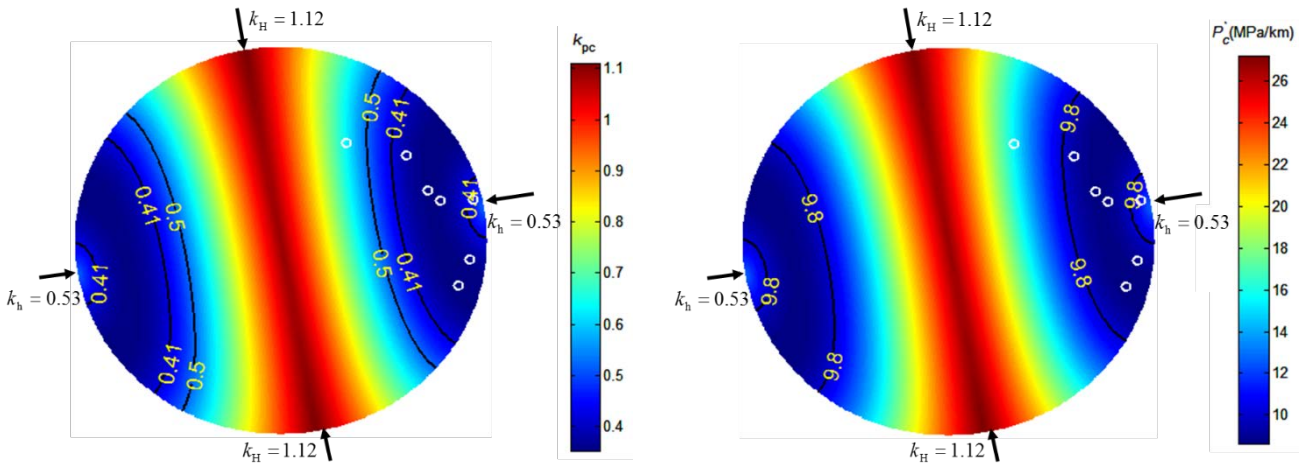

GPK2,3,4 (k_H=1.12, k_h=0.53)

Figure 3.10 Equal area stereo plots of estimated critical pressure k_{pc} for shearing (left column) and critical pressure gradient (right column) in lower hemisphere for Soultz site. In the plot of k_{pc}, the outer contour line, whose magnitude equals the minimum horizontal stress, defines the range of orientations possible for shearing before fracture opening, and the inner contour line with smaller value defines the range of orientations with high tendency for shearing in practice. In critical pressure gradient plot, the contour line, whose magnitude is 9.8 MPa/km because the water injection is considered, defines the range of orientations estimated for downward shearing. White dots are poles of permeable fracture zones detected at reservoir depth and most of them are predicted with high tendency for shearing with downward growth.

3.5 summary

A generic model to estimate the shearing initiation and propagation during hydraulic stimulation was developed based on the existing hydroshearing concept to consider the features of a massive volume injection in fractured crystalline rock through a long open well with the interval of hundreds of meters. From the geomechanical perspective, the shearing migration and associated growth of seismic events (upward or downward) depend on the fracture orientation, stress condition, fracture shear strength and injection fluid density.

The proposed model was applied to general studies on the effects of the stress condition on the shearing initiation and propagation, and also to selected field stimulation tests in major EGS projects. The lower bound of the critical pressure for shearing used in this study can be a simple but reliable indicator of the pressure at the onset of seismicity. Shear slip can usually be activated with less injection pressure for the NF and SS stress conditions than for the RF stress condition. Especially for extreme NF and SS stress regimes, the shear slip and associated seismicity can occur by a small injection pressure.

Considering the effects of the fracture slip and opening on the improvement of reservoir permeability and fluid diffusivity, the injection pressure accumulation tends to slow down with continuous injection. The maximum injection pressure that can be achieved in practice is

limited, constraining the portion of orientations for which the sliding is possible to occur. The fracture orientations with high tendency for shearing in practice are limited and only those requiring a critical pressure that is relatively easy to achieve during an injection operation are optimal for shearing. A way was proposed to conceptually compute the orientations possible for shearing and the orientations with high tendency for shearing in practice. The orientations with high tendency for shearing are featured as moderately, highly, and slightly dipped for NF, SS, and RF stress regimes, respectively, which is generally consistent with the field observations of seismic clouds. A narrow range of orientations can be sheared with high tendency in practice, which tends to result in a two-dimensionally stimulated zone with a small thickness. This can provide some insightful explanation to the observed mainly two-dimensionally featured seismic clouds for the major field stimulations in the previous EGS projects.

Upward growth of shearing prevails for most stress configurations, and only extreme NF and SS stress conditions may allow downward growth to occur, which may not be favorable for EGS project development. Employing a denser brine for stimulation tends to expand the stress range allowing downward growth of shearing, and it is practically applicable for activating slip at a deeper location of an open well with downward growth.

The proposed methodology was applied to the evaluation of Soultz site stimulation, for which the site stress condition and detected fracture zone orientations were covered. The analysis indicates downward shearing growth is dominant for natural fracture zones, which is generally consistent with the observed spatial feature of induced seismicity. The developed generic model can provide a primary assessment of the overall shearing growth and the migration of induced seismicity for massive stimulation during EGS project development.

Chapter 4. Hydraulic fracture initiation and propagation in EGS hydraulic stimulation

4.1 Introduction

Previous field experience of hydraulic stimulation demonstrates that the hydroshearing of pre-existing fractures and faults is the primary mechanism of permeability improvement (Jung, 2013), which is consistent with the induced seismicity when the injection pressure is lower than the minimum principal stress. However, the hydrofracturing mechanism cannot be excluded as it is an effective way to create fluid pathways. The early design and tests in Fenton Hill HDR project followed the concept of hydraulic fracturing and the wells were expected to be connected by a set of parallel fractures (Duchane and Brown, 2002). The hydraulic fracturing happened for the stimulation of Jolokia-1 well in Cooper Basin EGS site (Holl and Barton, 2015) and that of Gt GrSk 4/05 well in Groschonebeck EGS site (Zimmermann et al., 2008). Actually, tensile fractures by hydraulic fracturing are necessary to connect pre-existing structures in case that there are no optimal fractures crossing the open hole interval (Ito and Hayashi, 2003).

Compared with hydraulic fracturing treatments in the hydrocarbon field, there are three distinctive features with respect to the conditions of EGS stimulation: 1) an EGS well is usually completed with a long open

hole section, tens to hundreds of meters, in crystalline formation; 2) technical measures to isolate injection interval (e.g., isolation packers) are limited due to high temperature and 3) the deviated well design with varying well trajectory can be adopted in favor of configuring a multi-well system for heat extraction. The pressure shall accumulate on the wellbore wall of whole open hole interval during fluid injection. It is essential to estimate the location of fracture initiation in the open hole and the breakdown pressure when hydraulic fracturing happens during EGS stimulation. The fracturing propagation plays a vital role in the evolution of reservoir permeability and induced seismicity.

The basic equations describing the stress distribution on wellbore wall with arbitrary orientation can be found in various literature related to the study of inclined borehole failure (e.g., Bradley, 1979). Based on these stress equations and a certain fracturing criterion, hydraulic fracture initiation from arbitrarily oriented boreholes has been studied extensively (Hossain et al., 2000; Huang et al., 2012; Roegiers and Detoumay, 1988), which emphasizes the complication of fracture initiation added by the inclination of the borehole with respect to the in situ principal stress directions. Considering the feature of a long open hole with varying trajectory, the fracture initiation during EGS stimulation becomes more complicated.

In this chapter, the process of developing a generic model which can estimate the fracture initiation in open hole section and the overall

fracturing propagation during EGS hydraulic stimulation is presented, followed by general studies on the effects of in situ stress and open hole trajectory on hydraulic fracturing. The proposed model is then validated to the field case study of fracture initiation for Jolokia-1 hydraulic stimulation.

4.2 Theoretical foundations for hydraulic fracturing in EGS stimulation

4.2.1 Hydraulic fracture initiation in EGS open hole section

The fracture initiation mainly depends on: 1) in situ stress 2) applied injection pressure on wellbore wall, 3) orientation of the wellbore and 4) mechanical properties of the formation. Recognizing a long open hole section, even with varying trajectory, for EGS development, these governing parameters of fracture initiation shall be depth variable. In this regard, the fracturing is depth-dependent given that the fracture can initiate at any location of open hole section (e.g., the isolation packers can be applied on the wellbore wall fictitiously to seal off a short segment at the desired depth). In reality, the hydraulic fracturing should firstly occur at depth where the wellbore is most vulnerable to be fractured when subjected to the injection. Specifically, two fundamental questions need to be addressed with respect to fracture initiation in EGS hydraulic stimulation: the location where the fracturing is most preferable to happen and the associated breakdown pressure.

In spite of the complexity of the problem, the methodology presented here is within the framework of elastic hydraulic fracturing theory for simplified calculation, which shall be referred to as first order estimation consequently. The rock is treated as isotropic, homogeneous and linearly elastic material. The variability of rock strength and deformation properties with respect to well depth and the temperature is not considered for simplicity. Furthermore, the open hole trajectory is supposed to be smoothly varied with depth, which means small gradients of azimuth and inclination angle or low dog leg severity (DLS) of well trajectory. In this regard, it is assumed that the basic equations describing stress distribution around an inclined borehole are applicable at a specific depth of open hole section, even with varying trajectory.

The open hole configuration and stress conditions on wellbore wall at a specific depth are presented in Figure 4.1. The principal components of in situ stress are considered to be vertical and horizontal and a compression positive convention is followed. S_V , S_H and S_h denote field vertical and horizontal principal stresses, respectively ($S_H > S_h$). The minimum horizontal stress S_h is oriented from East direction with an angle of η measured counterclockwise. The well inclination angle refers to ψ and the azimuth angle refers to β. The well orientation is determined by the combination of ψ and β. Figure 4.1c shows stress components at a specific position of wellbore wall using a polar coordinate system. The circumferential position angle θ is measured

counterclockwise from x-axis as viewed downward from z-axis. It is highlighted that the stresses and well orientation are variable with depth, and thus all the variable notations shown in Figure 4.1 are ended with bracketed h, which means they are functions of the depth. In this chapter, depths are expressed in terms of true vertical depth (TVD) except specifically stated otherwise. For the stress, the notation S means a far field component while notation σ represents a component on wellbore wall.

In situ stress components associated with local coordinate system (x,y,z) which is aligned with wellbore orientation are obtained by applying stress tensor transformation upon field principal stresses.

$$\begin{Bmatrix} S_x(h) \\ S_y(h) \\ S_z(h) \\ S_{xy}(h) \\ S_{yz}(h) \\ S_{zx}(h) \end{Bmatrix} = \begin{bmatrix} \cos^2\psi(h)\cos^2\beta(h) & \cos^2\psi(h)\sin^2\beta(h) & \sin^2\psi(h) \\ \sin^2\beta(h) & \cos^2\beta(h) & 0 \\ \sin^2\psi(h)\cos^2\beta(h) & \sin^2\psi(h)\sin^2\beta(h) & \cos^2\psi(h) \\ -\frac{1}{2}\sin 2\beta(h)\cos\psi(h) & \frac{1}{2}\sin 2\beta(h)\cos\psi(h) & 0 \\ -\frac{1}{2}\sin 2\beta(h)\sin\psi(h) & \frac{1}{2}\sin 2\beta(h)\sin\psi(h) & 0 \\ \frac{1}{2}\sin 2\psi(h)\cos^2\beta(h) & \frac{1}{2}\sin 2\psi(h)\sin^2\beta(h) & -\frac{1}{2}\sin 2\psi(h) \end{bmatrix} \begin{Bmatrix} S_{\mathrm{h}}(h) \\ S_{\mathrm{H}}(h) \\ S_{\mathrm{V}}(h) \end{Bmatrix} \tag{4.1}$$

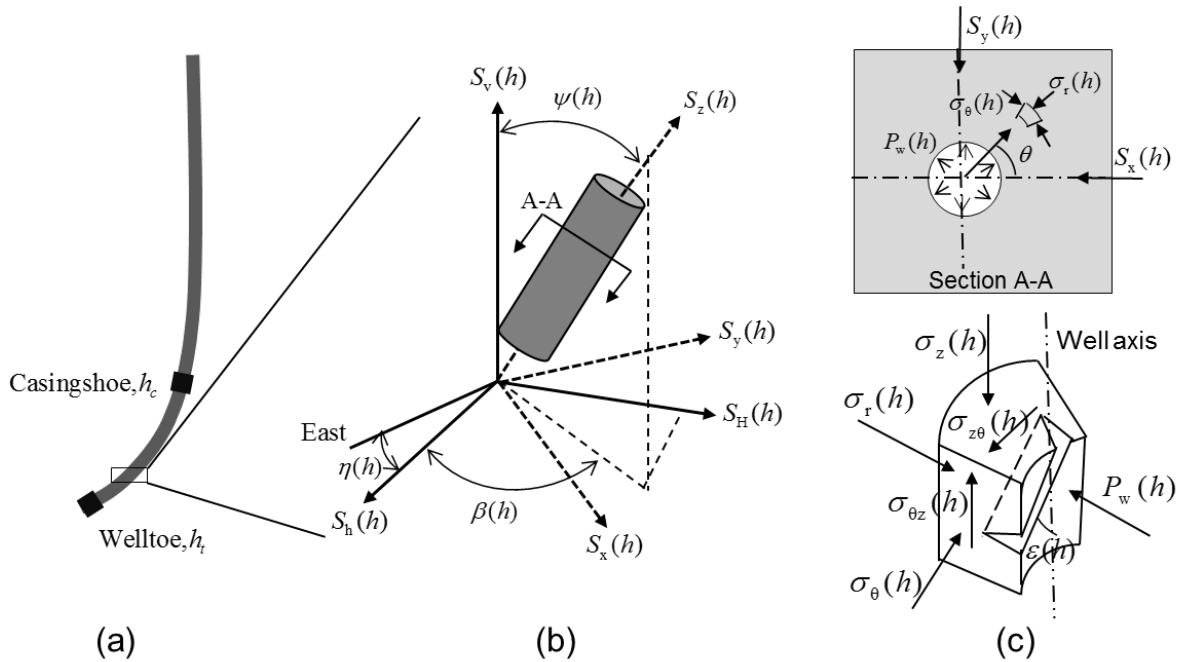

Figure 4.1 Well open section configuration and stress conditions on wellbore wall (modified from Hossain et al. (2000)). (a) well trajectory with a long open hole section from casing shoe to well toe; (b) well configuration at a specific depth of open hole section and in situ stress setting; (c) stress components on wellbore wall and hydraulic fracture trace (ε is angle between well axis and fracture trace line.

When a borehole is drilled into the formation, the stresses are significantly perturbed in the vicinity of the borehole resulting in the stress concentration. The stress components on the wall of an oriented wellbore are given as Eq. (4.2) (Bradley, 1979; Hossain et al., 2000; Huang et al., 2012).

$$
\begin{aligned}
&\sigma_r(h) = P_{\mathrm{p}}(h) \\
&\sigma_\theta(h) = S_x(h) + S_y(h) - 2(S_x(h) - S_y(h))\cos 2\theta - P_{\mathrm{p}}(h) - 4S_{xy}(h)\sin 2\theta \\
&\sigma_z(h) = S_z(h) - 2\nu(S_x(h) - S_y(h))\cos 2\theta - 4\nu S_{xy}(h)\sin 2\theta \\
&\sigma_{r\theta}(h) = \sigma_{rz}(h) = 0 \\
&\sigma_{\theta z}(h) = 2(-S_{xz}(h)\sin\theta + S_{yz}(h)\cos\theta)
\end{aligned}
\tag{4.2}
$$

where P_{p} is the applied well pressure and ν is the Poisson's ratio. On the wellbore wall, the radial stress σ_r is one of the principal stresses and equal to P_{p}. The other two principal stresses can be found as the eigenvalues of the stress tensor on wellbore wall and they are acting on a plane tangent to well axis. The principal stresses on wellbore wall are expressed as Eq. (4.3) and they are variable with circumferential position. It is clear that σ_1 and σ_2 are compressive, and only σ_3 can cause the tension (negative stress) on wellbore wall.

$$
\begin{aligned}
&\sigma_1(h) = \sigma_r(h) = P_{\mathrm{p}}(h) \\
&\sigma_2(h) = \frac{1}{2}\left[\left(\sigma_\theta(h) + \sigma_z(h)\right) + \sqrt{\left(\sigma_\theta(h) - \sigma_z(h)\right)^2 + 4\tau_{\theta z}(h)^2}\right] \\
&\sigma_3(h) = \frac{1}{2}\left[\left(\sigma_\theta(h) + \sigma_z(h)\right) - \sqrt{\left(\sigma_\theta(h) - \sigma_z(h)\right)^2 + 4\tau_{\theta z}(h)^2}\right]
\end{aligned}
\tag{4.3}
$$

According to hydraulic fracturing theory, a fracture initiates at a specific position of the wellbore wall where σ_3 reaches tensile strength of the formation, T_0 . The resulting fracture has the orientation perpendicular to the direction of σ_3 .

$$\sigma_3(h) = -T_0 \tag{4.4}$$

Considering the effects of in situ pore pressure and cooling induced thermal stress, a generalized concept of effective stress is adopted where both the pore pressure P_0 and thermal stress σ_{T} are included.

$$\sigma_3^{\mathrm{e}}(h) = \sigma_3(h) - P_0(h) + \sigma_{\mathrm{T}}(h) \tag{4.5}$$

Notice that the induced thermal stress is tensile or negative due to the cooling. Applying thermo-elastic theory, σ_{T} caused by a temperature perturbation of ΔT can be estimated using Eq. (4.6) (Jaeger et al., 2007).

$$\sigma_{\mathrm{T}}(h) = \frac{\alpha E \Delta T(h)}{1-\nu} \tag{4.6}$$

where α is the coefficient of thermal expansion and E is rock elastic modulus.

Thus Eq. (4.4) can be rewritten as

$$\sigma_3(h) = -T_0 + P_0(h) - \sigma_{\mathrm{T}}(h) \tag{4.7}$$

Combining Eqs. (4.3) and (4.7), the hoop stress σ_θ on wellbore wall becomes

$$\begin{aligned}
&\sigma_\theta(h) = C_1 / \mathrm{C}_2 \\
&C_1 = [\tau_{\theta z}{}^2(h) - (S_t - P_0(\mathrm{h}) + \sigma_T(\mathrm{h}))\sigma_z(h) - (S_t - P_0(\mathrm{h}) + \sigma_T(\mathrm{h}))^2] \\
&C_2 = (\sigma_z(h) + S_t - P_0(\mathrm{h}) + \sigma_T(\mathrm{h}))
\end{aligned} \tag{4.8}$$

Recall the expression of σ_θ in Eq. (4.2) and place it into Eq. (4.8). Simple mathematical manipulation provides the expression of the pressure required fracture initiation at a specific circumferential position θ of wellbore wall.

$$P_{\mathrm{w}}(h) = S_x(h) + S_y(h) - 2(S_x(h) - S_y(h))\cos 2\theta - 4S_{xy}(h)\sin 2\theta - C_1 / C_2 \tag{4.9}$$

For a specific depth of open hole section, the applied pressure on wellbore wall continues to increase until a fracture is initiated at a particular circumferential position (θ_{cr}), where the pressure firstly satisfies Eq. (4.9). In other words, the necessary pressure for fracture initiation at a specific depth is the minimum of P_{w} in terms of θ. To search this minimum, make

$$\frac{\partial P_{\mathrm{w}}(h)}{\partial \theta} = 0 \tag{4.10}$$

$$\frac{\partial^2 P_{\mathrm{w}}(h)}{\partial^2 \theta} > 0 \tag{4.11}$$

Direct solution of Eq. (4.10) and (11) is extremely difficult and no explicit expression is available. Alternatively, Eq. (4.10) can be solved using a common numerical method, e.g., Newton-Raphson method. Meanwhile Eq. (4.11) must be satisfied to ensure it is the minimum. Once the critical angle θ_{cr} is obtained, put it back into Eq. (4.9) for calculating the pressure required to initiate a fracture for a specific depth of open hole section.

$$P_{\mathrm{f}}(h) = [S_x(h) + S_y(h) - 2(S_x(h) - S_y(h))\cos 2\theta - 4S_{xy}(h)\sin 2\theta - C_1 / C_2]\Big|_{\theta_{\mathrm{cr}}(h)} \tag{4.12}$$

The generated fracture would be perpendicular to σ_3 of the particular position. The angle between wellbore axis and fracture trace line (ε in Figure 4.1) is called as trace angle with the following equation (e.g., Huang et al. 2012).

$$\tan(2\varepsilon(h)) = [\frac{2\tau_{\theta z}(h)}{\sigma_\theta(h) - \sigma_z(h)}]\Big|_{\theta_{\mathrm{cr}}(h)} \tag{4.13}$$

In reality, the trace angle of drilling induced tensile fracture can be detected from high-resolution borehole imaging loggings (e.g., Thorsen 2011).

When referring to wellhead pressure (WHP), it is simply treated by removing the corresponding fluid column pressure from bottom hole pressure (BHP). The WHP required for fracture initiation at a specific depth of open hole section is

$$P_{\mathrm{fwh}}(h) = P_{\mathrm{f}}(h) - \rho_{\mathrm{w}} g h \tag{4.14}$$

Where ρ_{w} is the density of injection fluid and g is the gravitational acceleration (9.8 m/s^2).

Subjected to injection, the WHP continues to increase until a fracture initiates at a particular depth of open hole section (h_{cr}), which is most vulnerable to the fracture initiation for given stress condition and open hole trajectory. Once fracture initiation location h_{cr} is obtained, put it back into Eq. (4.14) for computing the breakdown pressure P_{bwh} which is the minimum of P_{fwh}.

$$P_{\mathrm{bwh}} = P_{\mathrm{f}}(h_{cr}) - \rho_{\mathrm{w}}\, \mathrm{g}\, h_{cr} \tag{4.15}$$

Correspondingly, the initiated fracture trace angle in open hole section is

$$\tan(2\varepsilon(h_{\mathrm{cr}})) = \frac{2\tau_{\theta z}(h_{\mathrm{cr}})}{\sigma_{\theta}(h_{\mathrm{cr}}) - \sigma_{z}(h_{\mathrm{cr}})}\Big|_{\theta_{\mathrm{cr}}(h_{\mathrm{cr}})} \tag{4.16}$$

The methodology presented above is able to provide primary estimation of hydraulic fracturing initiation in EGS open hole section even with varying trajectory. The overall strategy is to perform exhaustive predictions of the location of fracture initiation and the magnitude of breakdown pressure with respect to the entire well depth, followed by the action to search the minimum fracturing pressure as the breakdown. The associated depth is considered as the most vulnerable

location for fracture initiation with the provided stress condition and open hole trajectory. The derivation process shows that the field stress, open hole trajectory and injected fluid are determining factors of fracturing initiation in EGS open hole section.

4.2.2 Hydraulic fracture propagation

Once a hydraulic fracture is initiated, it may propagate in a complex manner recognizing the local stress perturbation in the vicinity of wellbore. Nevertheless, the induced fracture shall eventually turn to align the plane normal to the orientation of minimum field principal stress (Yew and Weng, 2014), which requires a minimum energy for fracture development based on the mechanics of hydraulic fracturing.

Depending on the stress regime, the hydraulic fracture shall propagate vertically perpendicular to S_h (NF and SS stress regimes) or horizontally perpendicular to S_V (RF stress regime). Especially for the depth deeper than 2 km, the compilation of measured stress data supports that the minimum principal stress is generally horizontal (Brown and Hoek, 1978), implying the induced fracture is principally expected to be vertical. The EGS well is commonly completed in deep crystalline rock for necessary heat condition. In this regard, the injection induced fracture propagation in EGS reservoir can be simplified as vertical plane strain crack propagation subjected to the pressure loading (Figure 4.2).

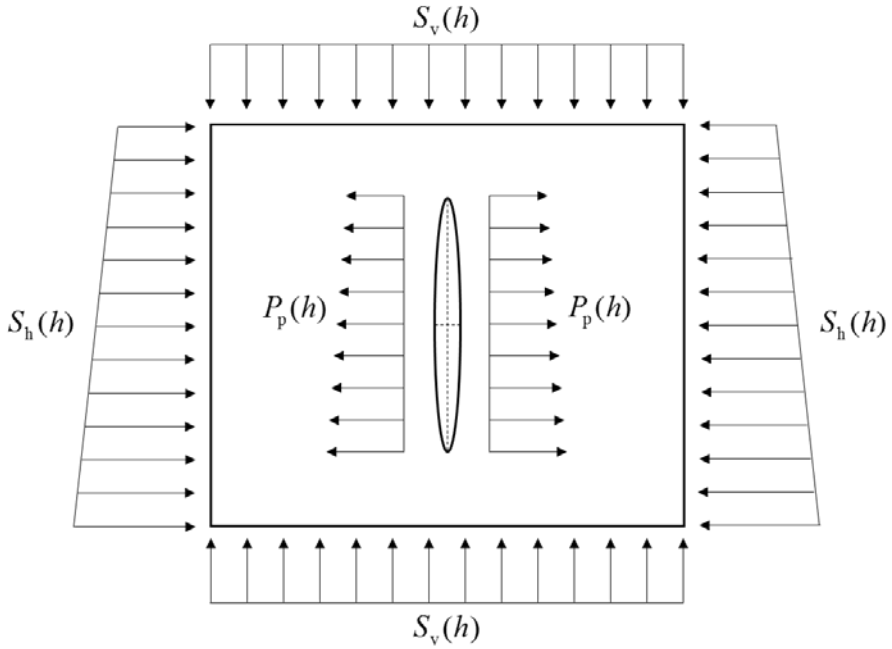

Figure 4.2 Vertical plane strain crack model subjected to insitu stress and injection pressure

Simonson et al. (1978) described that the propagation of a vertical hydraulic fracture (upward or downward) depends on the comparison between fluid pressure gradient and minimum stress gradient based on linear elastic fracture mechanics. Figure 4.3 is adopted to illustrate the physical process for determining fracture propagation direction in a straightforward manner. With continuous injection, the profile of applied pressure (dashed lines in Figure 4.3) moves toward the right hand side. For case I where fluid pressure gradient is bigger than the stress gradient, the positive net pressure first occurs at the bottom of the crack while the negative net pressure prevails in the upper section, which implies that the fracture tends to grow downward. Conversely, if the pressure gradient is less than the stress gradient, the positive net pressure is firstly reached at

the top of the crack and upward propagation of the fracture is desired (case II in Figure 4.3). Considering hydrostatic pressure distribution on the vertical fracture, the pressure gradient is directly determined by the applied fluid density.

$$P_{\mathrm{p}}'(h) = \rho_{\mathrm{w}} g \tag{4.17}$$

Clearly, the density of employed fracturing fluid impacts the propagation of a hydraulic fracture and applying a heavier brine tends to propagate a vertical fracture downward for the given stress condition.

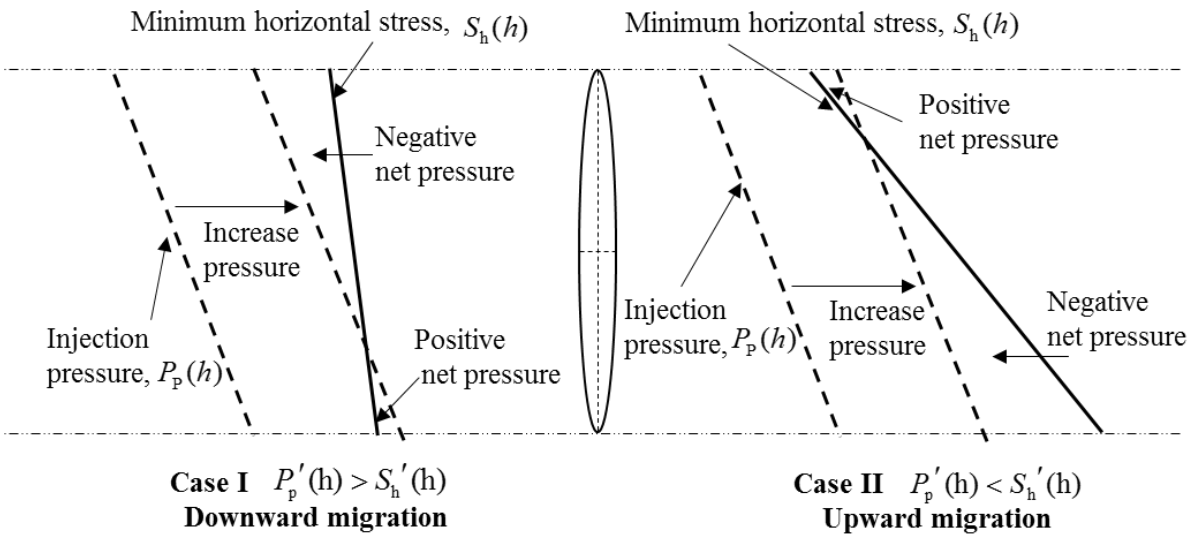

Figure 4.3 Demonstrating diagram of physical process to determine fracture propagation direction

4.3 Verification of stress computation of wellbore wall

The above stress derivation relies on the application of stress equations on inclined borehole wall by assuming the impacts of low dogleg severity (DLS) of well trajectory is negligible. This assumption is further verified by comparing finite element method (FEM) solution of the stress on borehole wall against that obtained using Eq. (4.3). A commercial code, COMSOL Multiphysics, was used which can provide accurate FEM solution of stress distribution for solid mechanics problems (COMSOL, 2013). As shown in Figure 4.4, the simulated model includes a rectangular block penetrated by the open hole section with building up inclination and the block is linear elastic (Young's modulus of 60 GPa and Poisson's ratio of 0.2). It is located below 4.0 km depth and subjected to a synthetic stress condition as $S_{\mathrm{V}} : S_{\mathrm{h}} : S_{\mathrm{H}} = 1:1.2:1.4$. As the vertical stress is treated as the rock overburden with a density of 2600 kg/m3, the stress magnitudes below 4.0 km are expressed as,

$$\begin{aligned} S_{\mathrm{V}}(h) &= 101.9 + 0.0255(h - 4000) \\ S_{\mathrm{h}}(h) &= 122.3 + 0.0306(h - 4000) \\ S_{\mathrm{H}}(h) &= 142.7 + 0.0357(h - 4000) \end{aligned} \tag{4.18}$$

Note that the vertical stress gradient is implemented by considering the gravity. Specifically, a vertical stress of 101.9 MPa is applied on the block upper surface and a roller boundary is placed on the block lower surface (Figure 4.4). Four cases with various open hole trajectory configurations were studied (Table 1), including a vertical well one (C0).

The synthetic wells are drilled parallel with the orientation of minimum horizontal stress, or the azimuth angle is 0°. The open hole section is linearly inclined with a given build-up rate (BUR) which is defined as the rate of change of the increasing inclination angle with respect to TVD. Besides the vertical case, three other tests are performed with the BUR of 0.03°/m (C1), 0.06°/m (C2) and 0.09°/m (C3). The attention is focused on the borehole wall stress for a depth interval of 500 m which corresponds to the well open section from 4.1 km to 4.6 km TVD. Note that the location and inclination angle of casing shoe are synchronized for these performed tests and the measured depth (MD) is different due to various open hole trajectories.

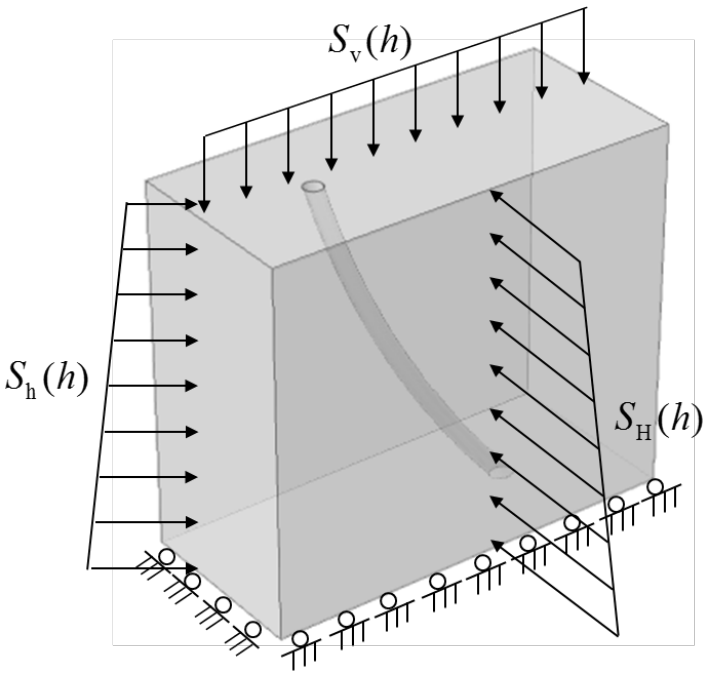

Figure 4.4 FEM model showing a block penetrated by the open hole with building up inclination and boundary conditions.

Table 4.1 Open hole trajectory settings for the performed tests of stress verification

Case	Azimuth (°)	BUR (°/m)	TVD (km)		MD (km)		inclination (°)	
			h_c	h_t	h_c	h_t	$\psi(h_c)$	$\psi(h_t)$
C0	0	0	4.1	4.6	4.1	4.6	0	0
C1	0	0.03	4.1	4.6	4.1	4.69	20	35
C2	0	0.06	4.1	4.6	4.1	4.74	20	50
C3	0	0.09	4.1	4.6	4.1	4.86	20	65

The results of the minimum principal stress on borehole wall for performed tests are shown in Figure 4.5. σ_3 is selected as the target parameter for the comparison because it is straightforwardly related to hydraulic fracture initiation and required breakdown pressure. The unfolding borehole wall image for stress plot visually presents the σ_3 distribution and more exact magnitude of the minimum σ_3, which determines the breakdown pressure according to the fracture initiation criterion, is provided in Figure 4.6.

In general, a good agreement is observed between the FEM solution of the stress on borehole wall and that obtained using Eq. (4.3), which supports the previous statement that stress equations of inclined borehole wall are applicable even for deviated wells with low DLS of the trajectory. Especially for vertical well case (C0), the great match between FEM result and analytical solution is found, indicating that the adopted

FEM mesh is sufficiently fine to obtain accurate stress distribution. Under given stress and well azimuth condition, the stress concentration on borehole wall is enhanced with increasing well inclination, which clearly demonstrates that the well trajectory impacts the stress distribution on borehole wall.

C0

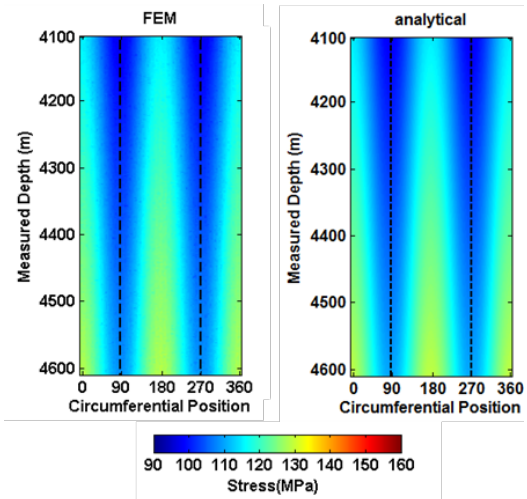

C1

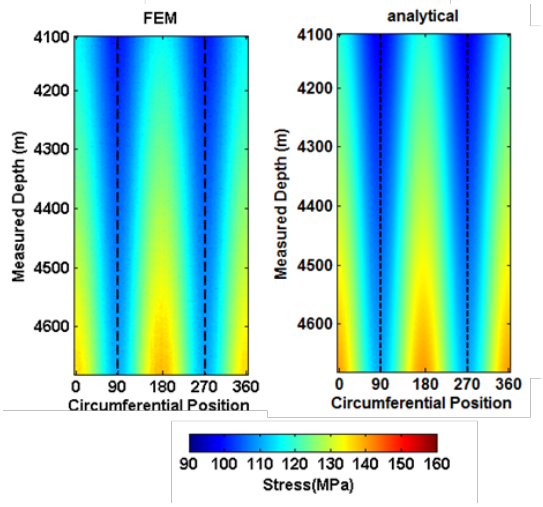

C2

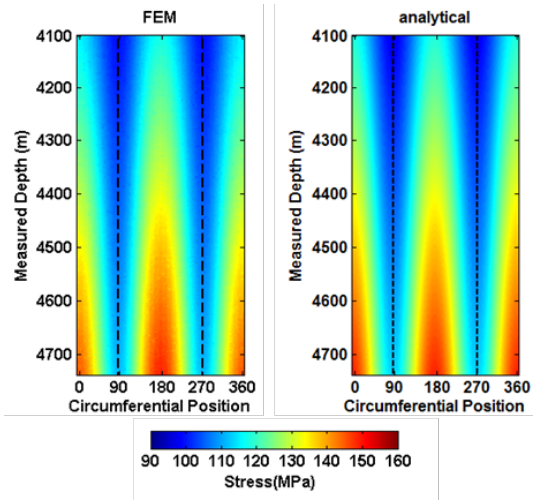

C3

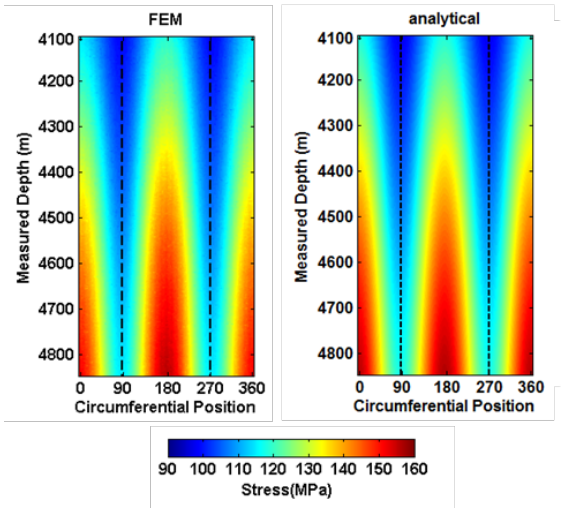

Figure 4.5 Comparison of σ_3 on borehole wall by FEM and that by Eq. (4.3). Two dashed lines represent a depth profile of the position of minimum σ_3.

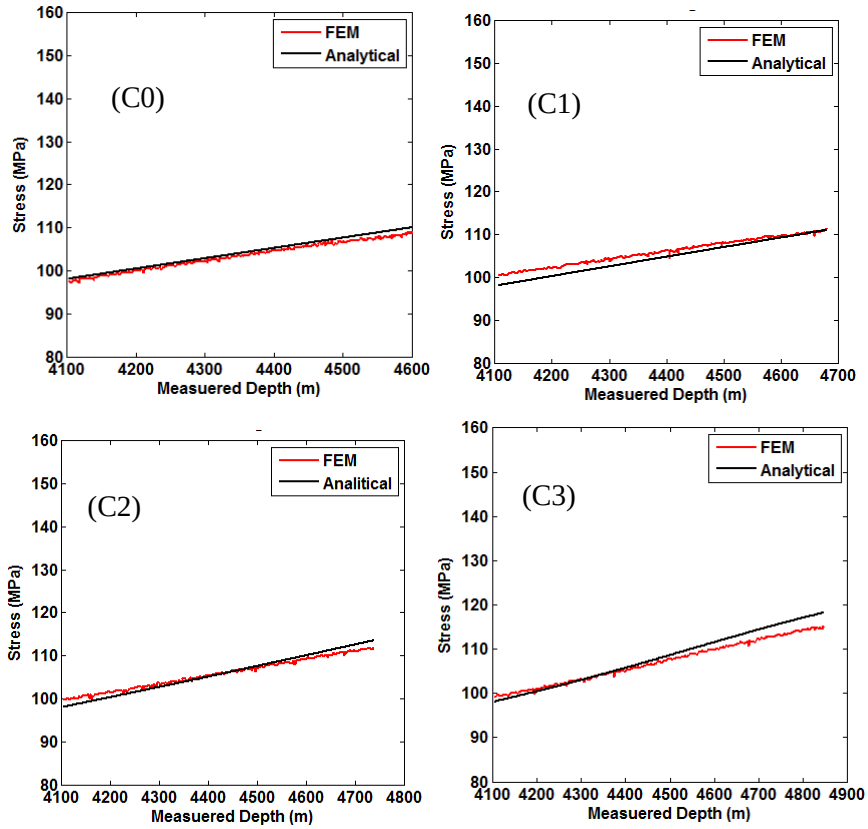

Figure 4.6 Comparison of minimum σ_3 profile on borehole wall computed by FEM and that by Eq. (4.3)

4.4 Effects of open hole trajectory and in situ stress on hydraulic fracturing in EGS stimulation

4.4.1 General configurations of studies

The studied stress conditions are identical with what presented in section 3.3.1.The ratios of maximum and minimum horizontal stress to vertical stress are defined as k_{H} and k_{h}, respectively. In kilometer-scale EGS reservoir of interest located in deep crystalline rock, the stress ratios can

be treated as constants, or the small variation is neglected. Equalizing vertical stress to the overburden, the three principal stresses are expressed as

$$\begin{aligned} S_{\mathrm{V}}(h) &= \rho_{\mathrm{r}} g h \\ S_{\mathrm{H}}(h) &= k_{\mathrm{H}} \rho_{\mathrm{r}} g h \\ S_{\mathrm{h}}(h) &= k_{\mathrm{h}} \rho_{\mathrm{r}} g h \end{aligned} \tag{4.19}$$

The general studies in this section consider a range of stress ratios from 0.5 to 2.0 as shown in Figure 3.3. This suggested stress range is common at depths below 1000 m (Brown and Hoek, 1978) and well covers the field stress states at reservoir depths for major existing EGS sites in the world (Xie et al., 2015).

The impacts of open hole trajectory and stress condition on hydraulic fracture initiation are coupled and complicated. To simplify the study and presentation, the open hole interval is either in the holding section or in the building section if the well is completed by directional drilling. The holding section basically corresponds to a straight but inclined open hole trajectory. For the building section, the open hole is assumed to be completed along a constant azimuth direction while the inclination is linearly varied with a given BUR with respect to TVD. For concise presentation, they are called as inclined open hole and building open hole respectively. Obviously the vertical open hole can be treated as a special case of inclined open hole whose azimuth and inclination are zero.

The tensile strength of rock is usually negligible for field hydraulic fracturing treatments considering the fact that its magnitude is small and ubiquitous flaws in the rockmass can further reduce it. Thus no tensile strength is included in this section. The thermal stress induced by the cooling is disregarded as well for simplicity. Actually, it is hard to estimate the temperature perturbation when hydraulic stimulation is operated because the surrounding rockmass has experienced multiple processes related to temperature alteration. The ignorance of cooling induced thermal stress tends to provide a conservative estimation of breakdown pressure because the temperature drop decreases compressive stresses on borehole wall. Nonetheless, the thermal stress can be considered for site specific application provided that the reliable temperature logging is available.

The rock density of 2600 kg/m^3 is assumed so the vertical principal stress gradient is 25.48 MPa/km. 0.2 is used for rock Poisson's ratio. Unless otherwise specifically stated, pure water injection (ρ_w =1000 kg/m^3) is considered and the pressure gradient is 9.8 MPa/km. No in situ pore pressure is considered corresponding to a hot dry rock condition.

4.4.2 Upward growth of hydraulic fracturing

For EGS projects subjected to NF or SS stress regime conditions, vertical hydraulic fracture propagation is expected in crystalline reservoir. For

configured stress condition as Eq. (4.19), the minimum horizontal stress gradient is

$$S_{\mathrm{h}}'(h) = k_{\mathrm{h}} \rho_{\mathrm{r}} g \tag{4.20}$$

$S_{\mathrm{h}}'(h)$ is no less than 12.74 MPa/km for the studied stress range ($k_{\mathrm{h}} \geq 0.5$). Obviously, the stress gradient is bigger than pressure gradient (9.8 MPa/km), which indicates upward growth of hydraulic fracturing according to the proposed methodology shown in Figure 4.3.

The issue of hydraulic fracture height growth has been a focus in the oil and gas engineering because of the concerns about upward propagation of hydraulic fracture to create potential connecting pathways resulting groundwater pollution (Davies et al., 2012; Flewelling and Sharma, 2014). Both field fracture growth data and theoretical mechanism studies support that vertical fracture growth is constrained in oil and gas sedimentary formations (Fisher and Warpinski, 2012; Flewelling et al., 2013; Simonson et al., 1978). The dominant mechanism lies in the contrasts of in situ stress and material properties between the cap rock and pay zone. Unlike the sedimentary layer condition in oil and gas reservoir, the EGS reservoir commonly targets to deep thick crystalline layer for necessary temperature condition. Continuous stress state and relative homogeneous properties for crystalline formation indicate less containment of vertical fracture propagation. In this regard, the upward growth of hydraulic fracturing is

expected to be more significant in EGS stimulation than in oil and gas hydraulic treatments.

For EGS development, the upward growth of fracturing augments the need of fracture initiation at deeper location of open hole section (e.g., well toe location) because this can connect a hotter temperature condition with the identical well depth. Besides, the upward vertical fracture implicates that the inclined or even horizontal well rather than vertical one, which enhances the possibility of penetration of the well into a hydraulic fracture, is an optimum option. This tends to create active connection between injection and production wells and eventually be beneficial to form a multi-well system.

4.4.3 Hydraulic fracture initiation

Implementing the previously stated configurations (Eq. (4.19) of in situ stress, zero tensile strength, zero thermal stress and no pore pressure) in Eqs. (4.1) and (4.8), Eq. (4.12) of the pressure required to initiate a fracture can be rewritten as

$$P_{\mathrm{f}}(h) = \lambda(\beta(h), \psi(h), \theta_{\mathrm{cr}}(h), k_{\mathrm{h}}, k_{\mathrm{H}})\rho_{\mathrm{r}} gh \tag{4.21}$$

where variable λ is defined as the coefficient of fracture pressure gradient. Notice that the circumferential angle $\theta_{cr}(h)$ is the function of $\beta(h)$, $\psi(h)$, k_{h} and k_{H}, and Eq. (4.21) is expressed as

$$P_{\mathrm{f}}(h) = \lambda(\beta(h), \psi(h), k_{\mathrm{h}}, k_{\mathrm{H}})\rho_{\mathrm{r}} gh \tag{4.22}$$

When the open hole interval lies in the holding section of a well, which means an inclined and straight trajectory with provided inclination β and azimuth ψ, the gradient of fracture initiation pressure is

$$P_{\mathrm{f}}'(h) = \lambda(\beta, \psi, k_{\mathrm{h}}, k_{\mathrm{H}})\rho_{\mathrm{r}} g \tag{4.23}$$

$P_{\mathrm{f}}'(h)$ is constant for an inclined open hole subjected to given stress condition. The fracture initiation pressure is positively proportional to its gradient and, intuitively, a bigger gradient corresponds to a bigger fracturing pressure at a specific depth.

As illustrated in Figure 4.7, the fracture initiation location in open hole section is determined by the comparison between applied pressure gradient and fracture pressure gradient. When $P_{\mathrm{p}}'(h) > P_{\mathrm{f}}'(h)$, the fracture is initiated at well toe location because the injection pressure firstly exceeds fracturing pressure there. On the contrary, the fracture shall start at casing shoe location when $P_{\mathrm{p}}'(h) < P_{\mathrm{f}}'(h)$.

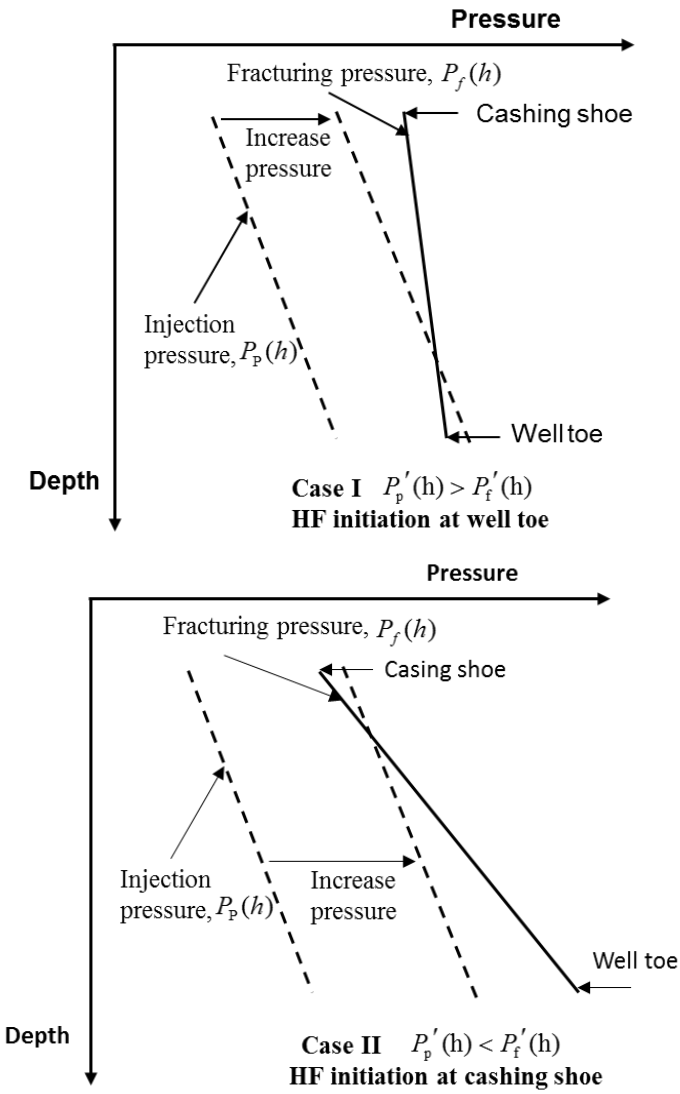

Figure 4.7 Demonstrating diagram for determining fracture initiation location when the open hole interval lies in well holding section.

Figure 4.8 shows fracture pressure gradient $P_f'(h)$ for various stress conditions when a vertical open hole trajectory is adopted. The results were computed by a 0.02 increment for k_H and k_h. The contour line of 9.8 MPa/km, representing applied pressure gradient $P_p'(h)$, is used to

distinguish the stress ranges for fracture initiation location based on proposed method shown in Figure 4.7. It is obvious that fracture initiation at casing shoe location prevails for most stress conditions and only severe SS stress case (high stress ratio of S_H to S_h) allows fracture initiation at well toe location.

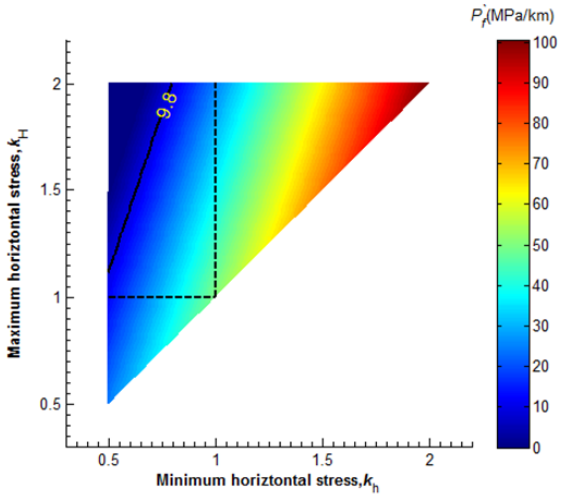

Figure 4.8 Fracture pressure gradient for vertical open hole trajectory. The contour line of 9.8 MPa/km represents applied pressure gradient and the stress conditions with $P_f'(h)$ less than 9.8 MPa/km allow fracture initiation at well toe location.

It should be recognized that, depending on the stress condition, the vertical open hole may not be the optimum option for reducing breakdown pressure. Figure 4.9a shows the magnitude of minimum fracturing pressure gradient searched from all orientations for inclined open hole scenario. The corresponding inclination (Figure 4.9b) and

azimuth (Figure 4.9c) defining the orientation of the open hole with the minimum $P_{\mathrm{f}}'(h)$ are also obtained.

The computed results show that the open hole orientation with the minimum $P_{\mathrm{f}}'(h)$ is horizontally parallel with S_{H} for NF stress regime, vertical for SS stress regime and horizontally parallel with S_{h} for RF stress regime, which is consistent with the statement that the wellbore oriented along the intermediate principal stress requires the minimum pressure for fracture initiation (Huang et al., 2012). Comparing the results shown in Figure 4.8 and Figure 4.9, it is inferred that the inclined open hole design may reduce the required breakdown pressure for NF and RF stress regimes. However, the minimum $P_{\mathrm{f}}'(h)$ is still over applied pressure gradient of 9.8 MPa/km, indicating that inclined open holes are not able to make fracture initiation at well toe location according to the criterion of determining fracture initiation location shown in Figure 4.7.

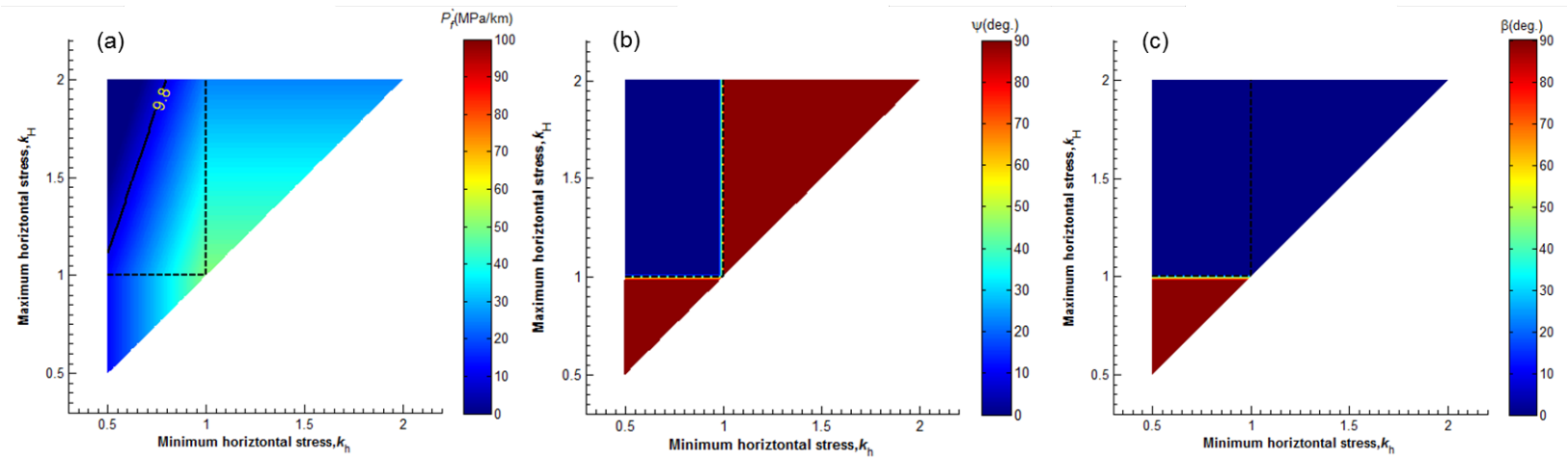

Figure 4.9 Minimum fracture pressure gradient for inclined open hole trajectory (a) and its corresponding well inclination (b) and azimuth (c). The well orientation with the minimum $P_f'(h)$ is horizontally parallel with S_H for NF stress regime, vertical for SS stress regime and horizontally parallel with S_h for RF stress regime.

For a building open hole trajectory, the inclination $\psi(h)$ varies with depth by a provided BUR, so the fracture pressure gradient expressed as Eq. (4.22) is not constant for the given stress condition. In this regard, the generic idea of determining fracture initiation in open hole section by comparing $P_{\mathrm{p}}'(h)$ and $P_{\mathrm{f}}'(h)$ is not applicable. Recognizing it is difficult to provide general solution, efforts were made to carry out some specific synthetic tests to demonstrate the effects of building open hole on hydraulic fracture initiation for EGS stimulation.

Table 4.2 lists the stress condition and open hole trajectory settings for the performed synthetic tests. A moderate NF stress condition (k_{h} = 0.6 and k_{H} = 0.8) is adopted and assume the minimum horizontal stress is oriented in East-West direction. The building open hole trajectory extends from 4.0 km to 4.5 km TVD and is intermediately inclined from 30° to 75° (0.09°/m of BUR). Six cases, one vertical as the benchmark and other five with an azimuth angle of 0°, 30°, 45°, 60° and 90° respectively, are included in this study.

Table 4.2 Stress and open hole trajectory settings for performed tests

Case	Stress		Azimuth (°)	BUR (°/m)	TVD (km)		inclination (°)	
	k_h	k_H			h_c	h_t	$\psi(h_c)$	$\psi(h_t)$
C0	0.6	0.8	0	0	4.0	4.5	0	0
C1	0.6	0.8	0	0.09	4.0	4.5	30	75
C2	0.6	0.8	30	0.09	4.0	4.5	30	75
C3	0.6	0.8	45	0.09	4.0	4.5	30	75
C4	0.6	0.8	60	0.09	4.0	4.5	30	75
C5	0.6	0.8	90	0.09	4.0	4.5	30	75

Figure 4.10 shows an unfolded borehole wall image plot for the computed wellhead pressure required for fracture initiation. These plots, which were obtained using one meter increment of the depth and one degree increment of circumferential position angle, can visually present the required fracturing pressure at any position of wellbore wall if a fracture is initiated. Intuitively, the position with minimum pressure is where the fracture shall initiate for the open hole (square mark in the plot) and this minimum pressure is the required breakdown pressure. The dashed line represents a depth profile of vulnerable position for fracture initiation where the minimum σ_3 lies. Physically, this can be treated as the potentially mapped longitudinal fracture trace along open hole section. By symmetry, there is one more profile which is 180 degrees apart in the plot. Actually, the wellbore image loggings frequently show an En echelon pattern of drilling induced tensile fractures and a set of

longitudinal fractures can be observed macroscopically. This longitudinal fracture commonly consists of many small inclined cracks which correspond to tensile fractures initiated along the well axis (e.g., Thorsen (2011) and Okabe et al. (1998)).

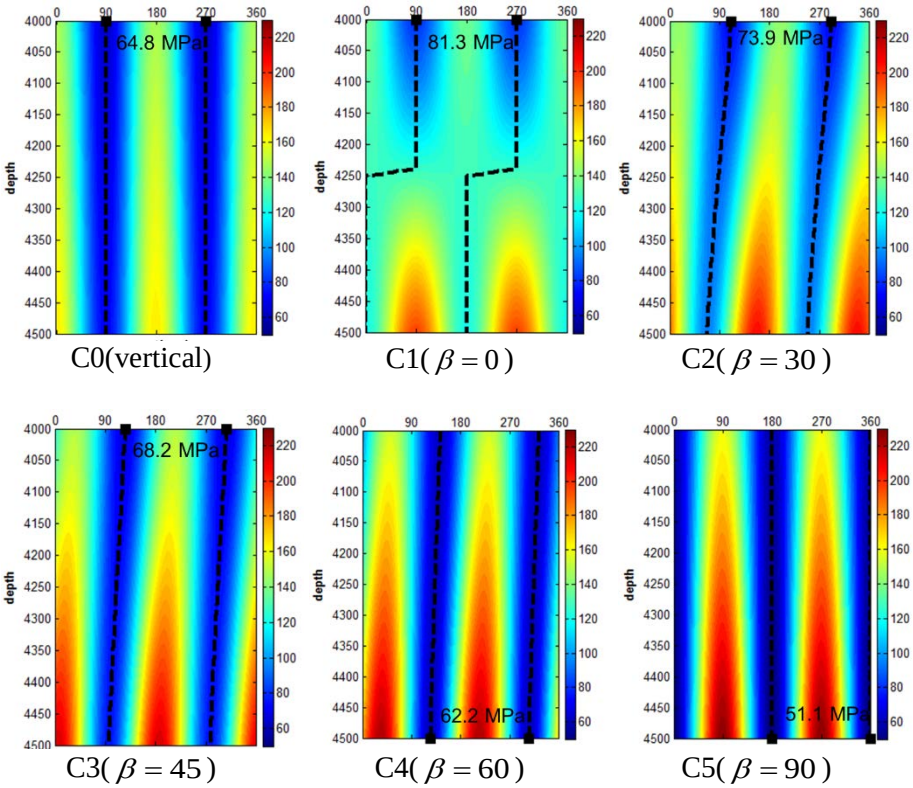

Figure 4.10 Unfolded wellbore wall image plots to show required fracturing pressure at any position of borehole wall for performed demonstrating tests subjected to NF stress condition (k_h = 0.6 and k_H = 0.8). Dashed lines represent a depth profile of vulnerable position for fracture initiation, and square marks indicate predicted fracture initiation location in open hole section and the associated breakdown pressure.

The results show that fracture initiation location shifts from casing shoe to well toe when the open hole azimuth increases sufficiently and

the predicted breakdown pressure monotonically decreases with increasing azimuth. Obviously, building open hole trajectory with high azimuth (C5) is optimal design for fracture initiation for current stress condition (k_h = 0.6 and k_H = 0.8) as it requests a low pressure to initiate the fracture at well toe location. Besides, the vulnerable circumferential position for fracturing is variable with well inclination because the angular position where the minimum σ_3 places varies with the deviation (Yew and Li, 1988). For case C1 where the open hole lies along the minimum horizontal stress, there is a particular inclination at which the vulnerable fracturing position shifts by 90 degrees. This phenomenon was also reported by (Yew and Li, 1988). It is caused by abrupt change of the orientation of the minimum σ_3 on wellbore wall with increasing well inclination.

Similarly, synthetic tests subjected to a SS stress regime (k_h = 0.8 and k_H = 1.2) and a RF stress regime (k_h = 1.2 and k_H = 1.4) are performed. The open hole trajectory configurations keep identical with those for a NF stress regime (Table 4.2). Figure 4.11 shows the results of tests under SS stress regime. The predicted fracture initiation location is at casing shoe section regardless of open hole azimuth. The required breakdown pressure decreases with well azimuth in a monotonic manner, however, the vertical case needs the minimum breakdown pressure, which is consistent with the results shown in Figure 4.9.

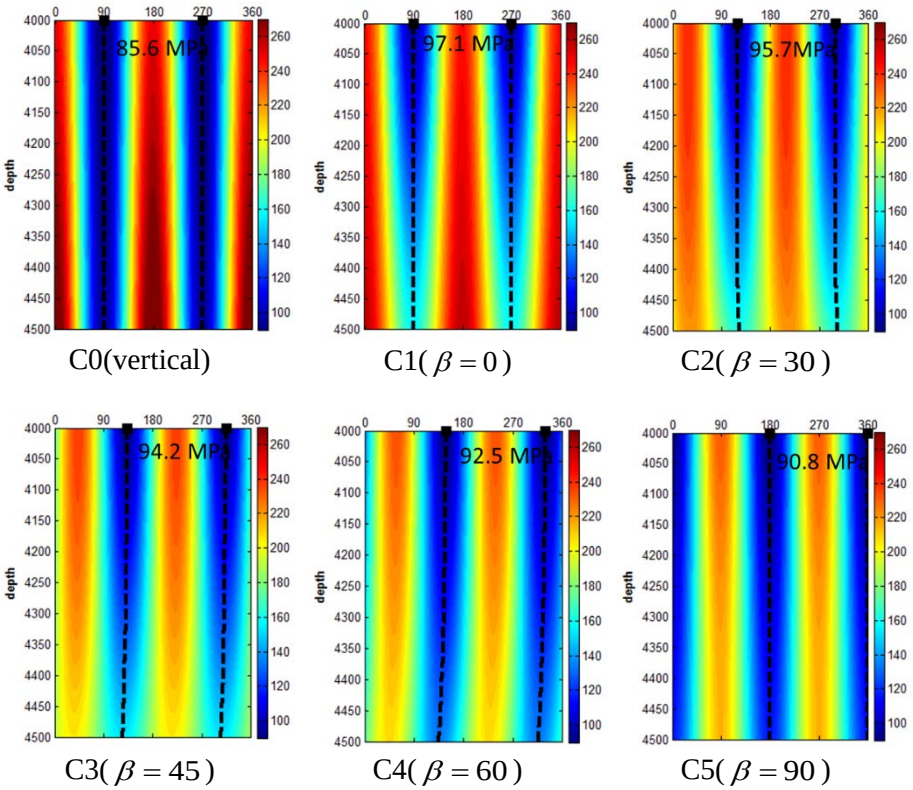

Figure 4.11 Unfolded wellbore wall image plots to show required fracturing pressure at any position of borehole wall for performed demonstrating tests subjected to SS stress condition (k_h = 0.8 and k_H = 1.2).

Figure 4.12 presents the test results of the scenario with RF stress regime. It is inspiring to observe that a fracture initiates at well toe location for all cases with a building trajectory, and the required breakdown pressures are much lower compared with vertical well case. The performed tests clearly demonstrate that the building open hole trajectory impacts hydraulic fracturing in terms of the magnitude of breakdown pressure and fracture initiation location.

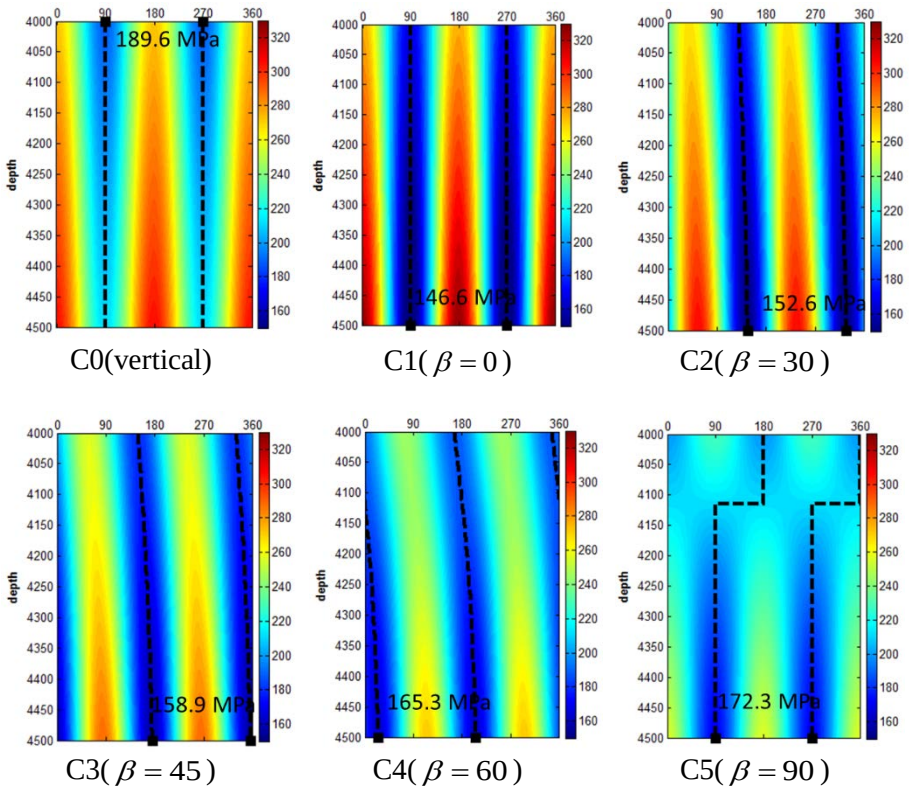

Figure 4.12 Unfolded wellbore wall image plots to show required fracturing pressure at any position of borehole wall for performed demonstrating tests subjected to RF stress condition (k_h = 1.2 and k_H = 1.4).

For EGS development, it is desired to stimulate deeper reservoir to access hotter geothermal resources by less drilling depth. In this regard, open hole trajectory optimization is targeted to allow fracture initiation at a deeper section using a lower injection pressure. The above studies imply that an inclined open hole design can reduce breakdown pressure but may not sufficient for fracture initiation at well toe location. A building open hole design may achieve both purposes simultaneously. However, the detailed site specific analysis is required because the result

heavily depends on open hole trajectory. Besides, it should be highlighted that a heavier fluid (e.g., NaCl brine) is beneficial for fracture initiation at a deeper location in open hole section because this tends to increase applied pressure gradient.

4.5 Validation against field hydraulic stimulation at Jolokia-1

Since 2002, Geodynamics Limited (GDY) has been developing an EGS system in Cooper Basin, approximately 900 km north of Adelaide, Australia. Four deeps wells (Habanero-1 to Habanero-4) were completed in the Habanero field and massive volume hydraulic stimulations were conducted to improve the reservoir conductivity mainly by shearing a major subhorizontal fault (Holl and Barton, 2015). The Jolokia-1 well which was hydraulically stimulated in 2010 is located about 9 km west of the Habanero field. Its open hole section holds a building trajectory of 540 m length along the north direction and the inclination increases from 14.5° at 4343 m TVD (casing shoe) to 39.1° at 4831 m TVD (well toe) (Jeffrey et al., 2012).

Figure 4.13 records the pressure and injection rate history for Jolokia-1 stimulation. In general, the injection was performed by a surface pressure limit of 10,000 psi using NaCl and NaBr brines. For NaCl brine injection, the injection rate was in the order of 1 L/s, which is one to two orders less than typical magnitudes observed in Habanero

stimulations at Cooper Basin (Baisch et al., 2009; Baisch et al., 2015). Little injectivity improvement was achieved by injecting NaCl brine and then the NaBr brine was injected to increase bottom hole pressure. The pressure applied using NaBr brine was approximately 20 MPa higher than the minimum principal stress, which induced obvious increase of injection rate (about 6 L/s). However, no long term increase of the injectivity was achieved. In this regard, it is believed that the hydraulic fracturing happened by applying NaBr brine (Holl and Barton, 2015). Unlike the stimulations in the Habanero field, where strong seismicity and obvious injectivity improvement occurred at a pressure level below the minimum principal stress, high-pressure stimulation in Jolokia-1 well caused only minor seismicity and much lower injection rates (Baisch et al., 2015). In this section, the developed model is applied to analyze the hydraulic fracturing initiation for Jolokia-1 stimulation.

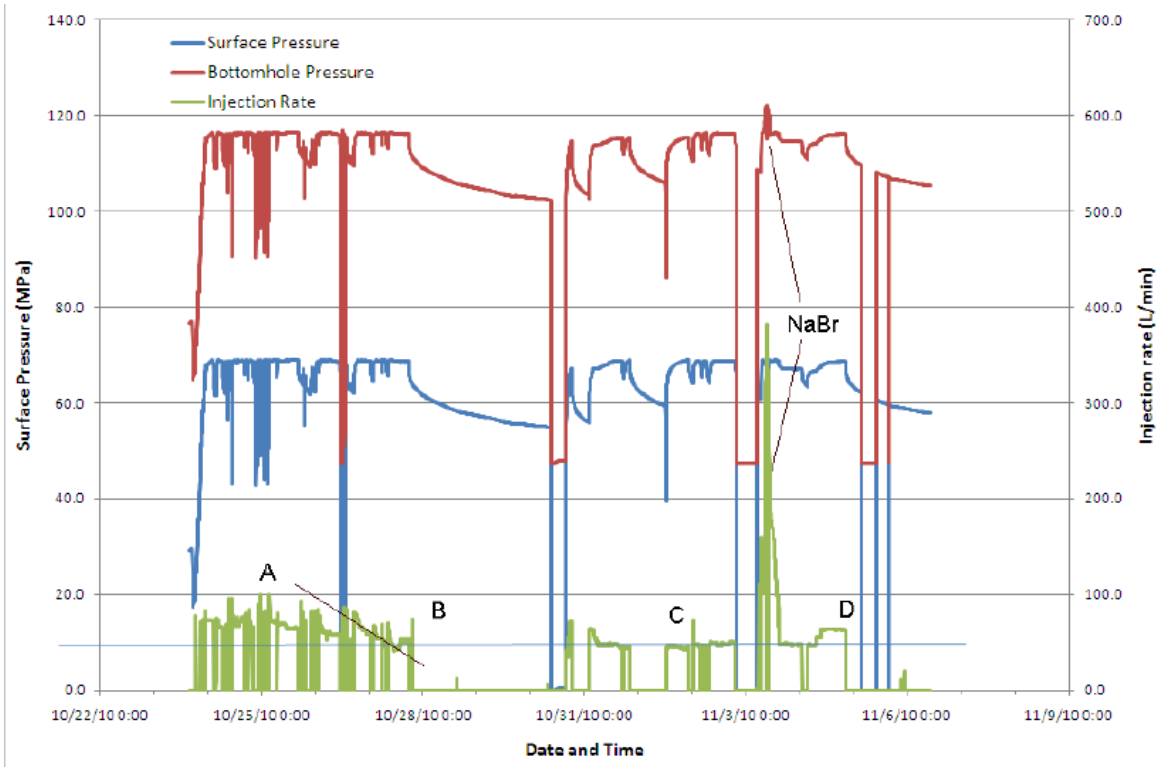

Figure 4.13 Pressure and injection rate history for Jolokia-1 stimulation (Jeffrey et al., 2012). The bottom hole pressure is calculated at 4370 m depth by adding fluid column pressure.

Table 4.3 lists the data in terms of the stress, open hole trajectory and pressure conditions for Jolokia-1 stimulation, compiled from a technical report by Jeffrey et al. (2012). Consistent borehole breakout and tensile induced fracturing are detected for Habanero and Jolokia deep wells, and the in situ stress is inversed from measured wellbore failure. The estimated stress ratios of Jolokia-1 deep reservoir are k_H = 1.51 and k_h = 1.03-1.22 depending on the interpretation of observed wellbore failure loggings, and S_H is oriented in E-W direction. The stress magnitudes shown in the table are based on average density of 2400 kg/m^3 for overburden rock. It is assumed that the open hole trajectory linearly increases from 14.5° to 39.1° for the simplification.

A significant overpressure condition occurs in the field and the pore pressure P_0 ranges from 75 MPa to 78 MPa for the open hole depth. The fracturing starts when the injection pressure reaches 125.6 MPa at well toe depth, which is supported by the recorded response of obvious increase of the injection rate during NaBr brine injection. Besides, 10 MPa of rock tensile strength is adopted and no cooling induced stress is considered as the injection rate applied is small (in order of 1 L/s).

Table 4.3 Stress, open hole trajectory and pressure condition for Jolokia-1 stimulation, compiled from Jeffery et al., (2012)

	TVD (m)	k_h	k_H	S_v (MPa)	ψ (°)	P_0 (MPa)	P_P (MPa)
Casing shoe	4343	1.03-1.22	1.51	102.6	14.5	75	119
Well toe	4831			114.8	39.1	78	125.6

Four scenarios are studied with the stress ratios of k_h varying from 1.05 to 1.20 by an increment of 0.05. In Figure 4.14, colored solid lines are computed depth profiles of fracture initiation pressure and colored dash lines represent injection pressure distribution in the open hole interval when it first satisfies fracturing pressure or the breakdown happens. The injection pressure profiles are prepared using a gradient of 13.67 MPa/km, corresponding to the density of 1395 kg/m^3 for NaBr brine. Because of building up inclination of the open hole trajectory, the profiles of fracture initiation pressure perform nonlinearly with respect to the depth. They also vary with the insitu stress condition. It is obvious that, except the case with k_h =1.05, the first intersection of applied pressure and fracturing pressure profile is at well toe for the other three cases and the applied pressure is below required fracturing pressure for the upper section of open hole, which means fracture initiation at well toe location for Jolokia-1 stimulation. Moreover, the certainty of fracture initiation at well toe is enhanced with the stress condition of a higher

ratio of k_h because the gap between applied pressure and required fracturing pressure is enlarged for the upper section of open hole.

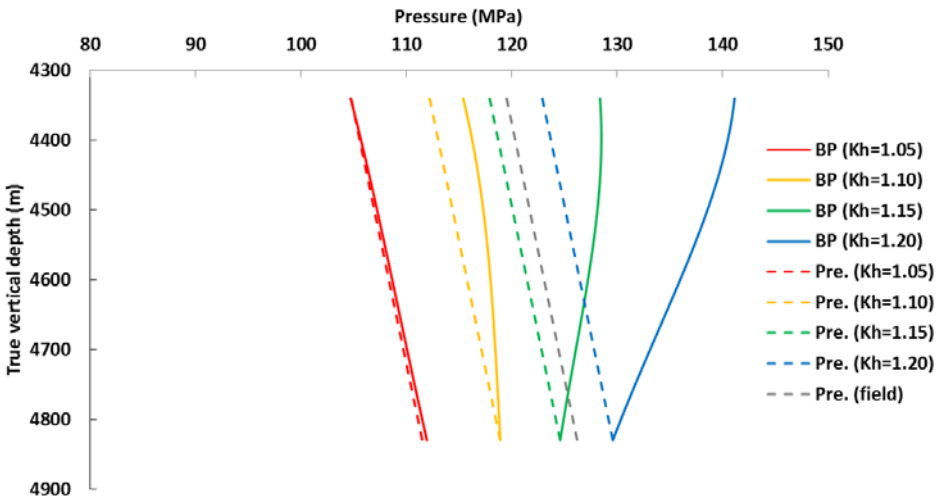

Figure 4.14 Depth profile of fracture initiation pressure (color solid lines) and injection pressure profile in the open hole section for the breakdown (color dashed lines). The case in grey represents field observation of injection pressure when the fracturing starts during the stimulation. Fracture initiation at well toe location prevails for provided stress conditions

Around 220 seismic events were recorded over the stimulation period and the following half year post the stimulation, and their hypocenters are located in close vicinity of open hole section (less than 100 m lateral distance from well trajectory), aligning steeply dipped fractures (Baisch et al., 2015). The induced seismicity can be linked to the shearing of natural fractures connected by induced tensile fractures when subjected to high injection pressure. However, it is not sufficiently fine to determine the location of fracturing initiation.

Jeffrey et al. (2012) supports fracture initiation from well toe section based on detected low instantaneous shut-in pressure (ISIP) drops at shut-in. With given open hole trajectory and stress condition for Jolokia-1, an axial fracture aligning S_H would be initiated and then reoriented to become horizontal away from the well, which forms a tortuous opening mode fracture. A high ISIP pressure drop after shut-in is expected for the fracture with significant tortuosity. The recorded low ISIP pressure drop is more consistent with fracture initiation at well toe location because a fracture initiating at the well toe, which is inclined by 39.1° from vertical, would develop less tortuosity than one starting from the casing shoe. In addition, the real field observation of injection pressure when the fracturing initiates (grey dashed line in Figure 4.14) is located between required pressures of the cases with k_h =1.15 and k_h =1.20. In this regard, the analysis of fracturing initiation can further constrain the stress ratio of k_h as 1.15-1.20.

4.6 Summary

A generic model is developed to estimate hydraulic fracture initiation location and the associated breakdown pressure for fluid injection subjected to a long open hole section even with varying trajectory during EGS system development. From the geomechanical perspective, the fracturing initiation in open hole section mainly depends on the field stress condition, temperature perturbation, open hole trajectory and

injection fluid density. The effects of open hole trajectory and in situ stress are coupled and complicated. The fracturing growth direction in host crystalline rock (upward or downward for NF and SS stress regimes) depends on the comparison between applied fluid pressure gradient and the minimum principal stress gradient.

For common stress range at deep formation (0.5-2.0 for stress ratios of horizontal to vertical), the upward growth of hydraulic fracturing is allowed for NF and SS stress regimes. It is expected that this upward growth of fracturing is more significant in EGS crystalline formation than in oil and gas sedimentary structures where the vertical fracture growth is constrained because of the contrasts of field stress and material properties. In favor of accessing hotter geothermal resources, it is necessary to initiate a fracture at deeper location in open hole section and this necessity is augmented by the upward growth of fracturing.

In kilometer-scale EGS reservoir of interest subjected to stress condition of constant ratio, the gradient of fracture initiation pressure is constant for an inclined open hole and the fracture initiation location is determined by the comparison of injection pressure gradient and fracture pressure gradient. Fracture initiation at casing shoe section prevails for common stress state at deep formation and the stress condition of high ratio (extreme SS stress state) may allow fracture initiation at well toe location. In NF and RF stress regimes, an inclined open hole tends to reduce fracture pressure gradient and breakdown pressure compared with

vertical trajectory but this decrease is commonly not sufficient to make fracture initiation at well toe section. For an open hole with building up trajectory, the performed synthetic tests demonstrate that the fracture initiation location may shift from casing shoe to well toe by a lower breakdown pressure, which is consistent with the target of open hole trajectory optimization. Employing a denser brine tends to induce fracture initiation at a deeper location in open hole interval because this results in the increase of applied pressure gradient.

The developed methodology of estimating fracture initiation in EGS open hole section was applied to the field case study of Jolokia-1 hydraulic stimulation for which the fracturing happened by injecting NaBr brine. The analysis indicates fracture initiation at well toe location for provided stress condition and open hole trajectory of Jolokia-1, which is consistent with the previous estimation according to recorded low ISIP drops at shut-in. By reversing observed breakdown pressure, the stress ratio of minimum horizontal to vertical is further constrained as 1.15-1.20.

Chapter 5. Conclusions and discussions

5.1 Conclusions

In this thesis, the main chapters (2, 3 and 4) are presented in the form close to journal publication. Detailed summaries and conclusions shall be referred to the end of each chapter.

A geomechanical review of the key characterization and performance parameters of field hydraulic stimulation tests on seven EGS or HDR projects was performed. The analytical geomechanical models were developed to provide primary estimation of shearing initiation location, the required pressure and the overall shearing growth direction corresponding to hydroshearing mechanism, and fracturing initiation and propagation corresponding to the hydrofracturing concept.

The comparative analysis on reservoir conditions, test parameters and test observations suggests that 1) the reservoir stress regime impacts the growth of stimulated region and the reverse faulting stress regime can be favorable for the layout of multiple well system as it may lead to a horizontally or sub-horizontally oriented stimulated zone; 2) there is strong dependency of injectivity on injection pressure and a high pressure makes a better hydraulic injectivity during stimulation and consequently afterwards for circulation; 3) the stimulated region and number of induced seismic events are mainly injection volume

controlled and the potential strategy to reduce seismic risks is either to extend stimulation in time or to separate stimulation in space; and 4) the differential stress condition is one of the necessary factors to raise a large magnitude event (LME) and the difference of maximum injection pressure achieved over that at onset of seismicity is an important additional factor to induce LMEs.

The shearing initiation and migration depend on the fracture orientation, stress condition, fracture shear strength and injection fluid density. General studies on the effects of the stress condition on the shearing initiation and propagation indicate that: 1)the pressure required to activate a shear slip and the associated seismicity is mainly impacted by the field stress; 2) optimal shearing orientations are featured as moderately, highly and slightly dipped for the NF, SS, and RF stress regimes, respectively, which is generally consistent with the field observations of seismic clouds; and 3) Shearing at casing shoe with upward growth prevails for most stress conditions, and only extreme NF and SS stress conditions may allow shearing at well toe with downward growth.

The fracturing initiation in open hole section mainly depends on the field stress condition, temperature perturbation, open hole trajectory and injection fluid density. The fracturing growth direction depends on the comparison between applied fluid pressure gradient and the minimum principal stress gradient. General studies on the effects in situ stress and

open hole trajectory on hydraulic fracturing indicate that 1) the upward growth of vertical fracture is expected for NF and SS stress regimes; 2) the fracture initiation at casing shoe section prevails for common stress range at deep formation; 3) an inclined open hole tends to decrease fracture pressure gradient for NF and RF stress regimes and 4) an open hole with building up trajectory may shift fracture initiation location from casing shoe to well toe by a lower breakdown pressure.

5.2 Discussions

The presented models for estimation of initiation and propagation of hydroshearing and hydrofracturing is based on the assumption of hydrostatic pressure distribution along the fracture, which disregards the transient evolution of pressure gradient during injection. In this regard, one meaningful future study is to implement the transient pressure distribution in the models and to evaluate its effects on shearing and fracturing. Better refined conclusions with respect to the effects of stress condition and well trajectory are expected.

The correlation analysis and generic studies here demonstrated important geomechanical factors impacting the initiation and propagation of shearing and fracturing, and therefore the induced seismicity. Especially, the comparison of pressure gradient and stress gradient plays a determinant role. The gradients make sense for large

scale problem and laboratory injection experiments are not a viable option to study the overall propagation of shearing and fracturing.

The outputs of field tests and general studies on the effects of field stress demonstrated that fractures optimally oriented for shear slip are moderately, highly and slightly dipped for the NF, SS, and RF stress regimes, respectively. This implicates the future strategy of well layout for better connection with stimulated reservoir: horizontal or highly inclined for NF and SS stress condition, and vertical or slightly inclined for RF stress regime.

As elaborated, the high differential stress condition or anisotropic stress is favorable for reducing the pressure required for activating shear slip and making downward growth of slip. The virgin stress difference may be enhanced by the stress perturbation caused by the complicated thermo-hydro-mechanical (THM) process during fluid injection. For example, the injection induced deformation generally results in a bigger stress change in horizontal direction than that in vertical because the formation can deform freely at the surface (Lee et al., 2013). The presented analytical models do not consider the stress perturbation and extending efforts are worthwhile for this issue.

Field tests or numerical simulations with field scale are necessary to provide more consolidated validations and elaborate information on the effects of each factors. In particular, numerical modellings provide cost effective ways to perform generic studies with respect to the strategies

of altering pressure and stress gradient even though field experiment must ultimately be carried out to verify model results. The validated models produce novel ideas for deep well placement (well orientation and spacing) and hydraulic stimulation design.

The presented models provide general description on initiation and propagation of shearing and fracturing, and also the associated induced seismicity. They lack the capabilities of the direct characterization of reservoir transmissivity or permeability enhancement which shall be the ultimate goal of hydraulic stimulation. The reservoir transmissivity prediction has to heavily depend on numerical methods considering the complex hydro-mechanical (HM) coupling process in the fractured formation where it is difficult to characterize the fracture properties such as size, roughness, dilation and connectivity. Some experiment and numerical studies discover that the permeability improvement in the direction perpendicular to the shear slip is more significant than that in the direction parallel to it (e.g., Yeo et al., 1998), which indicates the necessity of employing three-dimensional models for realistic representation of transmissivity evolution.

The hydraulic aperture plays a controlling role in fluid flow of fractured rock mass and its magnitude increase relies on the fracture dilation associated with shear slip. The appropriate shear dilation model corresponding to high confining stress condition is one prerequisite for studying the evolution of reservoir transmissivity. Numerous

experimental tests of fracture shear slip and dilation (e.g., direct shear test) under high loading conditions are irreplaceable to obtain realistic dilation model and parameters.

The top priority of future study is to build and validate a field scale numerical model which can address the HM coupling process during the whole injection and shut-in stage. Specifically, much effort is needed to make the simulation capture the transient pressure-injection rate response, the evolution of reservoir transimisivity and the occurrence of induced seismicity. Eventually, given site specific inputs, the well defined numerical models are useful to provide reliable predictions of potential stimulation tests and also to improve the interpretation of field test observations.

The Korean government has launched a pilot EGS project in Pohang since 2010. Two deep wells (PX-1 and PX-2) were completed below 4 km depth in the granite basement. First stage of hydraulic stimulation was carried out in February 2016 and more stimulations have to be performed to achieve the target of MW scale electricity generation. The developed analytical methods and subsequent numerical models are potentially applicable to the stimulation campaigns of Pohang EGS site.

References

Amadei, B., Stephansson, O., 1997. Rock stress and its measurement. Springer Science & Business Media. PP. 30-32.

Anderson, E.M., 1951. The dynamics of faulting and dyke formation with applications to Britain. Hafner Pub. Co.

Baisch, S., McMahon, A., 2014. Seismic real-time monitoring of a massive hydraulic stimulation of a geothermal reservoir in the Cooper Basin, Australia. Paper presented at the EAGE/DGG Workshop on Microseismic Monitoring, Karlsruhe, Germany. DOI: 10.3997/2214-4609.20140005.

Baisch, S., Rothert, E., Stang, H., Vörös, R., Koch, C., McMahon, A., 2015. Continued Geothermal Reservoir Stimulation Experiments in the Cooper Basin (Australia). Bulletin of the Seismological Society of America, 105(1), 198-209.

Baisch, S., Vörös, R., Weidler, R., Wyborn, D., 2009. Investigation of fault mechanisms during geothermal reservoir stimulation experiments in the Cooper Basin, Australia. Bulletin of the Seismological Society of America, 99(1), 148-158.

Baria, R., Baumgärtner, J., Rummel, F., Pine, R.J., Sato, Y., 1999. HDR/HWR reservoirs: concepts, understanding and creation. Geothermics, 28(4), 533-552.

Baria, R., Jung, R., Tishner, T., Nicholls, J., Michelet, S., Sanjuan, B., Soma, N., Asanuma, H., Dyer, B., Garnish, J., 2006. Creation of an

HDR reservoir at 5000 m depth at the European HDR project. Paper presented at the Thirty-First Workshop on Geothermal Reservoir Engineering, Stanford University, Stanford, California, USA. Retrieved 21 June, 2016 from http://www.geothermal-energy.org/pdf/IGAstandard/SGW/2006/baria1.pdf.

Baria, R., Michelet, S., Baumgärtner, J., Dyer, B., Nicholls, J., Hettkamp, T., Teza, D., Soma, N., Asanuma, H., Garnish, J., 2005. Creation and mapping of 5000 m deep HDR/HFR reservoir to produce electricity. Paper presented at the Proc. World Geothermal Congress, Antalya, Turkey. Paper No. 1627.

Barton, C.A., Zoback, M.D., Moos, D., 1995. Fluid flow along potentially active faults in crystalline rock. Geology, 23(8), 683-686.

Barton, N., 1973. Review of a new shear-strength criterion for rock joints. Engineering Geology, 7(1973), 287-332.

Batchelor, A., Baria, R., Hearn, K., 1983. Monitoring the effects of hydraulic stimulation by microseismic event location: a case study. Paper presented at the SPE Annual Technical Conference and Exhibition, San Francisco, California, USA. Paper No. SPE-12109-MS.

Baumgartner, J., Jung, R., Gérard, A., Baria, R., Garnish, J., 1996. The European HDR project at Soultz sous forets: Stimulation of the second deep well and first circulation experiments. Paper presented at twenty-first Workshop on Geothermal Reservoir Engineering, Stanford University, Stanford, California, USA. Paper No. SGP-TR-151-37.

Bertani, R., 2016. Geothermal power generation in the world 2010–2014 update report. Geothermics, 60, 31-43.

Bradley, W., 1979. Failure of inclined boreholes. Journal of Energy Resources Technology, 101(4), 232-239.

Breede, K., Dzebisashvili, K., Liu, X., Falcone, G., 2013. A systematic review of enhanced (or engineered) geothermal systems: past, present and future. Geothermal Energy, 1(1), 1-27.

Brown, D., 1995. The US hot dry rock program-20 years of experience in reservoir testing. Paper presented at the Proc. World Geothermal Congress, Florence, Italy. PP. 2607-2611.

Brown, D.W., Duchane, D.V., Heiken, G., Hriscu, V.T., 2012. Mining the earth's heat: hot dry rock geothermal energy. Springer Science & Business Media. PP. 313-422.

Brown, E., Hoek, E., 1978. Trends in relationships between measured in-situ stresses and depth. International Journal of Rock Mechanics and Mining Sciences & Geomechanics Abstracts, 15(4), 211-215.

Brudy, M., Zoback, M., Fuchs, K., Rummel, F., Baumgärtner, J., 1997. Estimation of the complete stress tensor to 8 km depth in the KTB scientific drill holes: Implications for crustal strength. Journal of Geophysical Research: Solid Earth (1978–2012), 102(B8), 18453-18475.

Byerlee, J., 1978. Friction of rocks. Pure and applied geophysics, 116(4-5), 615-626.

Charléty, J., Cuenot, N., Dorbath, L., Dorbath, C., Haessler, H., Frogneux, M., 2007. Large earthquakes during hydraulic stimulations at the geothermal site of Soultz-sous-Forêts. International Journal of Rock Mechanics and Mining Sciences, 44(8), 1091-1105.

Chen, D., 2010. Concepts of a basic EGS model for the Cooper Basin, Australia. Paper presented at the 2010 World Geothermal Congress (WGC 2010), Bali, Indonesia. Paper No. 3141.

Chen, D., Wyborn, D., 2009. Habanero field tests in the Cooper Basin, Australia: a proof-of-concept for EGS. Geothermal Resources Council Transactions, 33(1), 159-164.

COMSOL. 2013. Structural mechanics module user's guide, version 4.3b.

Cornet, F., Bérard, T., Bourouis, S., 2007. How close to failure is a granite rock mass at a 5km depth? International Journal of Rock Mechanics and Mining Sciences, 44(1), 47-66.

Davies, R.J., Mathias, S.A., Moss, J., Hustoft, S., Newport, L., 2012. Hydraulic fractures: How far can they go? Marine and petroleum geology, 37(1), 1-6.

Dezayes, C., Genter, A., Valley, B., 2010. Structure of the low permeable naturally fractured geothermal reservoir at Soultz. Comptes Rendus Geoscience, 342(7), 517-530.

DiPippo, R., 2012. Geothermal power plants: principles, applications, case studies and environmental impact: Butterworth-Heinemann. PP. 1-17.

Dorbath, L., Cuenot, N., Genter, A., Frogneux, M., 2009. Seismic response of the fractured and faulted granite of Soultz-sous-Forêts (France) to 5 km deep massive water injections. Geophysical Journal International, 177(2), 653-675.

Dreesen, D.S., Nicholson, R., 1985. Well completion and operations for MHF of Fenton Hill HDR Well EE-2. Retrieved from http://www.osti.gov/scitech/servlets/purl/5747481.

Duchane, D., Brown, D., 2002. Hot dry rock (HDR) geothermal energy research and development at Fenton Hill, New Mexico. Geothermal Heat Center Bulletin, 13-19.

Evans, K., Moriya, H., Niitsuma, H., Jones, R., Phillips, W., Genter, A., Sausse, J., Jung, R., Baria, R., 2005. Microseismicity and permeability enhancement of hydrogeologic structures during massive fluid injections into granite at 3 km depth at the Soultz HDR site. Geophysical Journal International, 160(1), 388-412.

Evans, K.F., 2005. Permeability creation and damage due to massive fluid injections into granite at 3.5 km at Soultz: 2. Critical stress and fracture strength. Journal of Geophysical Research: Solid Earth, 110(B4). DOI: 10.1029/2004JB003169.

Evans, K.F., Zappone, A., Kraft, T., Deichmann, N., Moia, F., 2012. A survey of the induced seismic responses to fluid injection in geothermal and CO 2 reservoirs in Europe. Geothermics, 41, 30-54.

Fehler, M.C., 1989. Stress control of seismicity patterns observed during hydraulic fracturing experiments at the Fenton Hill Hot Dry Rock geothermal energy site, New Mexico. International Journal of Rock

Mechanics and Mining Sciences & Geomechanics Abstracts, 26(3), 211-219.

Fisher, M.K., Warpinski, N.R., 2012. Hydraulic-fracture-height growth: Real data. SPE Production & Operations, 27(01), 8-19.

Flewelling, S.A., Sharma, M., 2014. Constraints on upward migration of hydraulic fracturing fluid and brine. Groundwater, 52(1), 9-19.

Flewelling, S.A., Tymchak, M.P., Warpinski, N., 2013. Hydraulic fracture height limits and fault interactions in tight oil and gas formations. Geophysical Research Letters, 40(14), 3602-3606.

Gaucher, E., Schoenball, M., Heidbach, O., Zang, A., Fokker, P., van Wees, J. D., & Kohl, T., 2015. Induced seismicity in geothermal reservoirs: Physical processes and key parameters. Paper presented at the Proc. World Geothermal Congress, Melbourne, Australia. Paper No. 31042.

Genter, A., Evans, K., Cuenot, N., Fritsch, D., Sanjuan, B., 2010. Contribution of the exploration of deep crystalline fractured reservoir of Soultz to the knowledge of enhanced geothermal systems (EGS). Comptes Rendus Geoscience, 342(7), 502-516.

Ghassemi, A., 2012. A review of some rock mechanics issues in geothermal reservoir development. Geotechnical and Geological Engineering, 30(3), 647-664.

Häring, M.O., Schanz, U., Ladner, F., Dyer, B.C., 2008. Characterisation of the Basel 1 enhanced geothermal system. Geothermics, 37(5), 469-495.

Holl, H., Barton, C., 2015. Habanero field: Structure and state of stress. Paper presented at the Proc. World Geothermal Congress, Melbourne, Australia. Paper No. 31034.

Hossain, M., Rahman, M., Rahman, S., 2000. Hydraulic fracture initiation and propagation: roles of wellbore trajectory, perforation and stress regimes. Journal of Petroleum Science and Engineering, 27(3), 129-149.

Huang, J., Griffiths, D., Wong, S.-W., 2012. Initiation pressure, location and orientation of hydraulic fracture. International Journal of Rock Mechanics and Mining Sciences, 49, 59-67.

Ito, T., Hayashi, K., 2003. Role of stress-controlled flow pathways in HDR geothermal reservoirs. In Thermo-Hydro-Mechanical Coupling in Fractured Rock. Birkhäuser Basel. PP. 1103-1124.

Ito, T., Zoback, M.D., 2000. Fracture permeability and in situ stress to 7 km depth in the KTB scientific drillhole. Geophys. Res. Lett, 27(7), 1045-1048.

Jaeger, J.C., Cook, N.G., Zimmerman, R., 2007. Fundamentals of rock mechanics: John Wiley & Sons.

Jeanne, P., Rutqvist, J., Dobson, P.F., Walters, M., Hartline, C., Garcia, J., 2014. The impacts of mechanical stress transfers caused by hydromechanical and thermal processes on fault stability during hydraulic stimulation in a deep geothermal reservoir. International Journal of Rock Mechanics and Mining Sciences, 72, 149-163.

Jeffrey, R., Wu, B., Zhang, X., Choi, X., Shen, B., 2012. An analysis of the stimulation of Jolokia-1 carried out during October and November 2010. CSIRO report.

Jung, R., 2013. EGS—Goodbye or Back to the Future. Paper presented at the ISRM International Conference for Effective and Sustainable Hydraulic Fracturing, Brisbane, Australia. DOI: 10.5772/56458.

Kagel, A., Bates, D., Gawell, K., 2005. A guide to geothermal energy and the environment. Geothermal Energy Association Washington, DC.

Kaieda, H., Sasaki, S., Wyborn, D., 2010. Comparison of characteristics of micro-earthquakes observed during hydraulic stimulation operations in Ogachi, Hijiori and Cooper Basin HDR projects. Paper presented at the Proc. of the World Geothermal Congress (WGC2010), Bali, Indonesia. Paper No. 3157.

Ladner, F., Häring, M.O., 2009. Hydraulic characteristics of the basel 1 Enhanced Geothermal system. Geothermal Resources Council Transactions, 33, 199-203.

Lee, J., 2014. Implicit and explict fractrue shear slip analysis for geological storage of carbon dioxide and nuclear waste. PhD dissertation, Seoul National University, Korea. PP. 1-10.

Lee, J., Min, K. B., Rutqvist, J., 2013. Probabilistic analysis of fracture reactivation associated with deep underground CO2 injection. Rock mechanics and rock engineering, 46(4), 801-820.

Majer, E.L., Baria, R., Stark, M., Oates, S., Bommer, J., Smith, B., Asanuma, H., 2007. Induced seismicity associated with enhanced geothermal systems. Geothermics, 36(3), 185-222.

Mayerhofer, M.J., Lolon, E., Warpinski, N.R., Cipolla, C.L., Walser, D.W., Rightmire, C.M., 2010. What is stimulated reservoir volume? SPE Production & Operations, 25(01), 89-98.

McClure, M., Horne, R., 2012. The effect of fault zone development on induced seismicity. Paper presented at the 37th Workshop on Geothermal Reservoir Engineering, Stanford University, Stanford, California, USA. Retrieved 21 June, 2016 from https://pangea.stanford.edu/ERE/pdf/IGAstandard/SGW/2012/Mcclure.pdf.

McClure, M.W., Horne, R.N., 2014. An investigation of stimulation mechanisms in Enhanced Geothermal Systems. International Journal of Rock Mechanics and Mining Sciences, 72, 242-260.

Meller, C., Kohl, T., Gaucher, E., Genter, A., 2012. Approach for determination of the failure probability of fractures at the Soultz-Sous-Forêts EGS project. Paper presented at the 37th Workshop on Geothermal Reservoir Engineering 2012, Stanford University, California, USA. Retrieved 21 June, 2016 from https://pangea.stanford.edu/ERE/db/GeoConf/papers/SGW/2012/Meller.pdf.

MIT, 2006. The future of geothermal energy: Impact of enhanced geothermal systems (EGS) on the United States in the 21st century. Massachusetts Institute of Technology. PP. 1-1 - 1-34.

Moeck, I., Kwiatek, G., Zimmermann, G., 2009. Slip tendency analysis, fault reactivation potential and induced seismicity in a deep geothermal reservoir. Journal of Structural Geology, 31(10), 1174-1182.

Morris, A., Ferrill, D.A., Henderson, D.B., 1996. Slip-tendency analysis and fault reactivation. Geology, 24(3), 275-278.

Mukuhira, Y., Asanuma, H., Niitsuma, H., Häring, M.O., 2013. Characteristics of large-magnitude microseismic events recorded during and after stimulation of a geothermal reservoir at Basel, Switzerland. Geothermics, 45, 1-17.

Murphy, H.D., Fehler, M., 1986. Hydraulic fracturing of jointed formations. Paper presented at the International Meeting on Petroleum Engineering, Beijing, China. DOI:10.2118/14088-MS.

Oikawa, Y., Yamaguchi, T., 2000. Stress measurement using rock core in an HDR field. Paper presented at the World Geothermal Congress 2000, Kyushu-Tohoku, Japan. PP. 3819-3822.

Okabe, T., Hayashi, K., Shinohara, N., Takasugi, S., 1998. Inversion of drilling-induced tensile fracture data obtained from a single inclined borehole. International Journal of Rock Mechanics and Mining Sciences, 35(6), 747-758.

Olasolo, P., Juárez, M., Morales, M., Liarte, I., 2016. Enhanced geothermal systems (EGS): A review. Renewable and Sustainable Energy Reviews, 56, 133-144.

Parker, R., 1999. The Rosemanowes HDR project 1983–1991. Geothermics, 28(4), 603-615.

Phillips, W.S., Rutledge, J.T., House, L.S., Fehler, M.C., 2002. Induced microearthquake patterns in hydrocarbon and geothermal reservoirs: Six case studies. In The Mechanism of Induced Seismicity. Birkhäuser Basel. PP. 345-369.

Pine, R., Batchelor, A., 1984. Downward migration of shearing in jointed rock during hydraulic injections. International Journal of Rock Mechanics and Mining Sciences & Geomechanics Abstracts, 21(5), 249-263.

Polsky, Y., Capuano Jr., L., Finger, J., Huh, M., Knudsen, S., Chip Mansure, A. J., Raymond, D., Swanson, R., 2008. Enhanced Geothermal Systems (EGS) well construction technology evaluation report. Sandia National Laboratory report. Retrieved 21 June, 2016 fromhttps://www1.eere.energy.gov/geothermal/pdfs/egs_well_contruction.pdf.

Regenauer-Lieb, K., Bunger, A., Chua, H.T., Dyskin, A., Fusseis, F., Gaede, O., Jeffrey, R., Karrech, A., Kohl, T., Liu, J., 2015. Deep geothermal: The 'Moon Landing'mission in the unconventional energy and minerals space. Journal of Earth Science, 26(1), 2-10.

Roegiers, J., Detoumay, E., 1988. Considerations on failure initiation in inclined boreholes. Paper presented at the The 29th US Symposium on Rock Mechanics (USRMS), Minneapolis, Minnesota, USA. Paper No. ARMA-88-0461.

Sanyal, S.K., 2010. Future of geothermal energy. Paper presented at the thirty-fifth workshop on geothermal reservoir engineering. Stanford University, Stanford, California, USA. Retrieved 21 June, 2016 from

https://pangea.stanford.edu/ERE/pdf/IGAstandard/SGW/2010/sanyal.pdf.

Schindler, M., Baumgärtner, J., Gandy, T., Hauffe, P., Hettkamp, T., Menzel, H., Penzkofer, P., Teza, D., Tischner, T., Wahl, G., 2010. Successful hydraulic stimulation techniques for electric power production in the Upper Rhine Graben, Central Europe. Paper presented at the Proc. World geothermal congress (WGC2010), Bali, Indonesia. Paper No. 3163.

Shin, K., Ito, H., Oikawa, Y., 2000. Stress state at the Ogachi site. Paper presented at the Proc. World Geothermal Congress 2000, Kyushu, Tohoku, Japan. PP. 1749-1752.

Simonson, E., Abou-Sayed, A., Clifton, R., 1978. Containment of massive hydraulic fractures. Society of Petroleum Engineers Journal, 18(01), 27-32.

Song, Y.H, Lee, D.J., Jeon, J.S., Yoon, W.S., 2015. Background and Progress of the Korean EGS Pilot Project. Paper presented at the Proc. World Geothermal Congress, Melbourne, Australia. Paper No. 31007.

Terakawa, T., Miller, S.A., Deichmann, N., 2012. High fluid pressure and triggered earthquakes in the enhanced geothermal system in Basel, Switzerland. Journal of Geophysical Research: Solid Earth (1978–2012), 117(B7).

Thorsen, K., 2011. In situ stress estimation using borehole failures—Even for inclined stress tensor. Journal of Petroleum Science and Engineering, 79(3), 86-100.

Tischner, T., Schindler, M., Jung, R., Nami, P., 2007. HDR project Soultz: Hydraulic and seismic observations during stimulation of the 3 deep wells by massive water injections. Paper presented at the 32nd workshop on Geothermal Engineering, Stanford University, Stanford, California, USA. Retrieved 21 June, 2016 from https://geo.stanford.edu/ERE/pdf/IGAstandard/SGW/2007/tischner.pdf.

Valley, B., 2007. The relationship between natural fracturing and stress heterogeneities in deep-seated crystalline rocks at Soultz-sous-Forêts (France). PhD Thesis, Institute of Geology, Swiss Federal Institute of Technology (ETH) Zurich, Switzerland. PP. 1-121.

Valley, B., Evans, K.F., 2007. Stress state at Soultz-sous-Forêts to 5 km depth from wellbore failure and hydraulic observations. Paper presented at the 32nd workshop on geothermal reservoir engineering, Stanford University, Stanford, California, USA. Retrieved from https://pangea.stanford.edu/ERE/pdf/IGAstandard/SGW/2007/valley.pdf

Van der Hoeven, M., 2013. World Energy Outlook 2013. International Energy Agency: Tokyo, Japan.

Weidler, R., Gerard, A., Baria, R., Baumgärtner, J., Jung, R., 2002. Hydraulic and micro-seismic results of a massive stimulation test at 5 km depth at the European Hot-Dry-Rock test site, Soultz, France. Paper presented at the 27th Workshop on Geothermal Reservoir Engineering, Stanford University, Stanford, California, USA. Retrieved 21 June, 2016 from

https://pangea.stanford.edu/ERE/pdf/IGAstandard/SGW/2002/Weidler.pdf.

Wyborn, D., 2010. Update of development of the geothermal field in the granite at Innamincka, South Australia. Paper presented at the Proc. of the World Geothermal Congress (WGC2010), Bali, Indonesia. Paper No. 3121.

Xie, L., Min, K.B., Song, Y., 2015. Observations of hydraulic stimulations in seven enhanced geothermal system projects. Renewable Energy, 79, 56-65.

Xie, L., Min, K.B., 2016. Initiation and propagation of fracture shearing during hydraulic stimulation in enhanced geothermal system. Geothermics, 59, 107-120.

Xie, L., Min, K.B., 2016. Hydraulic fracture initiation and propagation in deep inclined borehole (to be submitted).

Yeo, I. D., De Freitas, M. H., Zimmerman, R. W., 1998. Effect of shear displacement on the aperture and permeability of a rock fracture. International Journal of Rock Mechanics and Mining Sciences, 35(8), 1051-1070.

Yew, C., Li, Y., 1988. Fracturing of a deviated well. SPE Production Engineering, 3(04), 429-437.

Yew, C.H., Weng, X., 2014. Mechanics of hydraulic fracturing: Gulf Professional Publishing. PP. 1-23.

Zang, A., Yoon, J.S., Stephansson, O., Heidbach, O., 2013. Fatigue hydraulic fracturing by cyclic reservoir treatment enhances

permeability and reduces induced seismicity. Geophysical Journal International, doi: 10.1093/gji/ggt301.

Zimmermann, G., Reinicke, A., Brandt, W., Blöcher, G., Milsch, H., Holl, H., Moeck, I., Schulte, T., Saadat, A., Huenges, E., 2008. Results of Stimulation Treatments at the Geothermal Research Wells in Groß Schönebeck, Germany. Paper presented at the 70th EAGE Conference and Exhibition incorporating SPE EUROPEC 2008, Rome, Italy. DOI: 10.3997/2214-4609.20147634.

Zoback, M., Barton, C., Brudy, M., Castillo, D., Finkbeiner, T., Grollimund, B., Moos, D., Peska, P., Ward, C., Wiprut, D., 2003. Determination of stress orientation and magnitude in deep wells. International Journal of Rock Mechanics and Mining Sciences, 40(7), 1049-1076.

초 록

인공저류층 지열시스템 (Enhanced Geothermal System, EGS) 기술은 고온의 심부 결정질 암반으로부터 지열에너지를 회수하기 위한 기술로서, 지난 30 년간 지열에너지 산업의 최첨단 기술로 자리매김하고 있다. 대규모 수리자극은 EGS 저류층의 투수율을 증진시켜 유체 순환율을 상업적 발전이 가능한 수준까지 끌어올릴 수 있는 방법으로, 결정질 암반 내 시추공의 수십~수백 미터 길이의 나공 영역에 유체를 주입하여 실시된다. 현재까지 다수의 현장에서 EGS 수리자극이 실시되었고, 수리자극의 메커니즘을 이해하고 현장시험 결과를 해석하기 위한 많은 연구가 수행되었다. 그럼에도 불구하고, 수리전단 및 수압파쇄의 시작과 전파 등 저류층의 투수율 증진 정도를 파악하고 유발진동을 관리하기 위해 필수적인 수리자극의 근본적인 세부 거동에 대한 이해가 부족한 실정이다.

본 연구에서는 먼저 암반역학적 측면에서 과거의 7 개 EGS 및 HDR (Hot Dry Rock) 프로젝트에서의 현장 수리자극시험 사례를 살펴보고, 저류층 조건, 시험 인자 및 관측결과에 대해 비교 상관관계분석을 수행하였다. 해당 분석 결과는 저류층

내의 차분응력이 수리전단 및 유발진동 발생 거동을 좌우하는 결정적 인자임을 나타냈다.

한편 수리전단 메커니즘에 따라 수리전단 시작점의 위치, 수리전단 요구 압력 및 수리전단 전파방향을 예측할 수 있는 일반화된 모델을 개발하였다. 수리전단의 시작과 전파에 대한 응력조건의 영향을 알아보기 위한 분석은 유발진동 관측결과와 연관성을 보이는 기본적인 요소들이 존재함을 밝혀냈다. 수리전단 전파방향 분석 결과 대부분의 경우 상방(上方) 전파가 우세하나 고밀도의 주입유체를 사용하는 경우 하방(下方) 전파가 나타났다. 본 연구에서 개발된 수리전단 예측 방법론은 균열지열저류층에서의 EGS 수리자극시 발생하는 수리전단의 시작 및 전파 거동에 대해 일차적인 예측을 제공할 수 있는 적용 가능성을 지닌다.

본 연구에서는 또한 수압파쇄 메커니즘에 기반한 일반화된 예측 모델을 개발하였으며, 이는 나공 영역에서의 파쇄 시작 거동 및 수리자극 과정 동안의 전반적인 균열 전파 거동을 예측할 수 있다. 수압파쇄 거동에 대한 현지응력조건 및 나공 영역 궤적의 영향을 확인하기 위한 분석을 통해, 통상적인 심부 EGS 저류층의 응력조건 하에서는 수압파쇄 균열이 나공영역

최상단(케이싱 슈)에서 시작되어 상방 전파되는 수직 균열로 우세하게 나타나는 경향이 있음을 확인했다. 한편 심도가 깊어짐에 따라 점차 수직공에서 경사공으로 휘어지는 궤적을 갖는 나공 영역의 경우 수압파쇄균열의 시작 위치가 나공영역 최상단(케이싱 슈)에서 최하단(공저)으로 이동하며 보다 낮은 파쇄압력을 보인다.

주요어: 인공저류층 지열시스템 (EGS, enhanced geothermal system), 수리자극, 유발진동, 현지응력, 수리전단, 수압파쇄

학 번: 2011-31306